Graduate School Form 30
(Revised 08/14)

PURDUE UNIVERSITY
GRADUATE SCHOOL
Thesis/Dissertation Acceptance

This is to certify that the thesis/dissertation prepared

By Abdullah Karimi

Entitled
NUMERICAL STUDY OF HOT JET IGNITION OF HYDROCARBON-AIR MIXTURES IN A CONSTANT-VOLUME COMBUSTOR

For the degree of Master of Science in Mechanical Engineering

Is approved by the final examining committee:

M. Razi Nalim

Likun Zhu

Sohel Anwar

To the best of my knowledge and as understood by the student in the Thesis/Dissertation Agreement, Publication Delay, and Certification/Disclaimer (Graduate School Form 32), this thesis/dissertation adheres to the provisions of Purdue University's "Policy on Integrity in Research" and the use of copyrighted material.

M. Razi Nalim

Approved by Major Professor(s): _____

_____

Approved by: Sohel Anwar 12/09/2014

Head of the Department Graduate Program Date

NUMERICAL STUDY OF HOT JET IGNITION OF HYDROCARBON-AIR MIXTURES IN A CONSTANT-VOLUME COMBUSTOR

A Thesis

Submitted to the Faculty

of

Purdue University

by

Abdullah Karimi

In Partial Fulfillment of the

Requirements for the Degree

of

Master of Science in Mechanical Engineering

December 2014

Purdue University

Indianapolis, Indiana

For my parents

ACKNOWLEDGEMENTS

I would like to thank at first my advisor Dr. M. Razi Nalim for the continuous support and guidance during my years as graduate student. His intuitive and critical thoughts helped me carry out successful research. I am also thankful to Dr. Likun Zhu and Dr. Sohel Anwar for their time and advice.

I am grateful for the financial support provided by IUPUI Fellowship, Rolls Royce North America, and NSF EEC grant #1037694 during my work.

I am also thankful to my colleagues Sameera Wijeyakulasurya, Indika Perera, Tarek Elharis, Kevin Murphy, Manikanda Rajagopal, and Prasanna Chinnathambi at Combustion and Propulsion Research Lab, IUPUI.

Special thanks to my wife for all the support she provided during the time I worked on my thesis. Last but not the least I am grateful to my parents who always encouraged me to pursue my dreams.

TABLE OF CONTENTS

Page

Page

LIST OF TABLES

LIST OF FIGURES

Figure Page

Figure Page

Figure Page

Figure Page

Figure Page

Figure Page

Figure Page

ABSTRACT

Karimi, Abdullah. M.S.M.E., Purdue University, December 2014. Numerical Study of Hot Jet Ignition of Hydrocarbon-Air Mixtures in a Constant-Volume Combustor. Major Professor: Mohamed Razi Nalim.

Ignition of a combustible mixture by a transient jet of hot reactive gas is important for safety of mines, pre-chamber ignition in IC engines, detonation initiation, and in novel constant-volume combustors. The present work is a numerical study of the hot-jet ignition process in a long constant-volume combustor (CVC) that represents a wave-rotor channel. The mixing of hot jet with cold mixture in the main chamber is first studied using non-reacting simulations. The stationary and traversing hot jets of combustion products from a pre-chamber is injected through a converging nozzle into the main CVC chamber containing a premixed fuel-air mixture. Combustion in a two-dimensional analogue of the CVC chamber is modeled using global reaction mechanisms, skeletal mechanisms, and detailed reaction mechanisms for four hydrocarbon fuels: methane, propane, ethylene, and hydrogen. The jet and ignition behavior are compared with high-speed video images from a prior experiment. Hybrid turbulent-kinetic schemes using some skeletal reaction mechanisms and detailed mechanisms are good predictors of the experimental data. Shock-flame interaction is seen to significantly increase the overall reaction rate due to baroclinic vorticity generation, flame area increase, stirring of non-uniform density regions, the resulting mixing, and shock compression. The less easily ignitable methane mixture is found to show higher ignition delay time compared to slower initial reaction and greater dependence on shock interaction than propane and ethylene.

The confined jet is observed to behave initially as a wall jet and later as a wall-impinging jet. The jet evolution, vortex structure and mixing behavior are significantly

different for traversing jets, stationary centered jets, and near-wall jets. Production of unstable intermediate species like C_2H_4 and CH_3 appears to depend significantly on the initial jet location while relatively stable species like OH are less sensitive. Inclusion of minor radical species in the hot-jet is observed to reduce the ignition delay by 0.2 ms for methane mixture in the main chamber. Reaction pathways analysis shows that ignition delay and combustion progress process are entirely different for hybrid turbulent-kinetic scheme and kinetics-only scheme.

1. INTRODUCTION

1.1 Background

Intentional hot jet ignition of premixed combustible mixture finds application in internal combustion engines [1-2], pulsed detonation engines [3] and wave rotor combustors [4-6]. Such ignition is of particular interest for wave rotor combustors [5, 7-8]. Chemically active radicals and fast turbulent mixing in the jets create an explosion that is more energetic than a spark [3], allowing rapid ignition of lean mixtures. Further, the penetrating and distributed nature of ignition can overcome mixture non-uniformity. By enabling lean stratified mixtures, heat losses to the walls and pollutant emissions can be mitigated.

Hot-jet ignition involves complex flow phenomena such as vortex evolution, fluid mixing, and turbulence generation. The presence of reactive species in the jet complicates the chemical kinetics of fuel combustion. A high-speed compressible transient jet is usually accompanied by shock formation in a confined volume, leading to subsequent reshaping of flame fronts by shock waves and expansion waves. Chemically active hot jet created from spark ignition of combustible mixture in the pre-chamber is used to ignite the main constant volume combustor (CVC) mixture. The schematic of the experimental CVC rig is shown in Figure 1.1. This hot jet ignition rig is currently being investigated at Purdue School of Engineering and Technology, IUPUI for fundamental flow physics and chemical kinetics. This study helps in designing the hot/torch jet ignition system based wave rotor combustor (Figure 1.2) for gas turbine and power generation applications.

In the case of hot jet ignition studies, ignition delay time is an important parameter that controls the ignition characteristics of a fuel. The ignition delay time for a jet-ignited constant volume combustor may be defined as the time from jet initiation to the occurrence of rapid, visible, and pressure-generating heat release in the CVC chamber [5]. There are many definitions of ignition delay time used in the literature. Auto-ignition delay in shock-tube and rapid compression experiments reflect purely chemical processes, while jet ignition and spark ignition also include physical processes. Ignition delay in hot jet ignition includes time for transient jet vortex development, jet mixing with the gas in the CVC chamber, and chemical evolution. In addition, in the present study of hot jet ignition, reflecting shock and expansion waves generated due to confined geometry also affect the ignition process.

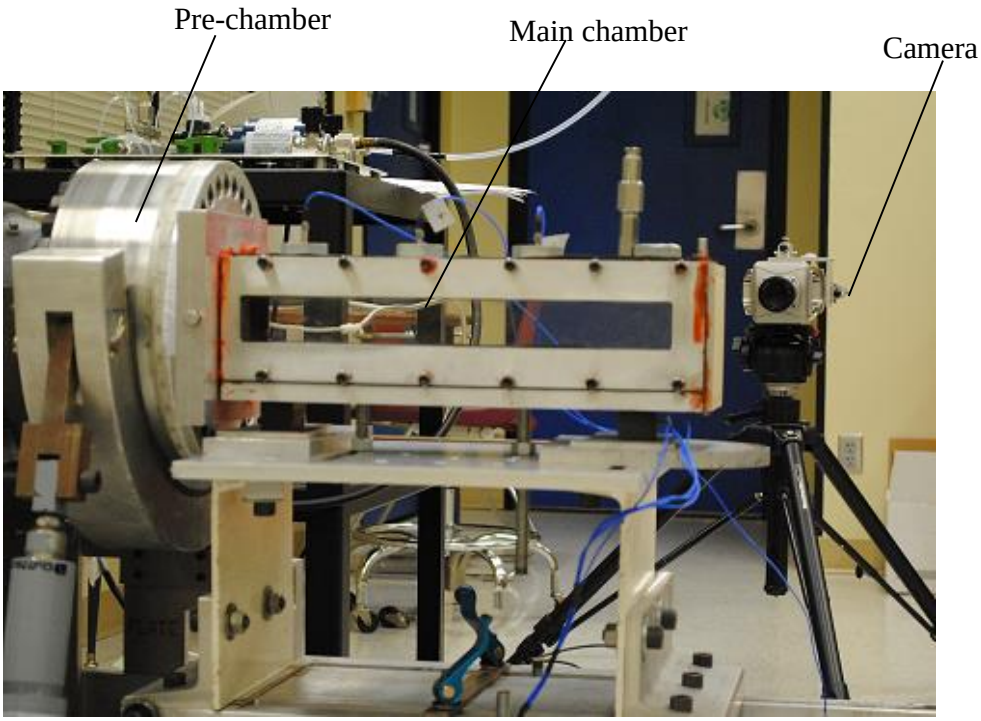

Figure 1.1 Constant Volume Combustor (CVC) Hot-Jet Ignition Rig

A combustible mixture can be ignited by an inert gas jet or reactive gas from another combustion source. Prior experiments mainly addressed mine safety using a steady non-reactive hot gas jet injecting into unconfined well-mixed stationary or quiescent

combustible mixture. Toulsan et al. [9] made a review of turbulent jet ignition systems for pre-chamber spark ignition engines (Figure 1.3). The pre-chamber mixture is more controlled and reliably spark-ignited and produces a hot jet that acts as a distributed ignition source, allowing reliable combustion of the main CVC charge over a broader range of air-fuel ratios, shorter flame travel distances, and more rapid combustion in traditionally slow-burning lean mixtures. Chemically reactive radicals (eg. H and OH) and jet-induced turbulence was estimated to be equivalent to two orders of magnitude higher energy than spark ignition [10]. Wolfhard [11] observed that nitrogen and carbon dioxide have similar ignition temperatures, while argon and helium have higher ignition temperatures. The ignition temperature was defined as the temperature at which the combustible gas mixtures can be ignited by laminar hot jets. Fink and Vanpée [12] developed an overall rate expression for ignition of methane and ethane-air mixtures by low-velocity hot inert gas jets. Cato and Kuchta [13] conducted experiments using laminar hot air jets and concluded that ignition depend on jet base temperature, jet dimensions, composition of the combustible mixture, and jet velocity. In contrast to the hot jet ignition reported here for confined constant-volume combustion, mine-safety experiments were typically without turbulence and at low velocities.

Tarzhanov et al. [14] investigated using hot detonation products to detonate stagnant propane-air mixtures and found that detonation initiation depends on the initial volume concentrations of the mixture, mass fraction of hot detonation products, and the energy deposited from the detonation products. Mayinger et al. [15] derived correlations between the induction time (ignition delay time), the mixing time of the jet, and the adiabatic auto-ignition time for the fuel-air mixtures. The experimental facilities in their work consist of two chambers separated by a partition with a single circular orifice.

Bilgin [16] developed a constant-volume combustor with long aspect ratio and square cross-section, representing a wave rotor channel. The CVC is ignited by a jet of hot combustion products from a separately fueled pre-chamber that could be spun to cause the jet to traverse one end of the CVC [17].

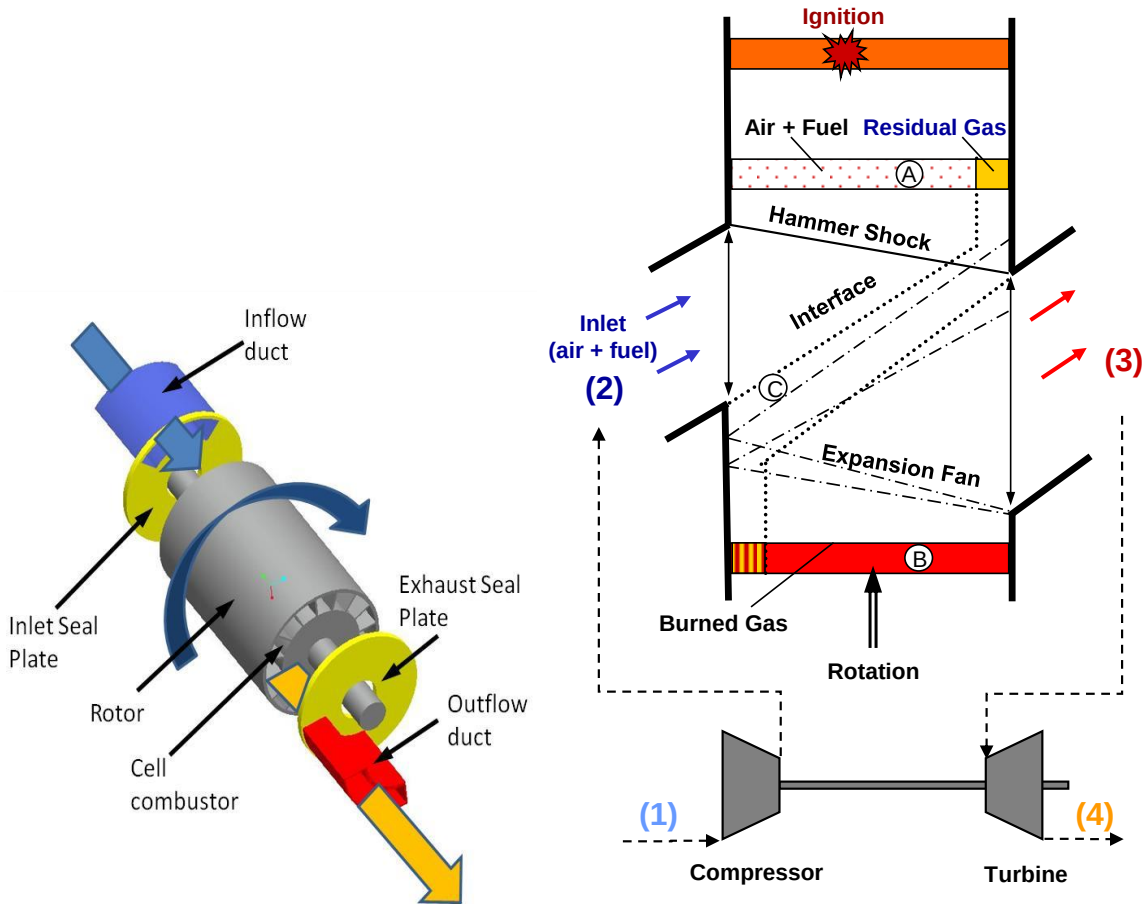

(a) (b)

Figure 1.2 (a) Schematic Diagram of Wave Rotor with 20 cells [4] (b) Flow Features in a Wave Rotor Cell [25]

The relative motion reproduces the action of a wave rotor channel, and pre-chamber may be representative of a previously combusted channel supplying hot gas. Bilgin proposed a correlation between the Damköhler number and ignition of a fuel-air mixture in the CVC. For the same geometry, Baronia et al. [18] performed numerical simulations for the stationary (non-traversing) torch jet case using global reaction mechanisms (one-step and four-step) for propane-air mixture. Bilgin's measurements were not well matched by Baronia's simulations, possibly due to lack of detailed chemistry and not accounting for more active chemical species in the jet. Perera [8] carried out experiments on the same CVC test rig for three hydrocarbon fuels (methane, ethylene, and propane) under varying equivalence ratios in the pre-chamber and the CVC chamber. The ignition delay time

variation for each fuel under constant experimental conditions and the ignitability limits, both lean and rich, for all three fuels in the CVC chamber were investigated. The variation of ignition delay time for fuels with different pre-chamber equivalence ratios and nozzle geometry were also observed.

The hot jet ignition system for internal combustion engines have been investigated for long time due to a number of advantages it provides. One of the first applications of such a system was in 2-stroke Ricardo Dolphin engine [19]. Torch cell engine designs used same concept in which the pre-chamber cavity is filled with the fresh main chamber charge during compression. Such torch cell designs were developed by Toyota, Ford, Volkswagen and others.

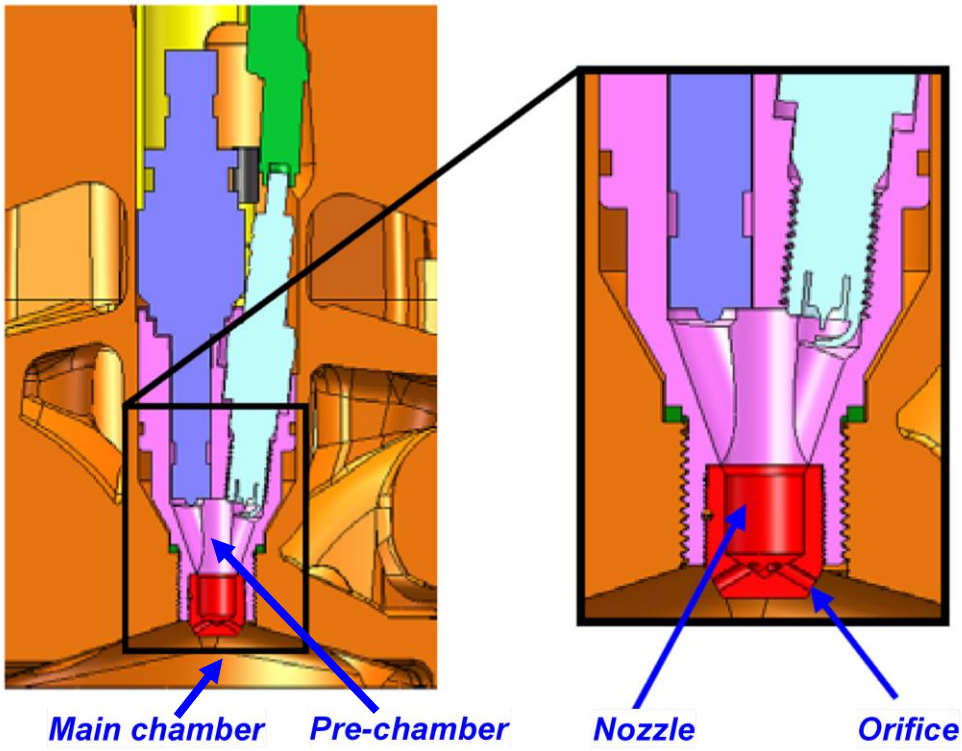

Figure 1.3 Pre-chamber Ignition in a 4-valve Pent Roof Combustion System [10]

Honda successfully developed a divided chamber stratified charge engine called Compound Vortex Controlled Combustion (CVCC) system with large pre-chamber [20]. The CVCC engine could comply the emissions standard in 1975 without a catalytic converter. The jet ignition, which uses smaller pre-chamber compared to divided chamber stratified charge concept, which was introduced by Nikolai Semenov in late 1950's. Gussak developed the first jet ignition engine under the name of LAG (Lavinia Aktivatisia Gorenia or Avalanche Activated Combustion). Gussak's extensive study established the importance of active radicals in such ignition processes. During 1990's Watson et al. developed hydrogen assisted jet ignition (HAJI) at the University of Melbourne. HAJI is an advanced pre-chamber ignition process that involves the use of a chemically active, turbulent jet to initiate combustion of ultra-lean mixtures in an otherwise standard gasoline fuelled engine.

The hydrogen assisted jet ignition (HAJI) system was first developed by Kyaw and Watson [21] and further explored by Hamori [22], Pouria [23] and Toulson et al. [9]. Active research on such a system called 'Turbulent Jet Ignition' is currently being carried out at MAHLE powertrain. The ongoing research efforts on jet ignition at University of Melbourne and Michigan State University are also noteworthy.

The detailed three-dimensional modeling of combustion coupled with fluid dynamics and detailed chemical kinetics was computationally prohibitive till few years back. Recently, this important field of continued research for the realistic modeling of turbulence chemistry interaction has drawn research attention because of practical application in combustion devices. The well stirred reactor assumption of individual cells that decouples fluid dynamics from chemistry has some flaws for modeling practical turbulent flows. Eddy break model (EBU) extended to include chemical kinetics (called hybrid EBU) is one of the models which can be suitably used to take into account the effects of both mixing and chemistry. The hot jet ignition for IC engine applications have been investigated by Mehrani et al [24], Toulson [9] and Hamori [22]. These studies carried out experiments on Cooperative fuel research (CFR) engine and compared results with spark ignited engines. Toulson [9] and Mehrani [24] also carried out preliminary CFD simulations. These works

did not consider the effect of mixing on the combustion and well-stirred reactor assumption for individual computational cells were made. The computational mesh was also not refined enough to capture quantitative details of the combustion progress and reaction pathways. The well-stirred reactor assumption for computational cells could give inaccurate combustion and heat release rate information.

1.2 Current State of Art

Modeling turbulent combustion is one of the most challenging problems in computational fluid dynamics. Full resolution of all turbulence scales coupled with sufficiently detailed chemistry treatment is still far from reach for the present computational power. In other words, direct numerical simulations (DNS) using detailed reaction mechanisms in a practical turbulent combustor for commercially used fuels are still beyond the computational power. In such a situation, judicious choice of practical modeling approaches with reasonable computational expense and still being able to capture the main features of flow physics becomes crucial. However, choosing the best possible approach constrained by computational resources is as important as interpreting the results. Significant differences can be obtained if different approaches are used and the best approach would be decided based on the experimental validation of results as well as the right intuition of the user.

In turbulent combustion modeling, there are two important factors; resolving turbulence and modeling combustion chemistry. In addition, the turbulence-chemistry interaction also play crucial role in numerical modeling of turbulent combustion. In past two decades, significant progress has been made in the computational power making it possible to carry out DNS of selected practical flows and large eddy simulation (LES) of a wide range of practical turbulent flows. DNS is very important for two reasons; first it resolves all the turbulence scales and with the increase in computational power it would be the coveted approach and second reason is that it is needed for the validation of Reynolds Averaged Navier Stokes (RANS) turbulence models. It should also be noted that with the current rate of progress in computational power, the full DNS of large scale problems

would still be impossible at practical time frame in near future. Keeping this in mind, LES has drawn great research efforts in recent years as it resolves the large scales making it better choice compared to RANS when details of flow is of importance.

Great progress has also been made in the detailed chemical treatment of combustion chemistry. Today there are reaction mechanisms available which involve thousands of reaction in hundreds of species for hydrocarbon combustion. However, the application of such large reaction mechanisms is beyond today's computational power for practical flow simulation. Coupling such detailed reaction mechanisms with DNS for practical combustors does not look possible in near future. Thus, efforts are also directed at developing reduced reaction mechanisms which can be applied for practical combustor flow simulation. A detailed review of the chemical reactions mechanisms, the development of reduced reaction mechanism techniques and their coupling with flow dynamics is discussed in Chapter 3 of the present thesis.

1.3 Scope of the Present Research

As seen above, the combustion modeling of practical turbulent flows is one of the most difficult problems to be resolved fully. The present work is an attempt on modeling turbulent combustion in a practical combustor using different modeling approaches. The constant volume combustor used in the present work has been experimentally investigated for hot jet ignition for practical application in wave rotor combustor. The turbulence is modeled using two-equation RANS turbulence model. A preliminary validation study of different RANS turbulence models and combustion models have also been carried out. The chemical kinetics is modeled using detailed reaction mechanisms for different fuels. This is one of the major contributions of the present work. No previous work has been found that model combustion using detailed reaction mechanisms for such an application. Some of the conclusions of the present work would also be important for modeling turbulent combustion in many other practical combustors (for example; hot jet ignition for otherwise spark ignited engines, HCCI engines and detonative combustion). Thus, present work

would be an important contribution in the literature for detailed combustion modeling of practical combustors.

1.4 Chapter Contents

The present thesis starts with the introduction and scope of the work in the present chapter. Chapter 2 presents a discussion on computational methods, and grids employed in the present work including grid sensitivity. The detailed description and validation of different turbulence and combustion models are described in Chapter 3. The non-reacting study of mixing in the constant-volume combustor is investigated in Chapter 4. This chapter also compares the jet penetration from numerical simulations with experimental results of high speed video images. In Chapter 5, a detailed study of combustion modeling for different types of fuel (methane, ethylene, propane, hydrogen, and hydrogen blended mixtures) is carried out. The effect of jet motion and lean and rich limits of different fuel-mixtures are also analyzed in this chapter. In Chapter 6, the combustion modeling results from different combustion models using detailed reaction mechanisms are investigated for constant volume combustor. This chapter also includes a study of the pre-chamber jet composition effect on the main chamber combustion. The conclusions, future scope of the work and the recommendations are described in the last Chapter.

2. COMPUTATIONAL METHODOLOGY

2.1 Introduction

A brief overview of computational methods used and the available computational resources are described in this chapter. The grid generation process and solver used are also discussed. The computational methods with a brief discussion of RANS turbulence modeling and combustion modeling are covered in this chapter. The chapter ends with a description of the methodology for grid and time-step independence.

2.2 Computational Methods

Commercial CFD code STAR-CCM+ was used primarily for most of the current research. The code uses a finite volume formulation of the Navier-Stokes equations. A second-order accurate spatial differencing scheme was used for the momentum, energy, turbulence, and species transport equations, while an implicit temporal discretization was used for transient computations. The code has two options of solver; segregated solver (pressure based) and coupled solver (density based). Since the flow in the current analysis is highly compressible and sometimes supersonic as well, coupled solver has been used for all the simulations. Furthermore, it has been observed that segregated solver is not good at capturing shock waves unless grid is highly refined. The computations were run on two dedicated 8-processor Dell Precision 690 machines (64 bit architecture, 2.66 GHz processor and 24 Gig RAM) as well as one 12-processor machine. Turbulence is modeled using two-equation SST k-ω model, except in Chapter 3. In Chapter 3, a study has been carried out for the validation of different RANS turbulence models for supersonic flow over backward facing step flow.

The combustion model primarily used in the present research is hybrid eddy break up model which takes into account both mixing and chemical kinetics. A detailed description of combustion models and a validation study is presented in Chapter 3. The chemical kinetics is modeled using different detailed reaction mechanisms for various fuel-air mixtures.

2.3 Computational Grids

Computational grids used in the present study are generated by using two methods; Proam, a grid generation tool which comes with StarCD suite, and automatic mesh generation from solid model in STAR-CCM+. The geometry is created in solid modeling tool Pro/E and then imported into STAR-CCM+ for automatic volumetric mesh generation. For complicated geometries, it becomes cumbersome to create grid using Proam; therefore, automatic grid generation available in STAR-CCM+ is employed.

Grid and time-step independence of results are carried out and discussed for different types of problems of the present research in relevant sections. For grid independence various parameters are analyzed. For example, grid sensitivity study is carried out for turbulence validation in Chapter 3 using three different grid sizes consisting of 57000, 123600 and 228000 cells. The static profile across the flow domain at 10 mm downstream of the backward facing step for a Mach number of 2 is presented for different grid sizes predicted using SST (Menter) k-ω turbulence model. Moreover, the normalized reattachment lengths for the three grid sizes are found to be 3.23, 3.50 and 3.56 respectively for 3 different grid sizes considered in the study. Therefore, the grid size with total number of cells 228000 is used for validating the turbulence model presented in Chapter 3. Similarly, grid independence is carried out for combustion modeling of constant volume combustor using global and detailed reaction mechanisms. Fuel consumption rates and mass fraction levels are compared to show the sensitivity of grid in predicted results.

3. TURBULENCE AND COMBUSTION MODELS

3.1 Introduction

Modeling turbulent flow using RANS approach needs the right choice of turbulence models. Several variants of two-equation models, one-equation model (Spalart Allmaras model) and Reynolds stress turbulence model (RSM) are most commonly employed. However, certain models are good for particular flow situations of interest and therefore a detailed validation of turbulence model that needs to be employed is crucial for more accurate turbulence modeling. For modeling turbulent combustion, the choice of turbulence-chemistry interaction models play important role as well. Therefore, in this chapter two test cases for validation of turbulence models and turbulence-chemistry interaction models are investigated. The results are validated with the published experimental data and important inferences are discussed.

3.2 Turbulence Model Validation

The flow over backward facing step (BFS) is a standard benchmark problem used to study separated flows. This flow geometry is preferred to evaluate turbulence models due to its simplicity [26]. There have been numerous studies on such a flow, both experimentally as well as numerically. Lately, the interest has been stimulated due to its application in hypersonic propulsive systems as flame-holder. The present chapter analyzes compressible supersonic flow over a BFS, computationally. The backward facing step compressible flow regime includes flow separation, reattachment and viscous-inviscid fluid interactions (Figure 3.1), who's appropriate and accurate representation requires careful and expensive computational modeling. In the present work, supersonic viscous turbulent flow over a BFS has been numerically investigated with special focus on understanding the effect of numerical modeling parameters such as RANS turbulence models, turbulence parameters

and wall boundary conditions on flow characteristics like pressure distribution, reattachment length in recirculation region.

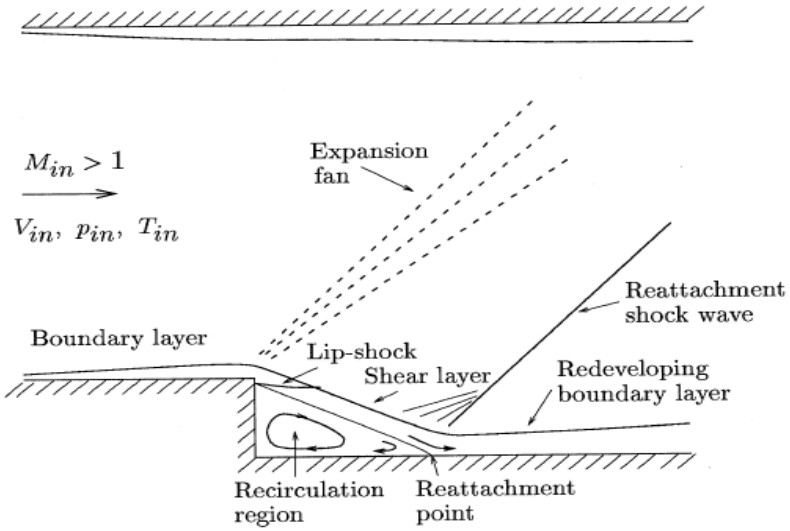

Figure 3.1 Supersonic Flow over a Backward Facing Step [27]

The geometry used in the present study is same as the one investigated experimentally by Hartfield [28], which is presented in Figure 3.2. Dimensions for the geometry and the number of computational grid points used are given in Table 3.1. Stagnation pressure and temperature are used as boundary conditions at the inlet; while, static pressure is specified at the exit boundary. When the flow becomes supersonic, downstream boundary conditions do not govern the flow due to flow velocities exceeding the speed of sound. Hence, the specification of outlet pressure boundary condition becomes obsolete, and the flow quantities at outlet are extrapolated from inside the computational domain. The walls are modeled as no-slip and adiabatic. The boundary conditions and values are listed in Table 3.2.

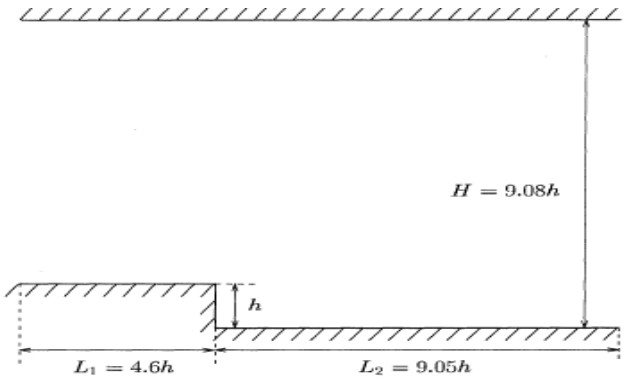

Figure 3.2 Computational Geometry Considered for the Study

Table 3.1 Geometric Dimensions

Step height (h, mm)	Other Dimensions (mm)	No. of cells
3.18	L_1 = 4.06h, L_2 = 9.05h, H = 9.08h	228000

Table 3.2 Boundary Conditions

Inlet (Supersonic Boundary)	Outlet (Static Pressure)	Walls
p = 34800 Pa, P = 273000 Pa, T = 301 K	p = constant	No slip and adiabatic

One of the objectives of this study is to investigate the effect of different RANS turbulence models on the flow behavior in a supersonic flow over BFS, especially in shear layer and reattachment regimes. The turbulence models used in this work are: Reynolds Stress Model [29], Standard k-ε model [30-31], Realizable k-ε model [32], Standard Spalart-Allmaras model [33], SST (Menter) k-ω model [34] and k-ε model with two-layer wall treatment. The governing flow equations were solved using a finite-volume method, with implicit time integration, velocity-pressure coupled equations, and second-order-accurate discretization, implemented in the STAR-CCM+ code.

Grid sensitivity study is carried out using three different grid sizes consisting of 57000, 123600 and 228000 cells respectively. The static pressure profile across the flow domain at 10 mm downstream of the step is presented in Figure. 3.3 for different grid sizes using SST (Menter) k-ω turbulence model. It is observed that the error in predictions from two finer meshes is very small. The normalized reattachment lengths for the three grid sizes are 3.23, 3.50 and 3.56 respectively. Therefore, the grid size with total number of cells 228000 is used for the further detailed investigation.

For the validation of present numerical predictions, comparisons have been done with the experimental work of Hartfield et al. [28] and previous numerical works [27, 35] in Figure 3.4 and Figure 3.5. The effect of different turbulence models on static pressure across the flow domain at 10 mm downstream of the step is presented in Figure 3.6 It can be seen in Figure 3.3 that the RSM model predictions agree well with the experimental PLIF measurements, than other models considered in this study. Moreover, the prediction from standard $k-\omega$ model is almost as good as that from RSM. The Realizable $k-\varepsilon$ model prediction is poor inside the shear layer and its spreading region. As can be seen in Figure 3.6, the current predictions using RSM and SST (Menter) $k-\omega$ turbulence models were able to capture the experimentally found pressure variation near the step wall accurately. Predictions from previous two works [27, 35] (which used high Reynolds number $k-\varepsilon$ and Spallart-Allmaras models respectively) cited in Figure 3.6, failed to capture this near wall pressure accurately. This is mainly because of the limitations of the turbulence models used in previous works.

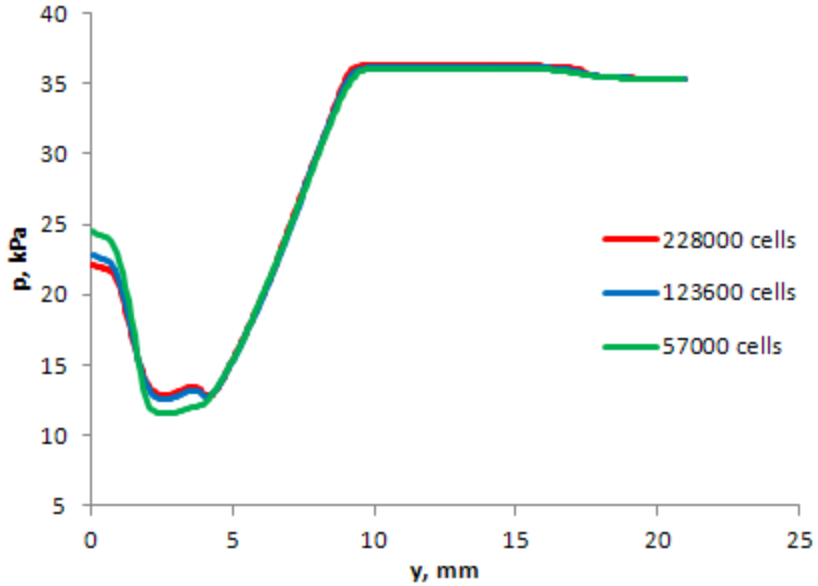

Figure 3.3 Static Pressure Profile at 10 mm Downstream of the Step for Different Grid Sizes

The static pressure contours predicted from the present numerical simulation using RSM turbulence model and published PLIF data are presented in Figure 3.4. A good agreement is noticed between the two sets of data. The static temperature contours compared in Figure 3.5 also shows good agreement with measured data.

Reattachment length is the distance from the step wall to the point at which wall shear stress zero ($dU/dz = 0$). Its value depends on various parameters, such as Reynolds number based on the step height (Re_h), state of the flow at the separation, the ratio of boundary layer thickness to step height at the edge of the step, turbulence intensity in the free stream, and expansion ratio. The reattachment length is shorter for higher free stream Mach numbers. Table 3.3 lists the reattachment length normalized by the step height for different turbulence models. The reattachment length is normalized by step height, to make comparisons of the predictions for different step heights. The experimentally measured [36] normalized reattachment length is 3.60 for a flow Mach number of 2 and for a step height of 6 mm; while, Halupovich et al. [27] predicts (using high Reynolds number k-ε turbulence model) this quantity to be 2.92, for a flow Mach number of 2 and a step height of 10 mm.

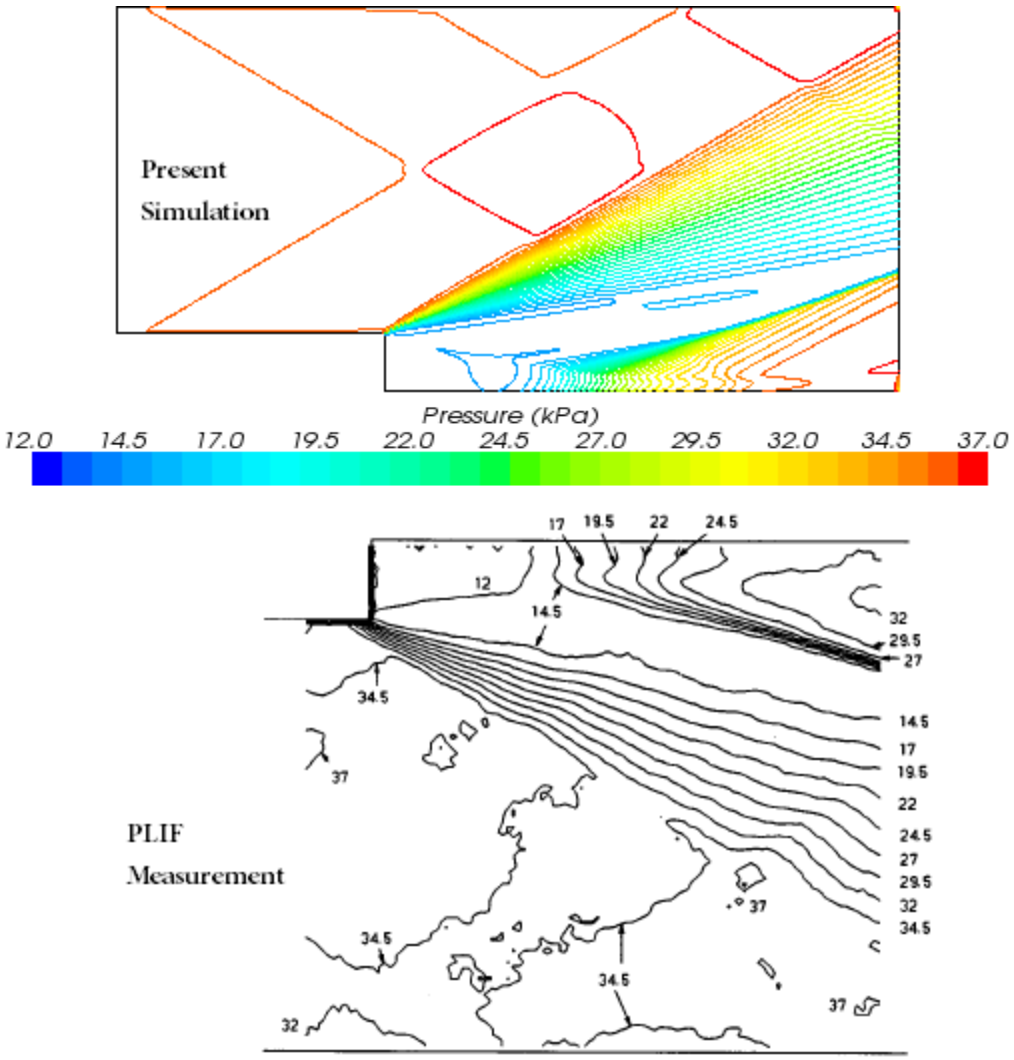

Figure 3.4 Static Pressure Contour in a Backward-Facing Step with Supersonic Flow Comparison with Experimental Data [28]

Table 3.3 shows that current predictions using standard k-ε model predicts this value to be 2.92, which is same as the predictions by Halupovich et al. [27]. The value of normalized reattachment length predicted by RSM model, SST (Menter) k-ω model, and 2 layer k-ε are higher are closer to the experimental value of Roshko and Thomke (although the step heights are different).

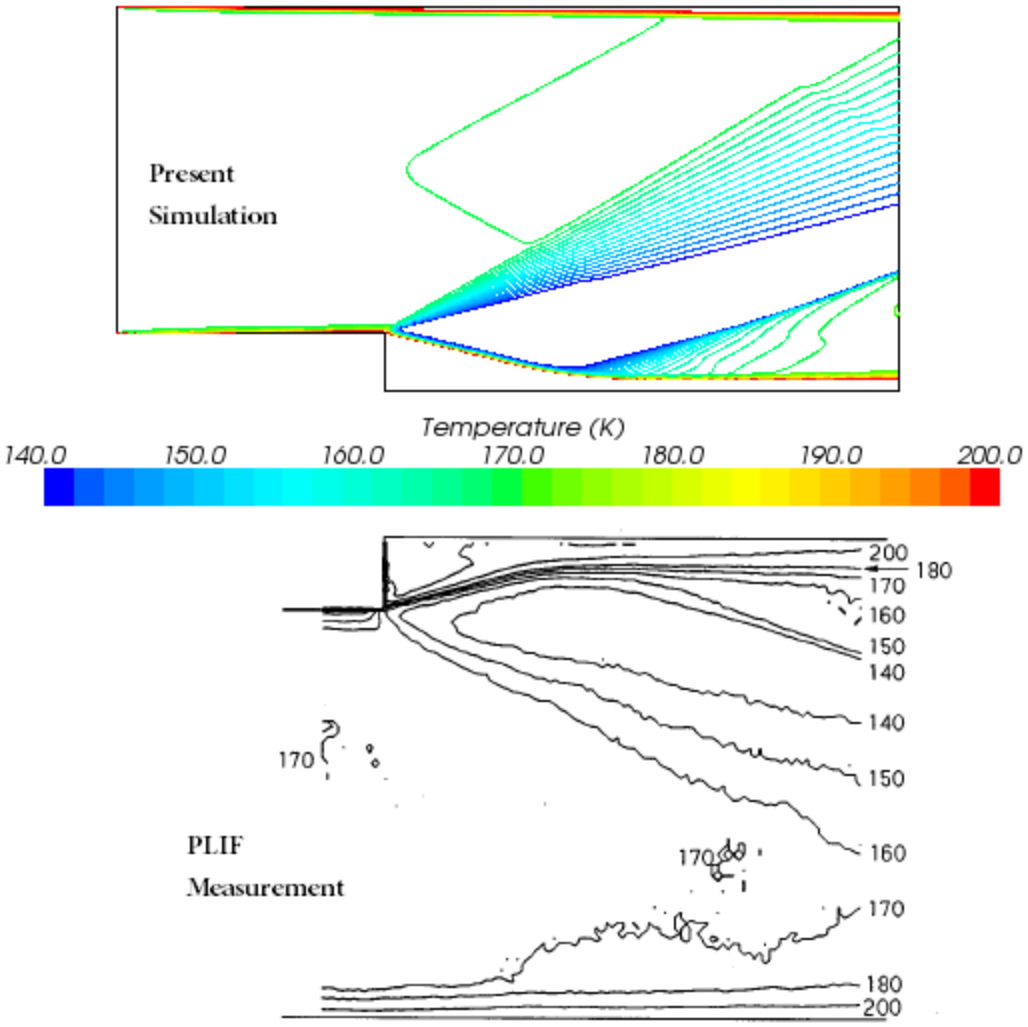

Figure 3.5 Static Temperature Contour in a Backward-Facing Step with Supersonic Flow Comparison with Experimental Data [28]

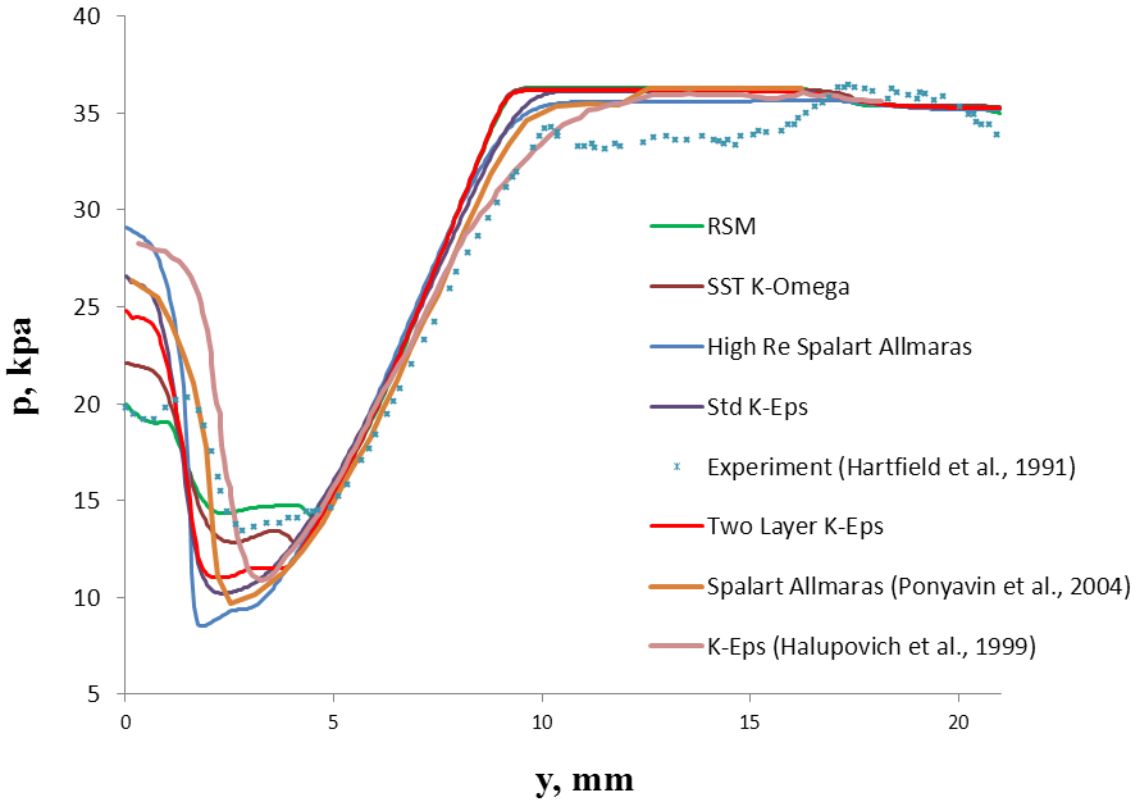

Figure 3.6 Static Pressure at 10 mm Downstream of the Step for Different Turbulence Models

Table 3.3 Normalized Reattachment Length (X_R/h)

High Re k-ε	2.92
Standard Spalart Allmaras	3.19
RSM	3.25
High Re Spalart Allmaras	2.68
SST (Menter) k-ω	3.56
2 layer k-ε	3.27

A more detailed study of other aspects of supersonic flow over backward facing step has been carried out in the published work of the author and co-workers [37].

3.3 Combustion Models

The objective of this section can be summarized as the investigation of different combustion models and the effect of reaction mechanism for predicting the temperature, velocity, and species distribution in non-premixed steady-flow cylindrical combustor that has been used as a test case in prior research. In this study, the comparison of different combustion models is carried out and the important inference obtained from the study are discussed. The global and quasi global reaction mechanisms are used because of computational expense. Flow is investigated within the cylindrical combustor and is assumed to be steady state and turbulent. The computational domain (Figure 3.7), considered in the present study, is the same as reported in Garreton and Simonin [38] and the numerical work of Silva et al. [39]. Computational mesh used in the present simulation is finer than that used in previous numerical works [39, 40]. The continuity, momentum, energy and k-ε equations along with chemical species transport equations are solved using different combustion models. The Eddy-Break up (EBU) model as incorporated in CFD code STAR-CCM+ presented by Spalding [41] and later developed by Magnussen and Hjertager [42], has been employed. To add the effect of finite rate chemistry by chemical kinetics, the reaction rate is obtained using modified Arrhenius form using single step [43], two-step [39], four-step [44] and 22-step quasi global reaction mechanism [43]. The fuel is injected in to the chamber through a cylindrical duct of diameter 6 cm, while air enters the chamber through a centered annular duct having a spacing of 2 cm. For such mass flow rates, the fuel and air velocities are 7.76 and 36.29 m/s, respectively. The Reynolds number at the entrance of the duct (Re ~ 18000) indicates that the inlet flow is fully turbulent. The inlet air is composed of oxygen (23% in mass fraction), nitrogen (76%) and water vapor (1%), while the fuel is composed of 90% methane and 10% nitrogen. The burner power is about 600 kW.

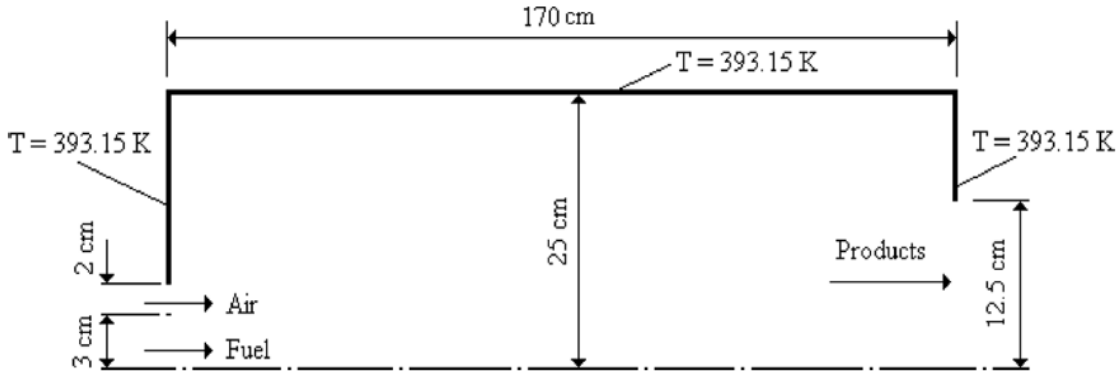

Figure 3.7 Computational Domain Considered for the Simulation

Initially, the standard EBU model has been employed to study the reacting flow inside the cylindrical combustor and followed by the finite rate chemistry using single-step global reaction. Later, the standard EBU model with four-step quasi global mechanisms [44] and the Presumed Probability Distribution Function (PPDF) approach have been investigated.

The axial variation of static temperature predicted by the standard EBU and PPDF models have been compared with the published numerical results [40] and experimental data [38] in Figure 3.8. It appears that there is relatively good agreement among the predictions using standard EBU in the present work and in prior numerical simulation work [40] but the predictions are poor when compared with measured data. Hence, it is clear that the 'mixed-is-burned' approach of EBU does not give good results in this problem. The poor prediction of the 'mixed-is-burned' approach is further shown by adiabatic equilibrium PPDF solution (which does not model finite rate chemistry) as presented in Figure 3.8.

The predictions corresponding to four-step standard EBU model indicates that several reactions will proceed at the same rate when combining the EBU model with a multi-step reaction mechanism. The reason for the above fact is that the reaction mechanism is controlled by the mixing rate of a species present at low concentration. If

this species is taking part in several reactions, the rates of these reactions are all the same; although it is probably more reasonable that the fastest reaction consumes the most [40]. The temperature variation predicted by the four-step Standard EBU and multi-species adiabatic equilibrium PPDF (which includes the species used in 4-step mechanism) are compared in Figure 3.8. It can be observed that the temperature prediction in reaction zone is improved as compared to single step reaction mechanism discussed earlier. Moreover, the axial variation plot indicates that the results predicted by the four-step EBU and multi species adiabatic equilibrium PPDF predictions are almost identical. The temperature profile for different reaction mechanisms is presented in Figure 3.9 and compared with published experimental [38] and predicted detailed kinetics modeling [45] data. The static temperature contours predicted using different combustion models are presented in Figure 3.10.

The Damkohler number (Da), defined as the ratio of characteristic turbulence time scale to characteristic chemical time scale, is used to understand the dominating effect between finite rate chemistry and turbulence mixing. When the Damkohler number is very large, the reaction rate is controlled by the turbulent mixing that brings reactants together at the molecular scale. When the Damkohler number is of order 1, finite rate kinetics must be considered. From Figure 3.11, it can be clearly observed that for Da < 1, chemical reaction rate is the limiting factor for combustion in the cold regime along the centerline in the core of the cylindrical combustor. As a result the combustion modeling without finite rate chemistry performs poorly in the region of low Damkohler number which has been observed from the previous plots of temperature as well.

It should be kept in mind that the Damkohler number can be defined in several ways depending on the situation under study. In the present study, the chemical time scale can be adequately understood by expressing it as the inverse of reaction rate multiplied by fuel molar concentration. Furthermore, the single-step global mechanism predicts well which also validates the worth of this global mechanism of methane for problems where the

detailed chemistry in terms of elementary reactions may not be worth the computational expense it would require.

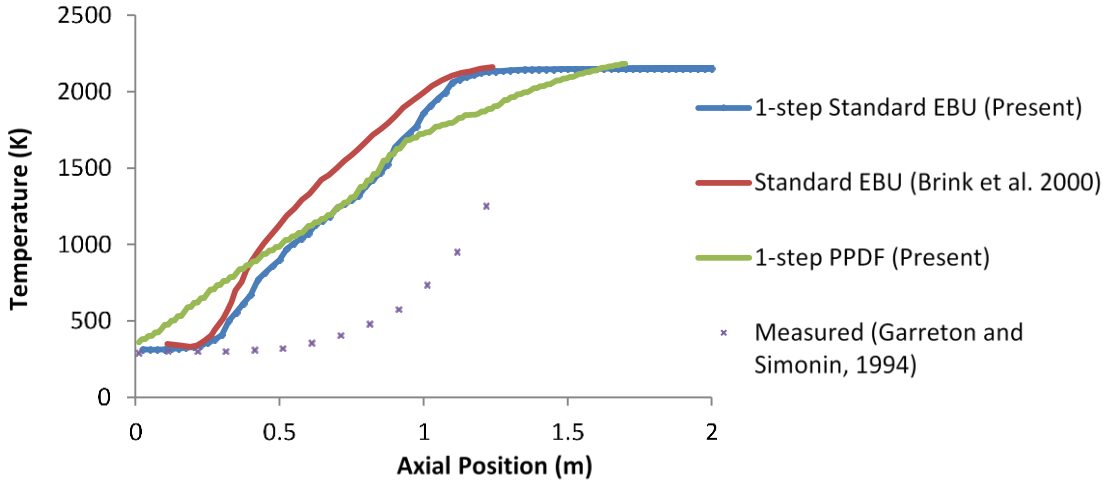

(a)

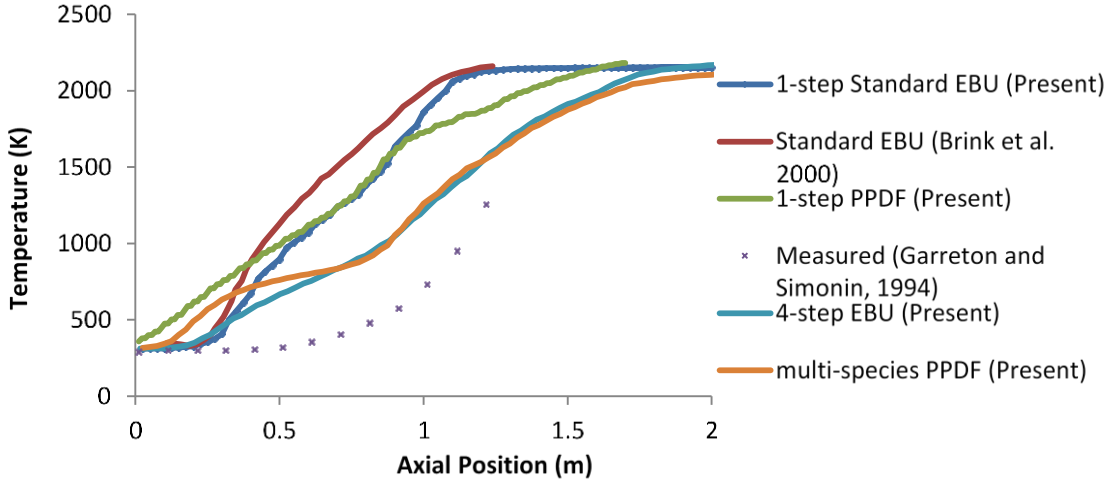

(b)

Figure 3.8 Temperature Comparison from Standard EBU and Adiabatic Equilibrium PPDF Combustion Models along the Centerline of the Furnace

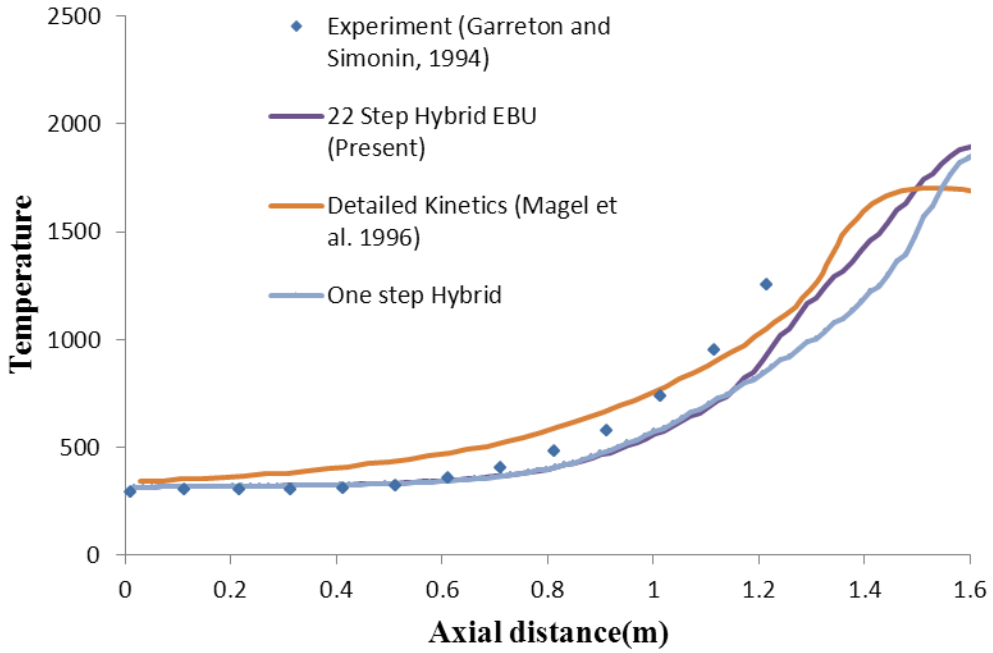

Figure 3.9 Temperature Comparison with Measured Data along the Centerline of the Furnace Using Hybrid EBU and Detailed Kinetics for Different Reaction Mechanisms

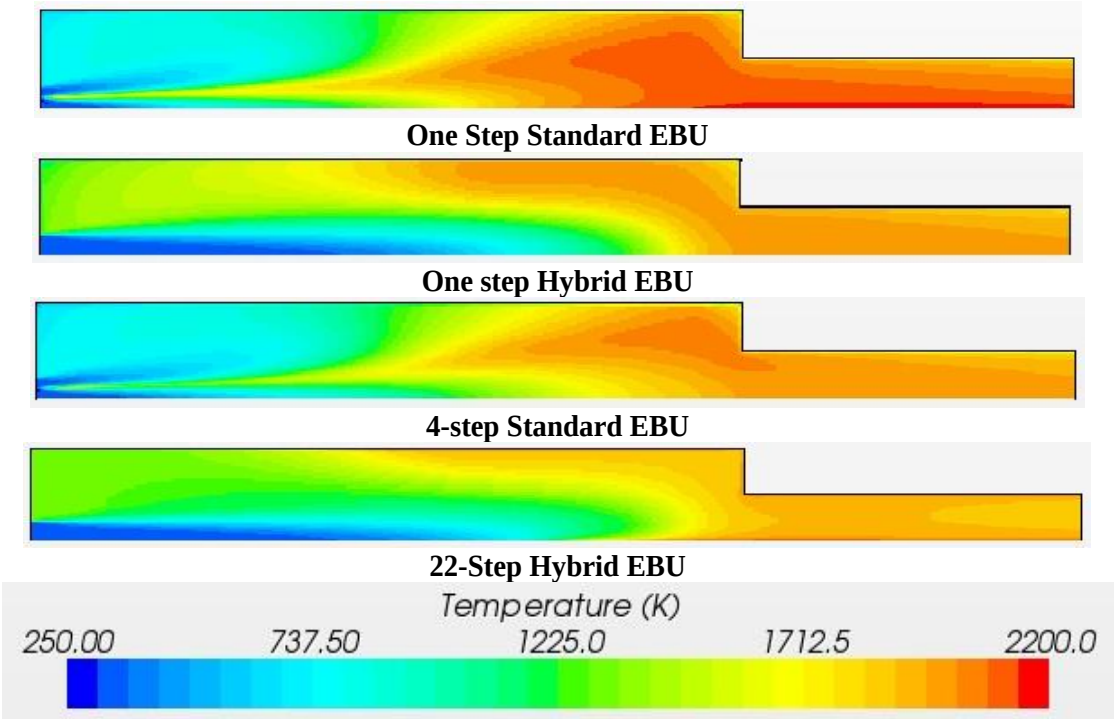

Figure 3.10 Temperature Distribution for Different Combustion Models

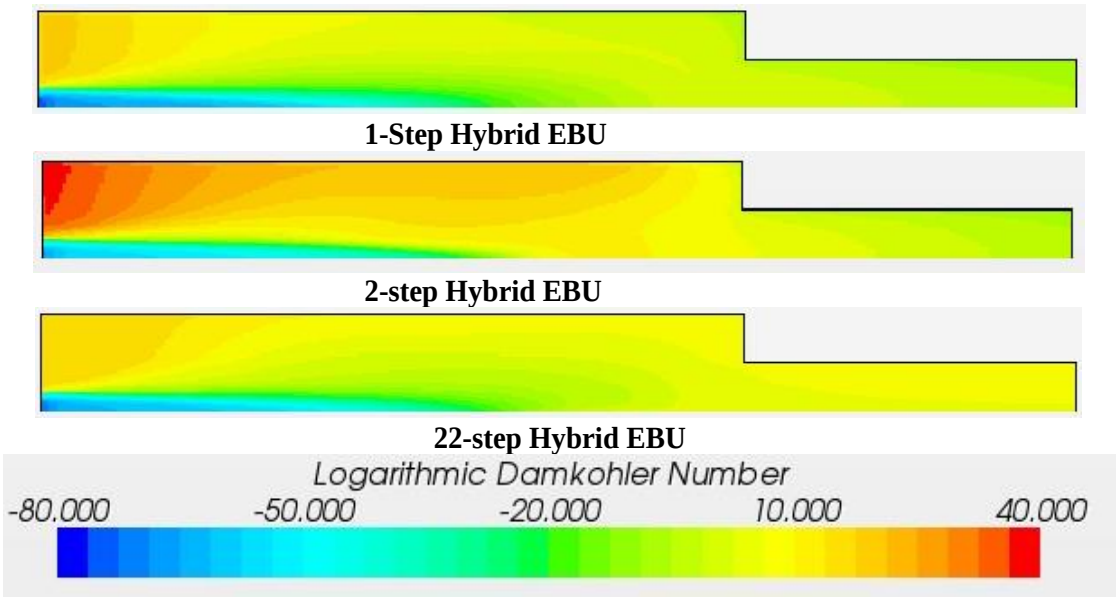

Figure 3.11 Logarithmic Damkohler Number Profile for Different Reaction Mechanisms used in Hybrid EBU Combustion Model

4. HOT JET MIXING AND PENETRATION

4.1 Introduction

The mixing of the hot jet with cold combustible mixture in a constant volume combustor plays an important role in ignition and combustion process. Similar turbulent transient jets have other applications as well including for example, in prechamber type IC engines, direct-injected internal combustion engines, fans, mixers, various spraying devices [46]. The fluid dynamics becomes more complex when the prechamber is spinning leading to traverse of the jet through the nozzle connected to the CVC chamber. Different prechamber spin speeds means different traverse speeds of the jet and the fluid mixing process is affected accordingly.

The two oft-studied turbulent jet types are wall jets and impinging jets. Wall jets occur in many industrial applications such as solid smoothing, inlet devices in ventilation and optimization of the film cooling of gas turbine blades. A turbulent wall jet is obtained by injecting a fluid at a high velocity tangentially to a flat plate boundary [47]. The wall-impinging jet has also wide engineering applications. In many practical applications of wall jets, the jet is injected at an angle to the solid boundary [48].

Horne [49] experimentally studied the laminar planar wall jet investigating unforced periodic velocity fluctuations in the shear layer. The jet velocity and wall length was varied in that work. Fujimoto et al. [50] studied the transient free and impinging jets for diesel engine application using high speed photography and particle image velocimetry. For the transient impinging jet the authors reported that the jet momentum in the main jet region decreases owing to impingement and the tip vortex is broken by the wall. The details of flow structure in various regimes like free jet region, impingement region, vortex region were investigated. Bruneaux [51] studied the flame structure and combustion process of the igniting diesel jet impingement on a perpendicular wall using simultaneous PLIF techniques. It was found that the central core of the jet is not significantly affected by the jet impingement. It is also concluded that the effect of jet impingement on wall on the structure of the OH and formaldehyde regions is consistent with its effect on the mixture structure since it has been shown [52] that mixing is enhanced at the jet tip by the jet–wall vortex. This higher mixing rate therefore creates leaner regions at the tip. Yu et al. [53] experimentally investigated, using PLIF, the jet structure and mixture formation process of wall-impinging gas jet injected by a low pressure gas injector in a constant volume chamber at room conditions. Experimental results showed that vortex structure with large scale is one of the important characteristics for wall-impinging jet, and the interaction among jet flow, impingement wall, and surrounding air plays a dominant role in the mixture formation. In the average image, the concentration field displays smooth decay from the jet center to the border, and the highest concentration regions are at the jet center and the jet impingement regions. It also reveals that the good mixture formation region is in the tip vortex regions.

For application in wave rotor constant volume combustor (WRCVC) the study of the jet mixing (stationary or traversing jets) are important to understand the jet mixing level and penetration characteristics. The understanding of such jet behavior is needed for efficient design of injector as well as prediction of ignition time delay for combustion in the confined volume. The traversing jet behaves like a jet parallel to the wall at the start and end of a channel traverse. One peculiar behavior in three dimensional wall jets widely

reported is that the spreading rates of a jet discharged parallel to a wall are considerably different from the rates observed for free jets [54]. In past research [55-58] it has been observed that the growth rates are larger (5-9 times) parallel to the planar wall compared to rates normal to it. Some [56] attributed the fact that this difference to the enhanced turbulent diffusion parallel to it while others [54, 58] concluded that this anisotropic growth rates are due to a resulting secondary flow causing substantial lateral outflow parallel to the wall with a strong entrainment velocity being induced normal to it. Launder & Rodi [59] attribute these anisotropic growth rates of the shear boundary to vortex-line bending. Craft et al., [54] use several turbulent models and found that the large lateral spreading rates are caused by anisotropic Reynolds stresses. Thus, employing linear eddy/turbulent viscosity RANS models to model the turbulence in the traversing jet situation would not be very accurate in its initial and later parts of the travel across a channel, which can be approximated by parallel wall jets. On the other hand using non-linear eddy/turbulent viscosity models or Reynolds stress model (RSM) which does not assume a linear relation between the Reynolds stresses and the mean strain tensor would be more accurate in this case as these can capture anisotropic turbulence and streamline curvature effects better. However, the addition of another set of equations to solve for Reynolds stresses in RSM, increases computational time and cost. Song and Abraham [60] explored in detail the transient round, radial wall jets. Modeling these types of jet phenomena requires different turbulence modeling strategies and is a great challenge with limited computational resources in modeling transient translating and confined jets which are currently analyzed.

In a configuration like wave rotor constant volume combustor, the injection of the jet into the confined volume produces complex flow features which are not found in standard wall jet and wall impinging jets. Moreover, the injector is moving across the combustion chamber opening; hence, the behavior of jet is also affected by the relative motion between the jet injector and the confined volume (channel/main chamber). To the best of the authors' knowledge, a comprehensive study of flow behavior of hot turbulent jet in such a traversing confined configuration has not been reported in published literature. Hence, the objective of the present chapter is to study the behavior of wall-jet, impinging

jet and their interactions in confined volume. The three-dimensional and two-dimensional traversing jets for various speeds of the injector nozzle relative to main CVC chamber are analyzed and compared with stationary jet. The planar wall jet and wall-impinging jet behaviors are seen for 2D simulations. Jet penetration from three-dimensional simulations is also compared with high speed video images from experiments [8].

4.2 Numerical Methodology

Bilgin [16] developed a constant-volume combustor with long aspect ratio and square cross-section, representing a wave rotor channel. The CVC chamber is ignited by a jet of hot combustion products from a separately fueled pre-chamber that could be spun to cause the jet to traverse one end of the CVC. The relative motion reproduces the action of a wave rotor channel, and pre-chamber may be representative of a previously combusted channel supplying hot gas. Bilgin [16] proposed a correlation between the Damköhler number and ignition of a fuel-air mixture in the CVC. For the same geometry, Baronia et al. [18] performed numerical simulations for the stationary (non-traversing) torch jet case using global reaction mechanisms (one-step and four-step) for propane-air mixture. Bilgin's measurements were not well matched by Baronia's simulations, possibly due to lack of detailed chemistry and not accounting for active chemical species in the jet. Perera [8] carried out experiments on the same CVC test rig for three fuels – methane, ethylene, and propane – under varying equivalence ratios in the pre-chamber and the CVC chamber. The ignition delay time variation for each fuel under constant experimental conditions and the ignitability limits, both lean and rich, for all three fuels in the CVC chamber were investigated. The variation of ignition delay time for fuels with different pre-chamber equivalence ratios and nozzle geometry were also observed. Chinnathambi [61] carried out experiments for different prechamber speeds (150, 750, 1000 and 1500 rpm) resulting in different traversing speeds of the jet.

The main CVC chamber has a square cross-section of side 39.878 mm (1.57 inches) and is 406.4 mm (16.0 inches) long. The pre-chamber internal cavity is of cylindrical design, 165.61 mm (6.52 inches) in diameter and width 39.1 mm (1.54 inches), forming an

internal volume of approximately $8.3574\times10^{-4}m^3$ (51 cubic inches). The exit diameter of the converging nozzle that connects the pre-chamber with the CVC chamber is 5.99 mm (0.236 inches). The small gap between the pre-chamber and CVC chamber is not modeled, as it is assumed that the gas outflow is negligible at low pressure before ignition occurs in the CVC chamber.

The transient simulations are carried out for turbulent, non-reacting, compressible flow using velocity-pressure coupled second order implicit scheme in commercial CFD code STAR-CCM+. Turbulence is modeled using widely employed Reynolds Averaged Navier Stokes SST (Menter) k-ω model and turbulence parameters are specified in terms of turbulence intensity and turbulence length scale. The flow is driven by the initial pressure difference between pre-chamber and main CVC chamber similar to shock tube problem. Table 4.l lists the initial conditions used in the pre-chamber and main chamber. The computational domain is discretized using polyhedral meshes and different mesh densities are used in pre-chamber, nozzle and main chamber (Table 4.2). Grid is refined in the initial region of main chamber near nozzle exit and grid sensitivity analysis is done to make sure that the results are grid independent. Three different grids are used and error between coarse and fine grids is compared.

A two-dimensional (2D) model of the combustor and jet is also used to simulate the transient, turbulent, reacting and compressible flow at reasonable computational cost. For the 2D simulation, the height and length of the CVC chamber and nozzle are the same as those in the test rig. The varying vertical width of the nozzle is taken equal to the corresponding diameter. While this does not preserve the area ratio, it does retain the relative height ratio of the confined jet. However, the volume ratio of the pre-chamber to the test channel is preserved, neglecting the small volume of the nozzle. This allows the same volume flow rate between the experiment and 2D numerical calculations, preserving mass and energy realism and the nominal pressure history. The simulation uses the velocity-pressure coupled, second-order implicit scheme available in the computational code used for this work [62].

Table 4.1 Initial Conditions

Pre-chamber Initial Pressure (Pa)	Main Chamber Initial Pressure (Pa)	Pre-chamber Initial Temperature (K)	Main-chamber Initial Temperature (K)
649000.00	101325	2200	298

Table 4.2 Computational Cells

Mesh density	No of cells in Pre-chamber	No of cells in Nozzle	No of Cells in CVC chamber	Total number of cells
Coarse Mesh	61463	16446	308349	386258
Fine Mesh	61463	16446	484373	562282
Fine Mesh 2	61463	16446	7176309	795548

4.3 Stationary Jet: Penetration and Mixedness

The simulations are carried out for the flow conditions described in Table 4.1. Grid sensitivity analysis is carried out and the fine Mesh 2 is found to show little difference in results as compared with the fine Mesh listed in Table 4.2 and therefore Fine 2 Mesh is used for the rest of the three-dimensional simulations.

The jet penetration is estimated by plotting injected gas mass fraction iso-surface in the main chamber. Injected mass fraction from present simulation, and high speed video images from experiments are presented in Figure 4.1 [8]. In Figure 4.2, jet penetration in the main chamber is compared with present simulation and measured data from high speed video images. Velocity vector profile at mid-plane in the initial region of the main chamber at time t = 0.7 ms for case 1 is presented in Figure 4.3. It indicates that two vortices are formed besides the hot jet. Jet penetration structure is presented in Figure 4.4 at time 0.7 ms. Mass flow history through the nozzle exit and the area averaged Mach number history at the nozzle exit are plotted in Figures 4.5 and 4.6, respectively. It is seen in Figure 4.6

that after 0.4 ms the mass flow rate appears to be constant until 1.0 ms for which simulation has been carried out, which ensures that the steady state condition has been established.

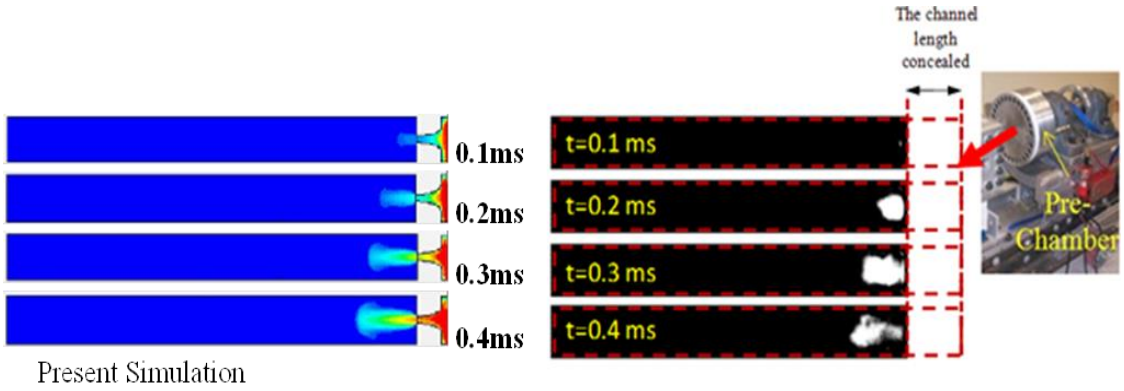

Figure 4.1 Jet Penetration Comparison from Simulations and Experimental Visualization [5]

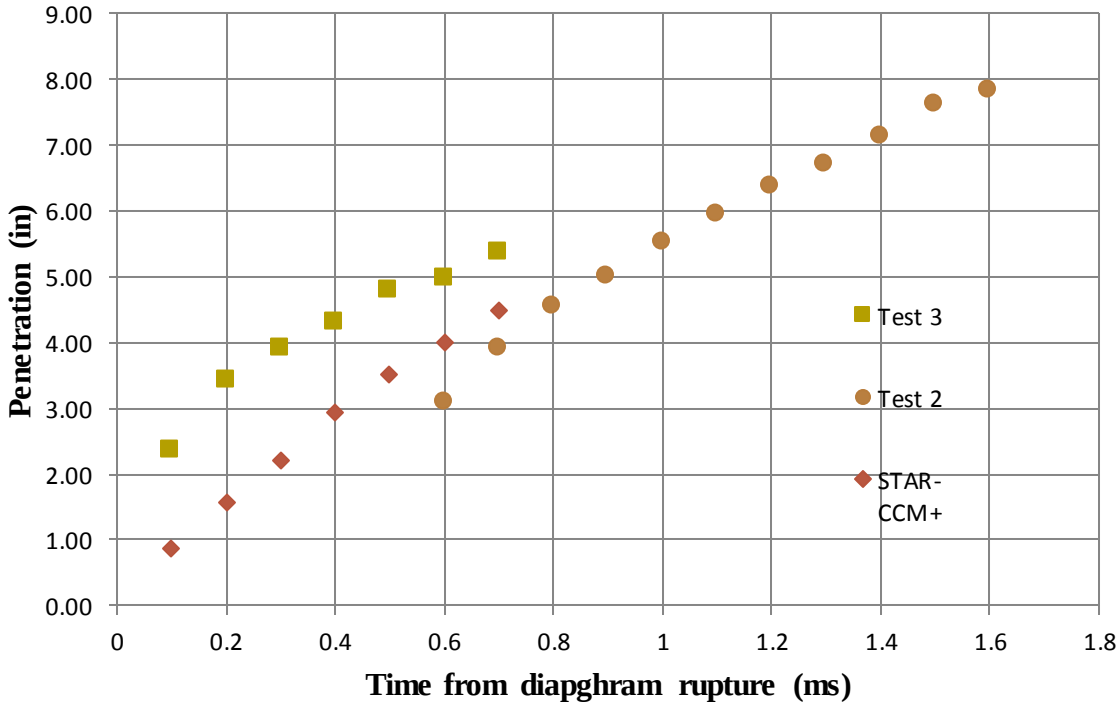

Figure 4.2 Jet Penetration Comparison for Simulations with Measured Data at Different Times

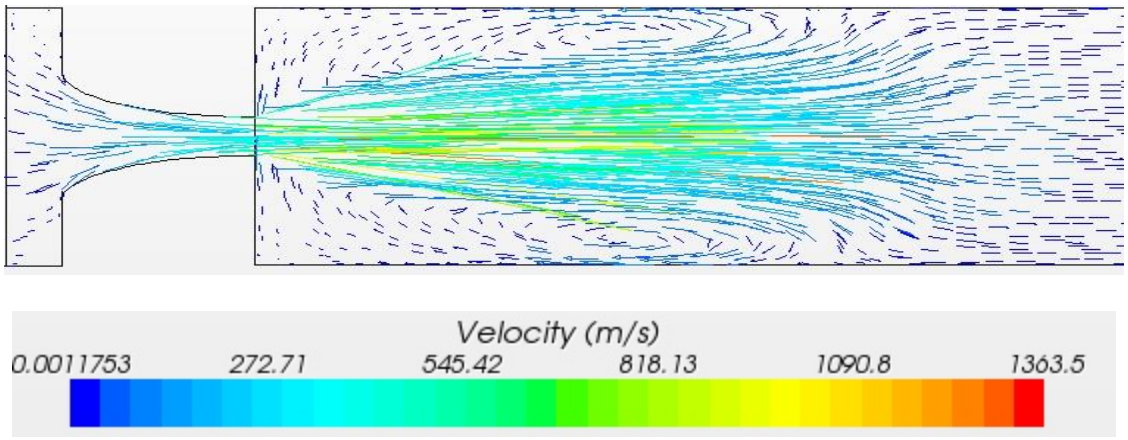

Figure 4.3 Velocity Vector Profile at Mid-section Plane for the Initial Region of Main Chamber at Time t = 0.7 ms

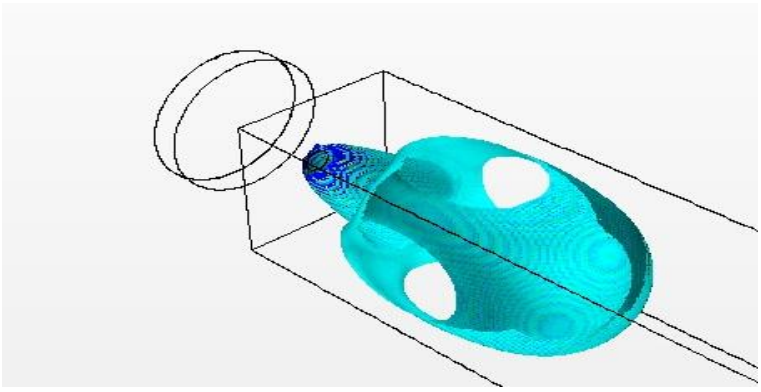

Figure 4.4 Three-dimensional View of the Jet Entering the Channel at time t = 0.7 ms. Contours Shown are the 0.01 Iso-surface of Injected Mass Fraction

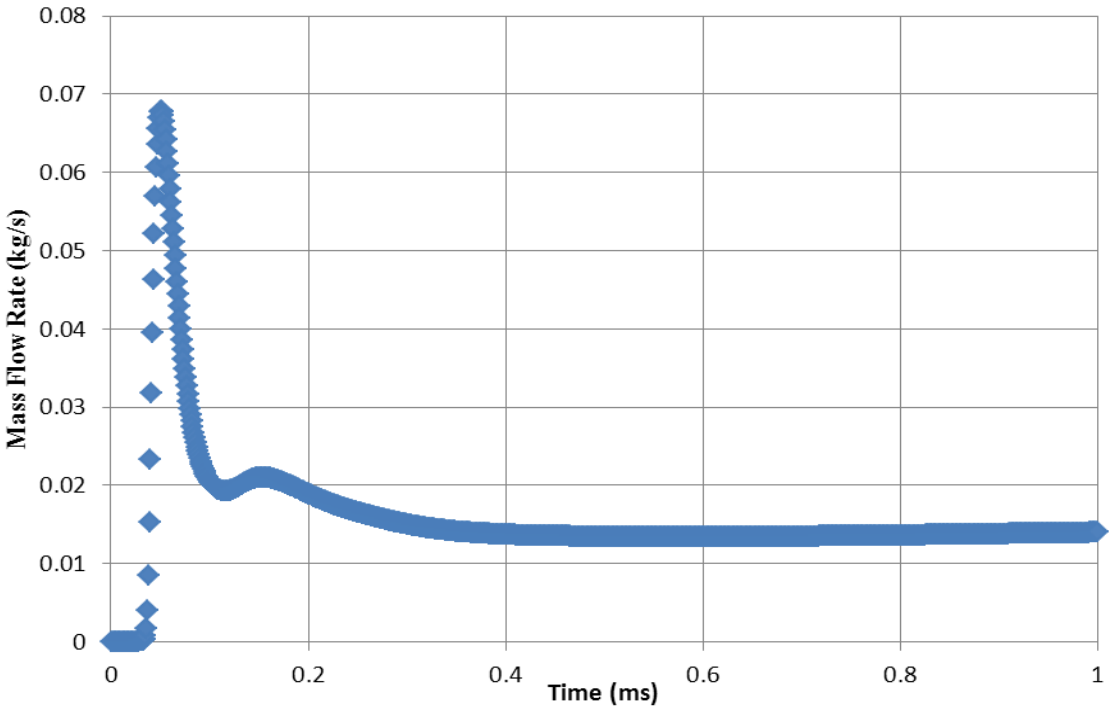

Figure 4.5 Mass Flow Rate History at Nozzle Exit Injected Into the Main Chamber

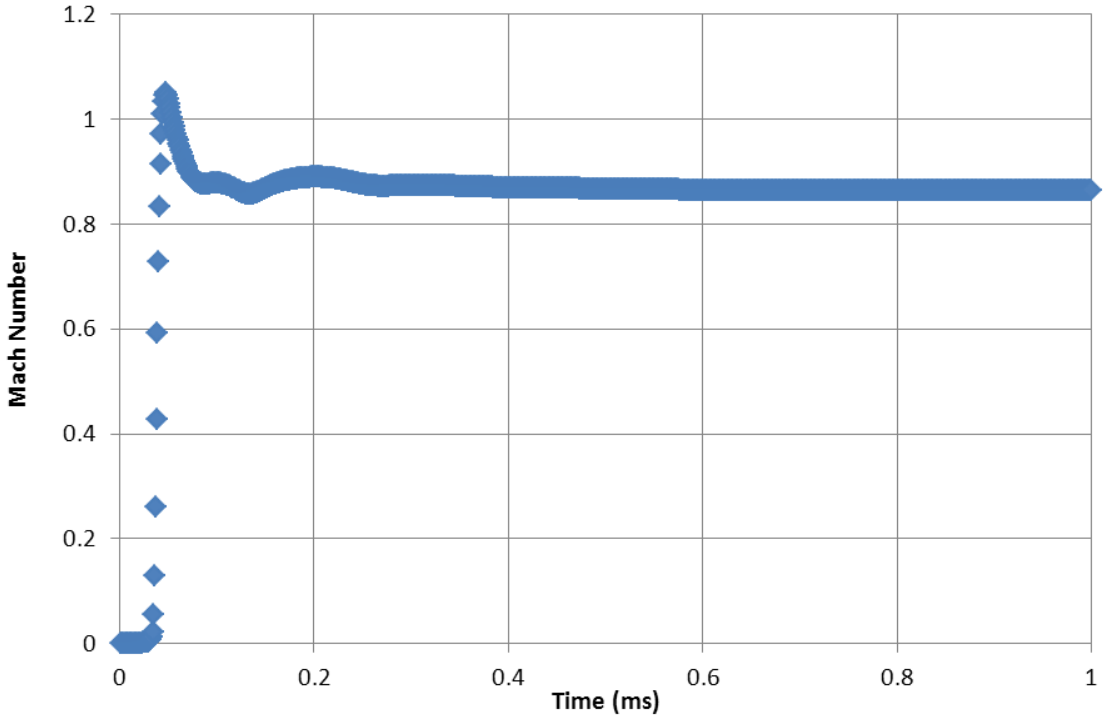

Figure 4.6 Area Averaged Mach Number History at the Nozzle Exit

4.3.1 High Temperature Mixedness (HTM)

The study of mixing hot jet with a cold combustible mixture in the CVC chamber is important in understanding the ignition probability at various time levels. The injection of hot jet into the main CVC chamber changes the local equivalence ratio; hence, a quantity needs to be defined which would provide better insight on ignitability with the passage of time. For this purpose, a quantity called High Temperature Mixedness (HTM) is defined which is the ratio of 'hot gas' mass within a certain mass fraction range and above a 'critical temperature' in the main chamber to the total injected hot jet mass. Mathematically it can be defined as follows:

$$HTM = \frac{\left\langle m_{LL \le Y_{HG} \le UL} \right\rangle \; for T_{cell} > T_{critical}}{m_{HG,Total}} \tag{4.1}$$

A similar approach of this mixedness analysis has been used by several researchers in the past to quantify the mixing process as well as to utilize it in multi-zone combustion modeling [63]. Total injected mass history in the main chamber is plotted in Figure 4.7. Figure 4.8 presents the HTM for different mass fraction ranges at critical temperature of 500 K. It can be seen that there is significant increase in HTM when the lower level of hot jet mass fraction is decreased keeping the upper level at the same value of 0.9. Figure 4.9 shows the HTM varying the upper level of mass fraction for same critical temperature of 500 K indicating small variations implying that most of the hot jet during mixing is present in low mass fraction range in the main chamber. It can also be observed from Figure 4.9 that by the time t = 1.0 ms, approximately 70 % of the hot injected gas in the mass fraction range of 0.1 to 0.8 is above the temperature of 500 K. Moreover, approximately the same percentage of the hot jet with a lower mass fraction range in the main chamber is also above the critical temperature 500 K.

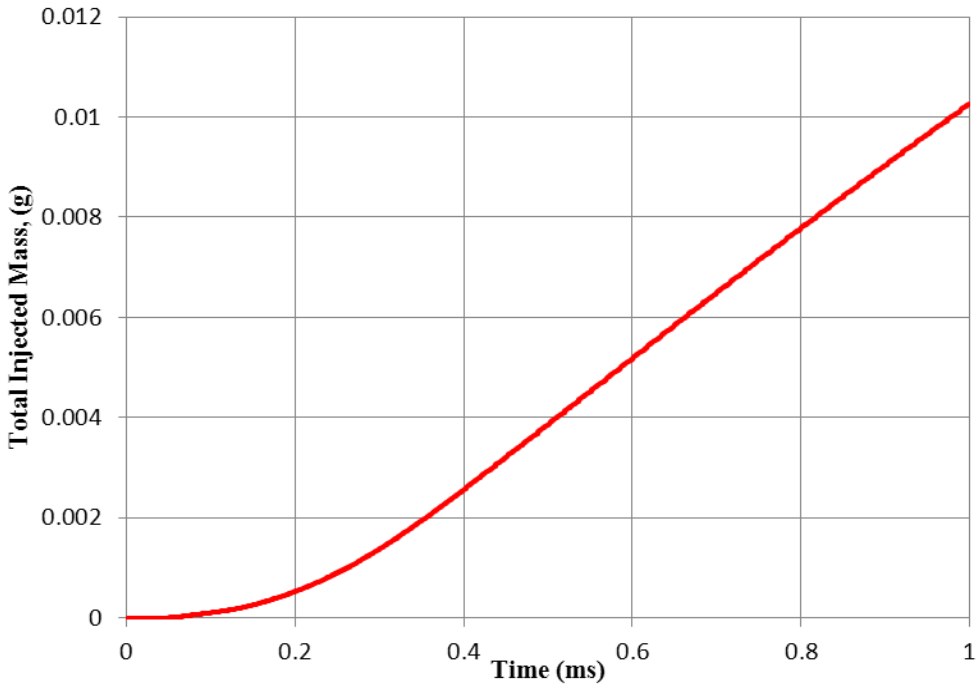

Figure 4.7 High Temperature Mixedness for Different Mass Fraction Ranges of Hot Jet (Tcritical = 500K)

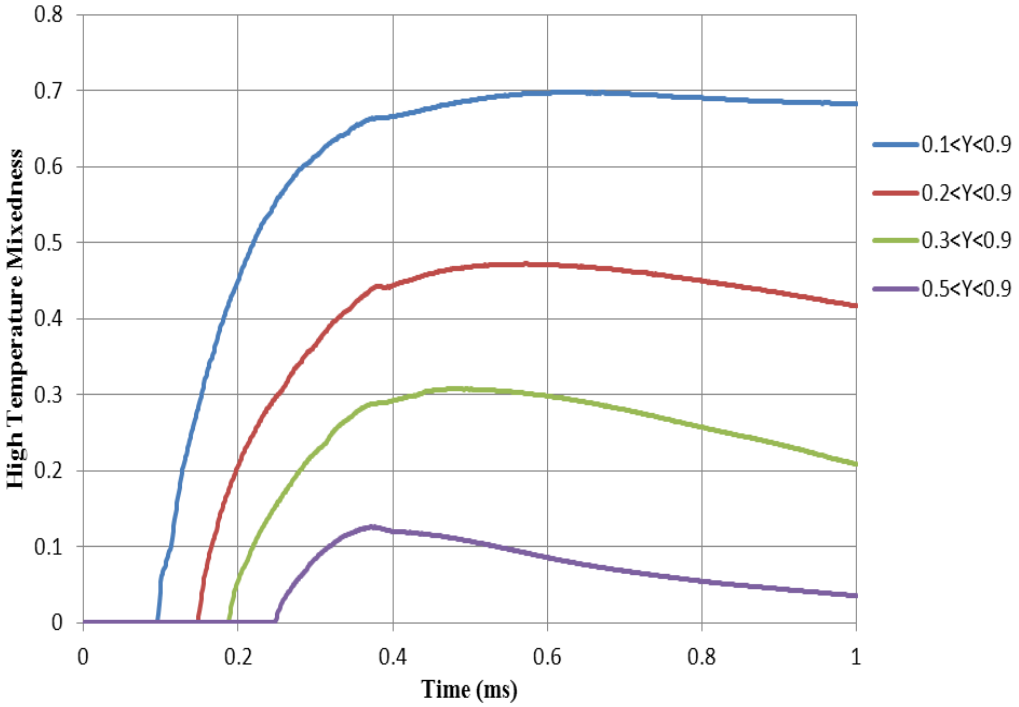

Figure 4.8 High Temperature Mixedness for Different Mass Fraction Ranges of Hot Jet ($T_{critical}$ = 500K)

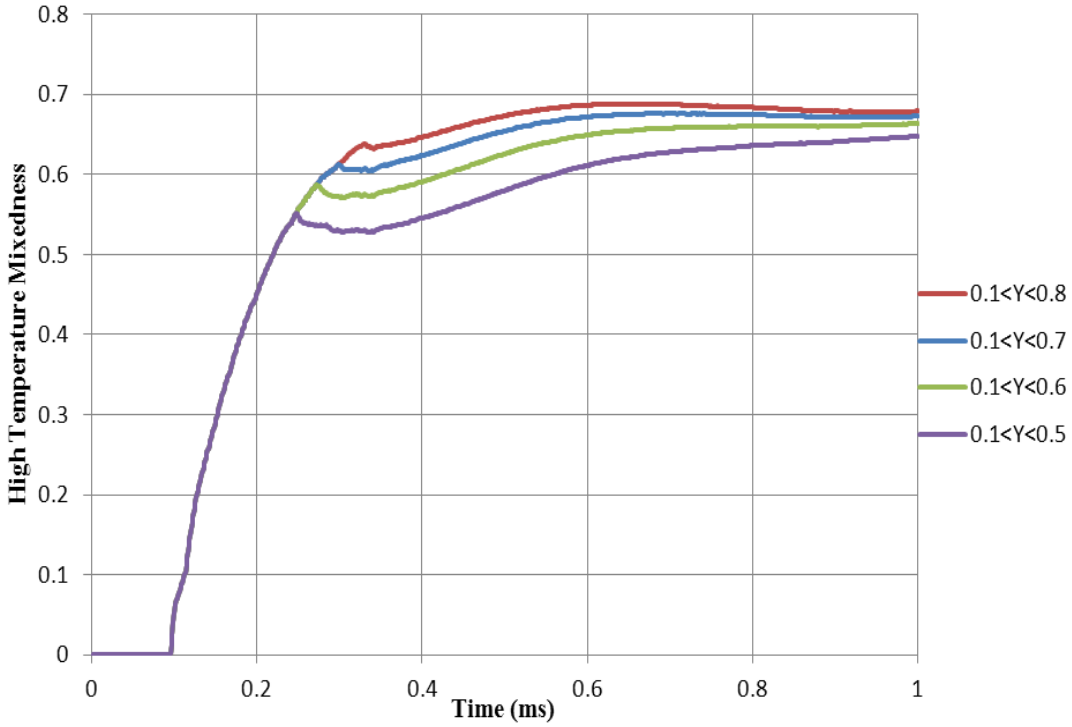

Figure 4.9 High Temperature Mixedness for Different Mass Fraction Ranges of Hot-Jet ($T_{critical}$ = 500K)

The variations of HTM for various hot jet mass fraction lower and upper limits are plotted in Figure 4.10. The HTM is high for low hot jet mass fraction upper limit as seen for $0.1 < Y < 0.4$ and $0.0 < Y < 0.3$. The ignition of cold combustible mixture in the main chamber is dependent on the mixing and subsequent rise of temperature in the main chamber. To estimate the hot jet mass in the main chamber at higher temperatures, the HTM plots for the critical temperature of 700 K is shown in Figure 4.11, which illustrates that at time t = 1ms less than 50 percent of the injected gas of the mass fraction range 0.1-0.9 is above the temperature of 700 K. Moreover, the HTM for mass fraction range 0.5-0.9 is very low for the critical temperature of 700 K. HTM for three different critical temperatures of 500 K, 700 K, and 1000 K is shown in Figure 4.12 for different mass fraction ranges.

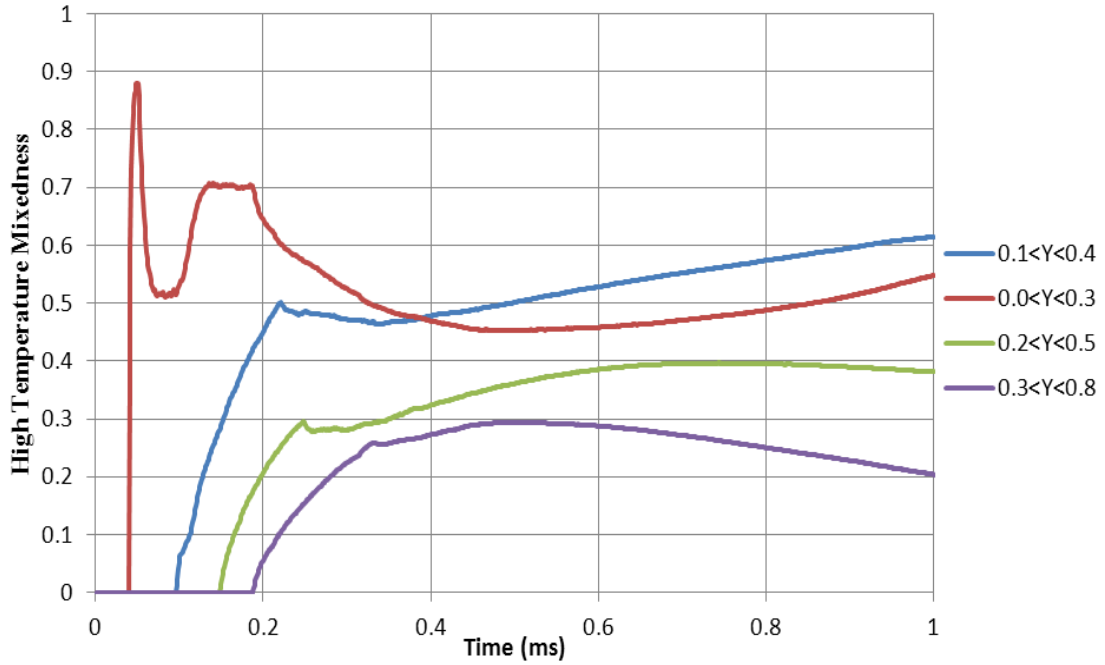

Figure 4.10 High Temperature Mixedness for Different Mass Fraction Ranges of Hot Jet ($T_{critical}$ = 500K)

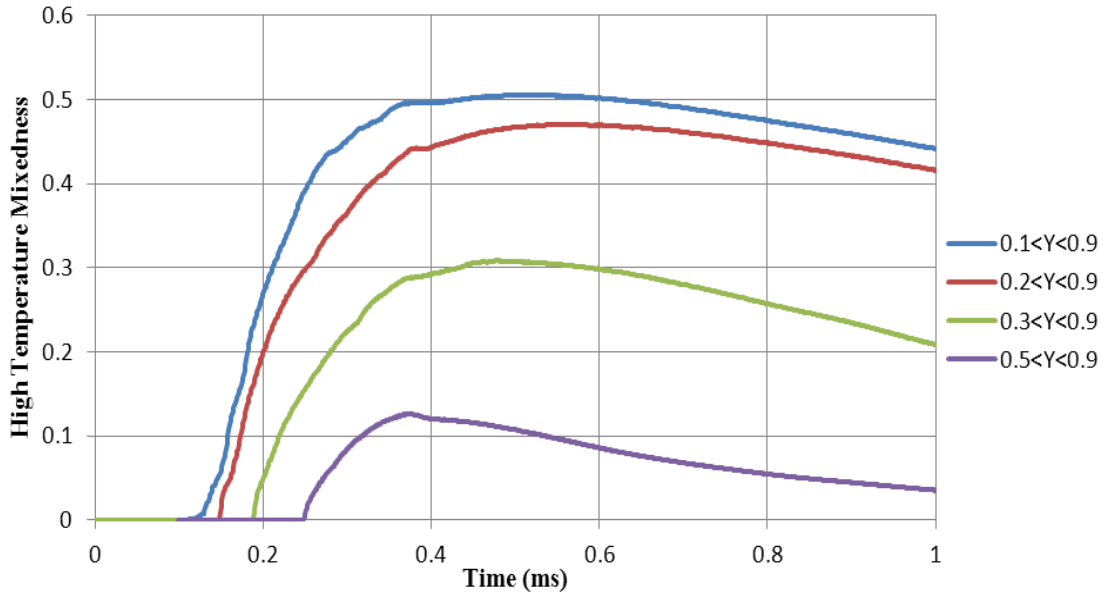

Figure 4.11 High Temperature Mixedness for Different Mass Fraction Ranges of Hot Jet ($T_{critical}$ = 700K)

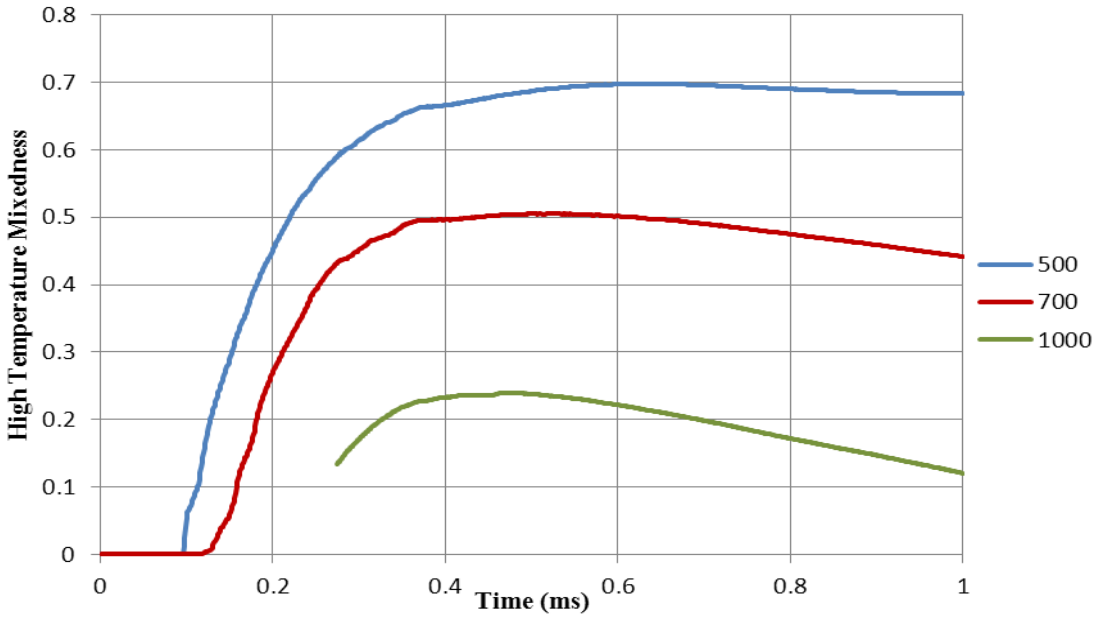

Figure 4.12 High temperature Mixedness for Different Three Different Critical Temperatures ($T_{critical}$ = 500, 700, 1000 K) at 0.1 < Y < 0.9

The HTM for three different critical temperatures and the hot jet mass fraction range of 0.5 < Y < 0.9 is plotted in Figure 4.13.For mass fraction range of 0.5 < Y < 0.9, all the hot jet are at temperature greater than 1000K. For example, the hot jet in the mass fraction range of 0.5 < Y < 0.9 is above temperature 1000 K; hence, HTM using 500 K and 700 K as critical temperatures gives the same value. This is further verified from Figure 4.14 where it is seen that the HTM is nearly equal for critical temperatures 500 K and 700 K but it is lower for critical temperature 1000 K. This can be attributed to the lower value of hot jet mass fraction lower limit than that in Figure 4.13.

The hot jet penetration contours (using mass fraction of injected gas) above critical temperatures of 500K and 700K are shown in Figure 4.15 and 4.16 while Figure 4.17 presents the hot jet mass fraction contour in the range of $\langle m_{0.2 \leq Y_{HG} \leq 0.8} \rangle$ and above critical temperature of 700 K. It can be seen that the core of the jet is at higher temperature as well as high injected gas mass fraction. It can be inferred that the ignition would be expected to initiate in the core jet region surrounded by fuel mixture in the main chamber.

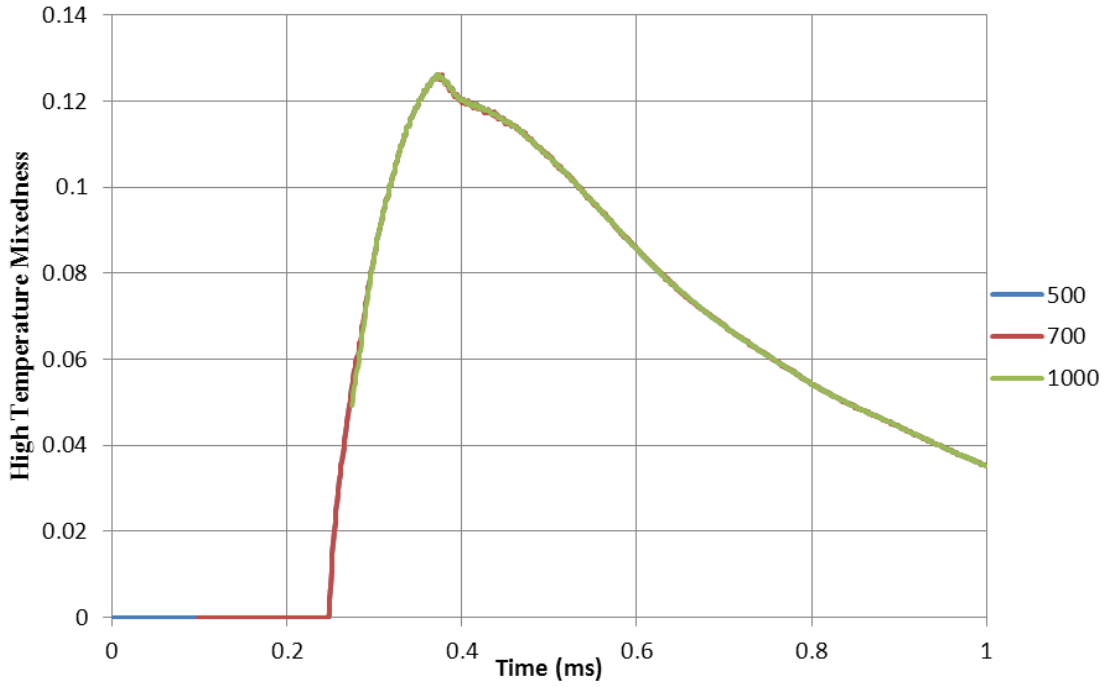

Figure 4.13 High Temperature Mixedness for Different Three Different Critical Temperatures and $0.5 < Y < 0.9$ ($T_{critical}$ = 500, 700, 1000 K)

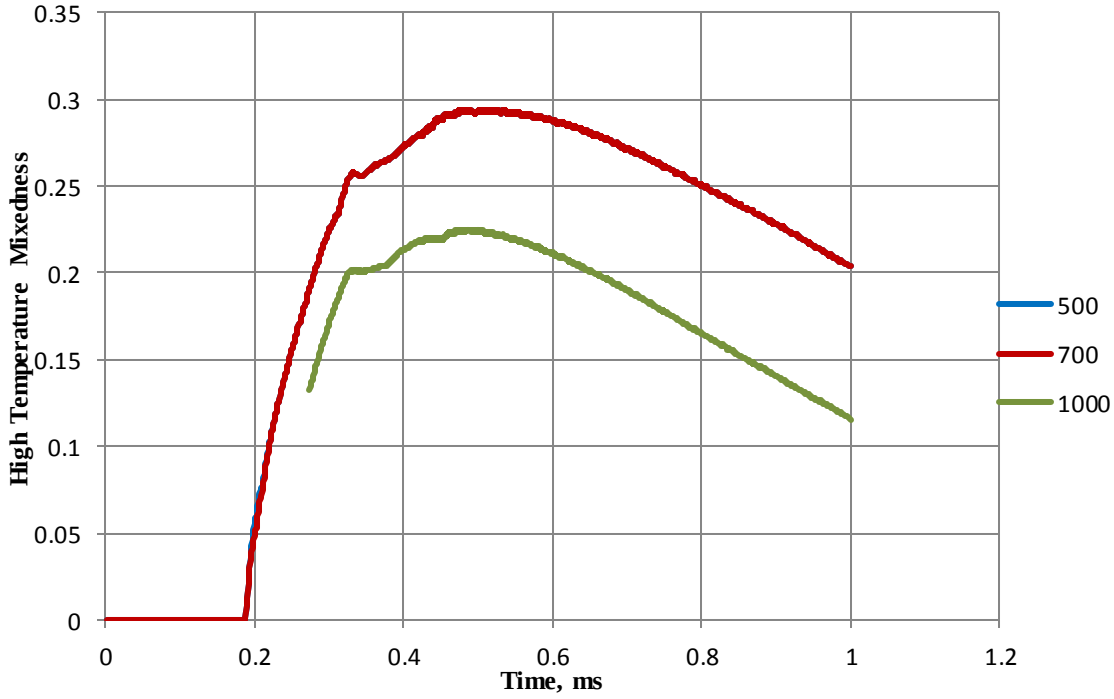

Figure 4.14 High Temperature Mixedness for Different Three Different Critical Temperatures and $0.3 < Y < 0.8$ ($T_{critical}$ = 500, 700, 1000 K)

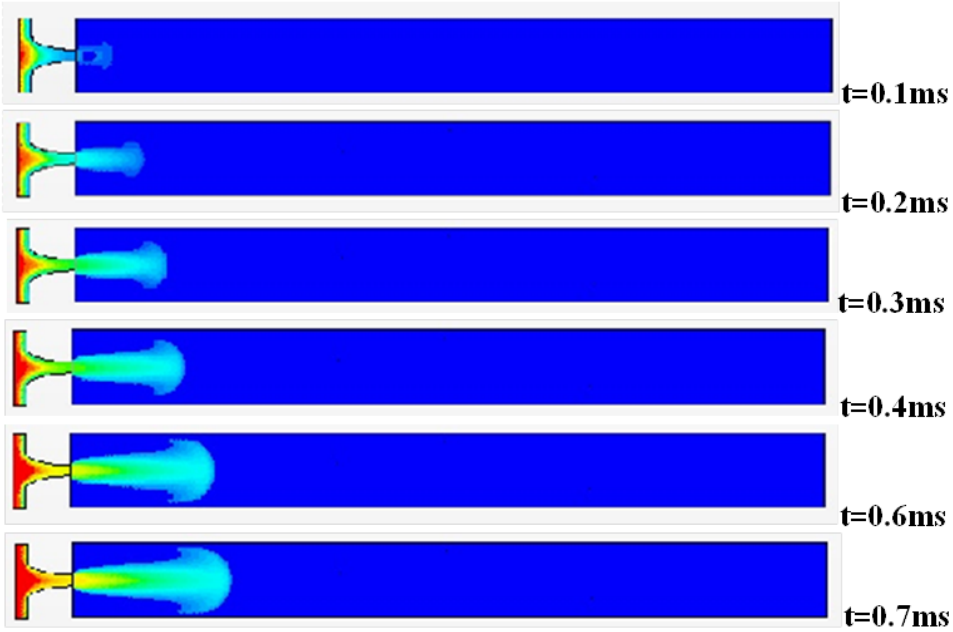

Figure 4.15 Injected Gas Mass Fraction in the Main Chamber above Critical Temperature of 500K

Figure 4.16 Injected Gas Mass Fraction in the Main Chamber above Critical Temperature of 700 K

Figure 4.17 Injected Gas for $\langle m_{0.2 \leq Y_{HG} \leq 0.8} \rangle$ above Critical Temperature of 700 K in the Main Chamber

4.4 Traversing Jet: Penetration and Flow Behavior

Figure 4.18 presents the jet penetration for the prechamber speed of 150 RPM from three-dimensional simulations as well as the high speed video images from representative test cases. The initial conditions for the simulation are same as listed in Table 4.1.

The two-dimensional simulation for studying behavior for traversing jet has also been carried out. Mass fraction of the injected gas at different time instants is shown in Figure 4.19 for jet traverse speed of 0.98 m/s which corresponds to 150RPM prechamber spin. The jet after entering the CVC chamber remains attached to the wall and then impinges on the lower wall. The formation of counter-rotating vortices can be seen after 0.35 ms.

The jet core appears to impinge second time at around 0.6 ms. A more detailed analysis of the effect of jet traverse and fluid dynamics on the ignition and combustion process is presented in Chapter 5 and 6 of this thesis.

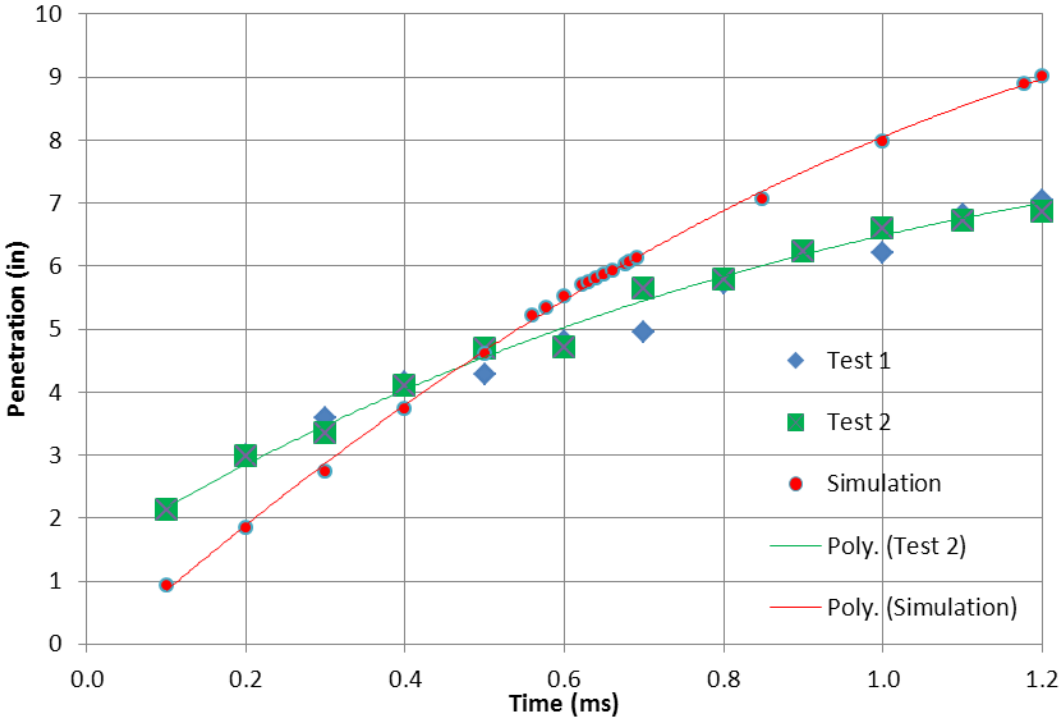

Figure 4.18 Jet Penetration Comparison of Three-dimensional Simulations with High Speed Video Images of the Experiments [64] for the Prechamber Speed of 150RPM

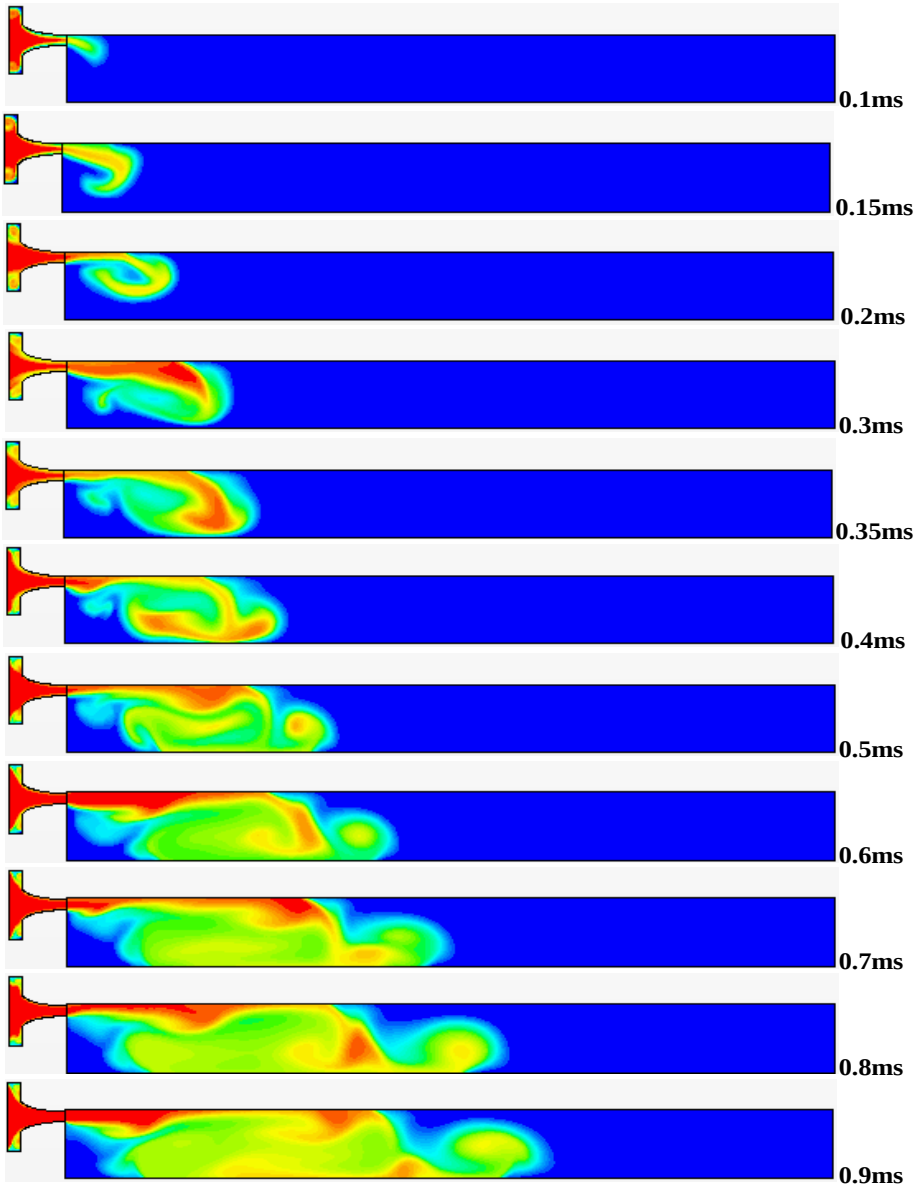

Figure 4.19 Injected Gas Mass Fraction at Different Times of Transient Two-dimensional Simulation for Jet Traverse Speed of 0.98 m/s (150RMP)

5. COMBUSTION MODELING OF DIFFERENT FUEL-AIR MIXTURES

5.1 Introduction

The ignition of combustible mixture using hot inert jet or combusted products has been rarely studied numerically using global reaction mechanisms, and no studies are known that use detailed or skeletal reaction mechanisms. The Present thesis work seeks to use detailed numerical simulations to investigate the ignition by a hot jet and ensuing combustion of different hydrocarbon fuels (methane, propane, ethylene) and hydrogen-hydrocarbon mixtures with varying percentage of hydrogen. Chemical kinetics is modeled using several detailed reaction mechanisms after verifying the inadequacy of a four-step global reaction mechanism for propane. The hot jet is modeled as the equilibrium products of rich ethylene combustion in the pre-chamber. The role of shock-flame interaction on ignition in the CVC chamber is also investigated. The reaction pathways are discussed for the detailed methane mechanism. The predicted ignition delay times have been compared with the published experimental data [5].

5.2 Model Description

The constant-volume combustor (Fig. 5.1) is an evolution of the rig initially used by Bilgin [16] and later for ignition delay studies by Perera et al. [5]. The main CVC chamber has a square cross-section of side 39.88 mm (1.57 inches) and is 406.4 mm (16.0 inches) long. The pre-chamber internal cavity is of cylindrical design, 165.6 mm (6.52 inches) in diameter and width 39.1 mm (1.54 inches), forming an internal volume of approximately 8.36×10^{-4} m^3 (51 cubic inches). The exit diameter of the converging nozzle that connects the pre-chamber with the CVC chamber is 5.99 mm (0.236 inches). The small gap between the pre-chamber and CVC chamber is not modeled, as it is assumed that the gas outflow is negligible at low pressure before ignition occurs in the CVC chamber.

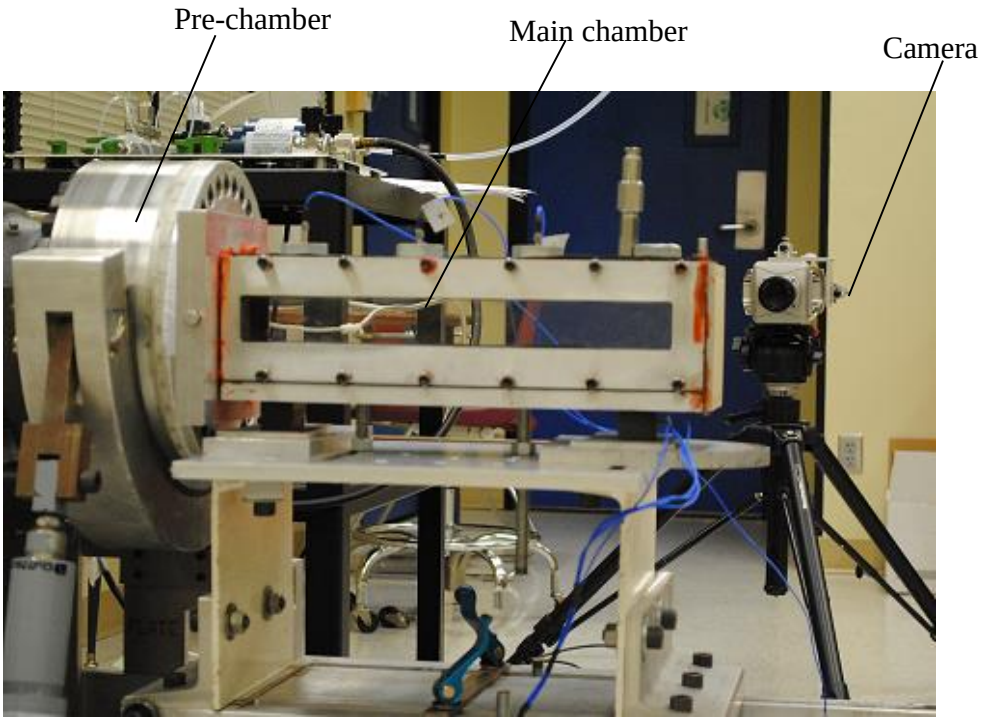

Figure 5.1 Constant-volume Combustor Rig

A two-dimensional (2D) numerical model of the combustor and jet are used to simulate the transient, turbulent, reacting and compressible flow at reasonable computational cost. The simulation uses the velocity-pressure coupled, second-order implicit scheme available in a general-purpose computational fluid dynamics (CFD) program [62]. The computational domain is discretized using polyhedral meshes with varying mesh density in the pre-chamber, nozzle, and CVC chamber (Figure 5.2). For 2D calculations, the height and length of the channel and nozzle are the same as those in the test rig. The varying vertical width of the nozzle is taken equal to the corresponding diameter. While this does not preserve the area ratio, it does retain the relative height ratio of the confined jet. Moreover, the volume ratio of the pre-chamber to the test channel is preserved, neglecting the small volume of the nozzle. This allows the same volume flow rate between the experiment and numerical calculations, preserving mass and energy realism and the nominal pressure history. Turbulence is modeled using the shear-stress-transport (SST) two-equation k-ω model [34]. The flow is driven by the initial pressure difference between pre-chamber and CVC chamber when an intervening diaphragm is

suddenly splayed away, similar to a shock tube. The initial pressure in the pre-chamber is specified as the pressure at diaphragm rupture measured from experiments [5]. The initial temperature and composition of the pre-chamber is obtained by chemical-equilibrium calculation for combustion of ethylene-air mixture at an equivalence ratio of 1.1 using the program developed by Depcik [65], which correlates well with NASA's equilibrium program [66]. The initial conditions for the pre-chamber and CVC chamber are listed in Table 1 and are the same for all the simulations in the present work. No slip and adiabatic boundary conditions are used for all walls.

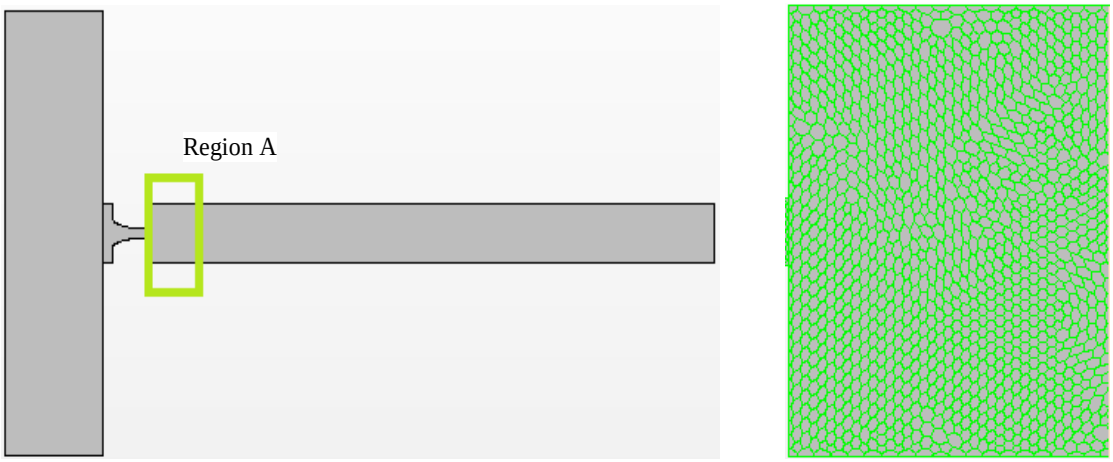

(a) Geometry used for the analysis (b) Enlarged view of Region A polyhedral mesh,

Figure 5.2 Geometry used for Simulation

Combustion is modeled using a hybrid eddy-break-up model that considers the roles of both turbulent mixing and finite-rate chemistry. The eddy-break-up (EBU) model was presented by Spalding [41] and later developed by Magnussen and Hjertager [42]. The underlying principle behind the 'mixed-is-burnt' EBU model is that the chemistry is fast compared to mixing and the combustion is controlled by turbulent mixing. In the simple EBU model, reaction rates are calculated as functions of the mean species concentrations, turbulent mixing timescale, and, depending on the specific model used, temperature. In the present hybrid EBU model, each individual chemical reaction rate is limited by a maximum rate based on the local turbulent vorticity timescale. Species are transported according to individual advection-diffusion transport equations for species, with diffusive fluxes

accounting for both molecular and turbulent diffusion. It is intended to identify the rate-limiting process as either turbulent mixing or chemical kinetics.

In the hybrid EBU model, the reaction rate of each species is computed as the minimum of a turbulent-mixing-controlled reaction rate and chemical kinetic reaction rate. For illustration, a global fuel-oxidation reaction is considered, of the form:

$$v_F F + v_O O \rightarrow v_{P1} P_1 + v_{P2} P_2 + ... + v_{Pj} P_j \tag{5.1}$$

The molar rate of fuel depletion $R_{F,mix}$ based on the turbulent micromixing process depends on the mass fractions of reactant and product species, and the turbulent mixing rate, which is taken to be the turbulent specific dissipation, ω:

$$R_{F,mix} = \frac{\rho}{M_F} \omega A_{EBU} \min\left[\overline{Y_F}, \frac{\overline{Y_O}}{s_O}, B_{EBU} \left(\frac{\overline{Y_{P1}}}{s_{P1}} + \frac{\overline{Y_{P2}}}{s_{P2}} + ... + \frac{\overline{Y_{Pj}}}{s_{Pj}} \right) \right] \text{moles/m}^3\text{-s} \tag{5.2}$$

Eq. (5.2) provides that the overall reaction requires both reactants and products to be present in proportion to their stoichiometric coefficients, but with different weighting. In this work, the values of A_{EBU} and B_{EBU} are kept at the nominal values of 4.0 and 0.5 respectively for all the reactions [42].

In the above equation:

$$s_O = {v_O M_O}/{v_F M_F}, \qquad s_{Pi} = {|v_{Pi}| M_O}/{v_F M_F} \tag{5.3}$$

When a detailed mechanism or any multi-step reaction mechanism is used, the EBU model is applied to each of the multiple reactions. For each reaction rate, a turbulence-limited reaction rate $R_{j,mix}$ is calculated based on its own reactants and products.

The molar reaction rate for reaction j predicted from finite-rate chemistry is obtained using modified Arrhenius form, using the detailed chemical mechanism selected for a particular fuel:

$$R_{i,kin} = -A_j T^{\beta_j} \prod_{\text{all reactants}} \left(\frac{\rho Y_i}{M_i} \right)^{p_{ij}} e^{-E_{aj}/RT} \tag{5.4}$$

In the species transport equations, the reaction source term for each species is:

$$S_i = M_i \sum_{j=1}^{n_R} v_{ij} R_j \tag{5.5}$$

where the actual reaction rate is the minimum of the reaction rates from the Arrehnius kinetic rate of Eq. 5.4 and the turbulence-mixing rate of Eq. 5.2. This can be expressed as:

$$R_j = -\min\left(\left| R_{j,kin} \right|, \left| R_{j,mix} \right| \right) \tag{5.6}$$

One-step global reaction mechanisms validated for a particular flame propagation phenomenon, such as a laminar flame, are generally not applicable to ignition phenomena. The hot jet ignition process in the CVC is a complex transient reaction-mixing-diffusion problem that requires detailed modeling of chemistry. Nevertheless, some multi-step reaction mechanisms, skeletal mechanisms, and reduced mechanisms may be adequate for estimating ignition delay, and justifiable relative to the computational cost of a detailed

mechanism. Reduced mechanisms include algebraic equations for minor species concentrations assumed to be in steady-state, which must then be added to the main time-integration computation

5.3 Grid Independence

A grid-sensitivity study is presented considering methane-air mixture in the CVC chamber and using a 21-species reaction mechanism, DRM19 within the hybrid approach described above. Two different grid sizes were used for the CVC chamber with minimum cell sizes of 1.0 mm (20,834 total cells), and 0.5 mm (63,728 total cells). The solutions for the two finer grids were found to differ slightly, as presented in Figures 5.3-5.4 for the cumulative formation of carbon dioxide and the rate of fuel consumption. In Figure 5.5, it is seen further how the details of the jet and flame propagation with the two grids also have jet-structure visible differences, but similar history of jet penetration and flame position. The critical feature of ignition delay time as characterized by the rapid acceleration of fuel consumption rate beginning at about 1.2 ms from the start is not significantly different between the two grids. Therefore, it is deemed that the variations are acceptable relative to the variability observed in experiments. Therefore, the grid with minimum cell size of 1.0 mm in the CVC chamber is used for the detailed simulations. It should be noted that the present study is not intended to resolve the flame thickness or for estimating flame speed after ignition. The mesh used here is intended to predict the ignition delay time influenced by mixing in relatively large-scale jet vortex structures, but may not be adequate for predicting subsequent flame propagation controlled by relatively smaller turbulence scales.

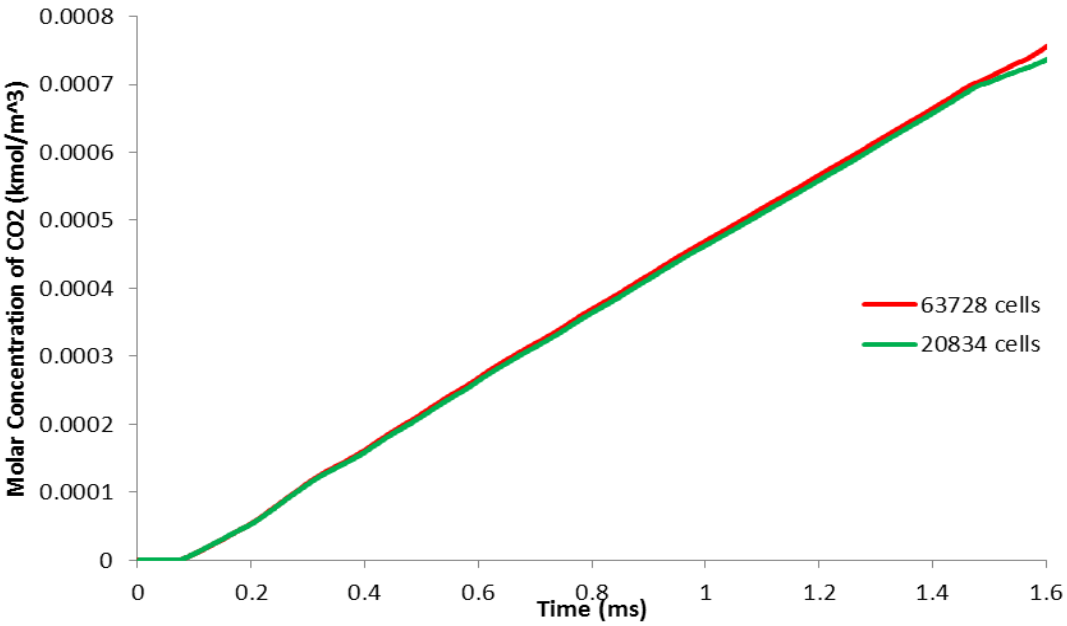

Figure 5.3 Molar Concentration History of CO_2 Integrated over the CVC Chamber for the two Grids for Methane Mixture using DRM19 Reaction Mechanism

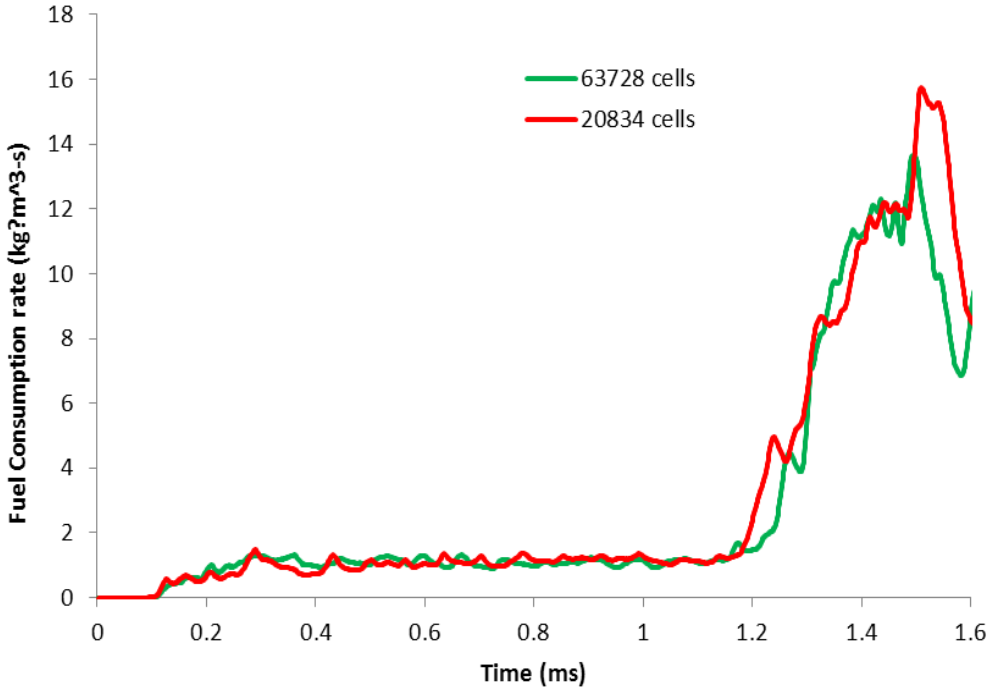

Figure 5.4 Fuel Consumption Rate Integrated over the CVC Chamber for the two Grids for Methane Mixture using DRM19 Reaction Mechanism

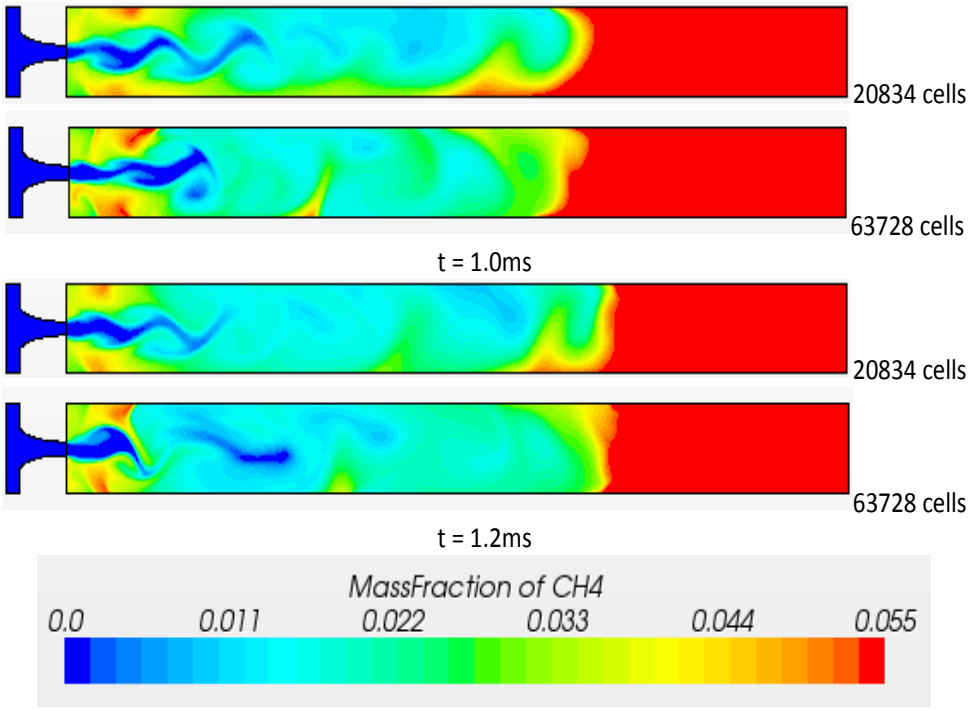

Figure 5.5 Methane Mass Fraction Levels for two Different Grids for Methane Mixture in the CVC Chamber using DRM19 Reaction Mechanism

5.4 Ignition Delay Predictions

The prediction of ignition behavior using appropriate chemical kinetic mechanisms is a limited goal of this work. It is intended to elucidate the major determinants of ignition and combustion acceleration, as a first step towards a definition and measurement of ignition delay time for a transient jet.

5.4.1 Reaction Mechanisms

Single-step mechanisms, few-step global reaction mechanisms, and quasi-global mechanisms that oversimplify key initiation steps are generally not validated for ignition delay prediction, and their application for hot jet ignition study will be of limited usefulness. With this caution in mind, a 4-step global reaction mechanism for propane that is reported to be validated for ignition delay in flow reactors and shock tubes [67] was evaluated early in the present study. Using the modeling approach for the CVC hot-jet ignition system described above, the reactive flow in the combustion chamber was simulated using the

four-step reaction mechanism and a detailed propane combustion mechanism [68]. The history of total reaction rate of fuel in the CVC chamber predicted by the two mechanisms (Figure 5.6) differs significantly qualitatively and quantitatively. Single-step and few-step global mechanisms have implied representations of flame species diffusion and intermediate species chemistry that generally do not apply to jet ignition. Moreover, auto-ignition effects during shock-flame interaction require detailed representation of initiation reactions. Henceforth, detailed or skeletal reaction kinetic mechanisms are used for the further detailed investigation presented here.

5.4.2 Ignition Chemistry for Methane

The detailed reaction mechanism used in the present work for methane is GRI Mech 3.0 [69]. Incorporating the well-studied and unusual reaction pathways and autoignition timescale of methane, it involves 53 species among 325 elementary reactions. For lower computational expense, a skeletal mechanism of 21 species, DRM19 [70], derived from GRI-Mech 3.0 is also used. A review of DRM19 is given by Amir et al. [71]. The average fuel consumption rate in the CVC chamber predicted by GRI-Mech 3.0 and DRM19 is presented in Figure 5.7(a). It is noted that for methane, the reaction rates are relatively small until the shock-flame interaction at about t = 1.2 ms. These two mechanisms are in good agreement on the peak value of fuel consumption rate, but show important differences. Figure 5.7(b) presents the total concentration of CH_3, which is an important intermediate species, in the CVC chamber. It is observed that DRM19 over-predicts the CH_3 molar concentration beyond time t = 1.3 ms. The timing of peak CH_3 corresponds closely with peak fuel consumption with either mechanism. Considering the computation cost savings and typical variations observed in experiments [8], predictions using DRM19 are deemed adequate and are the basis on discussion henceforth.

A comparison of ignition behavior, for methane mixture in the CVC chamber, with the high-speed video images of the experiments [8] is presented in Figure 5.8. Although the comparison is qualitative, there is a good match between the regions of high flame (soot)

luminosity and predicted flame temperatures over about 2000 K. The early stages of the jet and its penetration into the colder gas in the CVC chamber are also approximately matched.

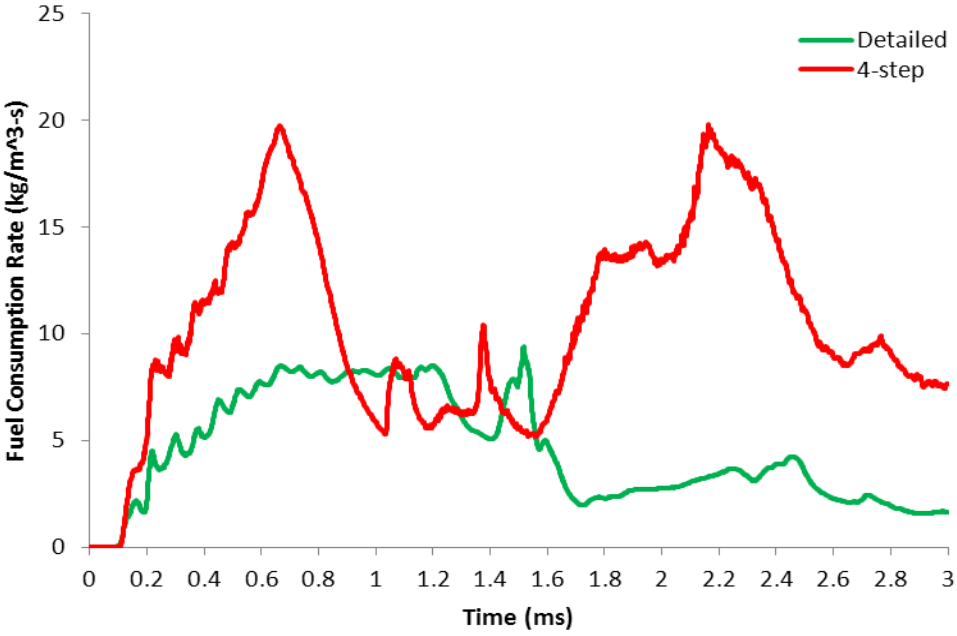

Figure 5.6 CVC Chamber-Integrated Fuel Consumption Rate for Propane-air Mixture, Predicted using 4-step Global Reaction Mechanism and Detailed Reaction Mechanism

The fuel mass fraction over time is presented in Figure 5.9(a), indicating that despite jet penetration and mixing, significant reaction of methane did not occur until the first reflected shock or compression wave arrives at t = 1.2 ms. This is supported by the plot of overall fuel consumption rate in Figure 5.10(a). This observation must be interpreted carefully, considering the spatial distribution of methane over time, and the expected kinetics of methane oxidation at the mixture that is initially at room temperature. First, the rapid disappearance of methane after the shock arrival is observed to occur over a distributed region of mixed gas that includes chamber and jet gases. Thus the increase in reaction rate is primarily associated with the bulk temperature and concentration changes of the partially mixed gas region, apparently due to bulk stirring driven by density gradients in the region. The shock interaction with the density gradient at the boundary of this region is probably secondary. The shock does enhance mixing both within the region and at the

boundary of the region, but the boundary has not yet become a 'flame'. Second, there is some compression by the shock throughout the jet mixing region, which may elevate temperatures to a level where methane reactions are significantly accelerated.

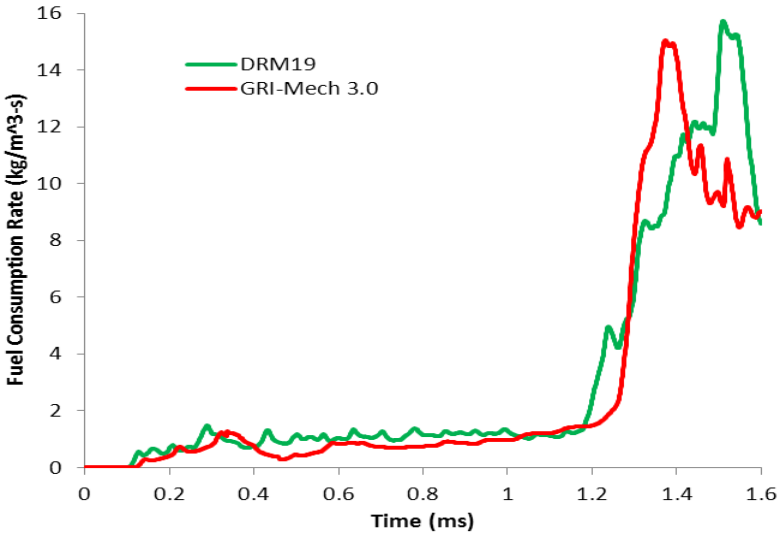

(a) Fuel consumption rate

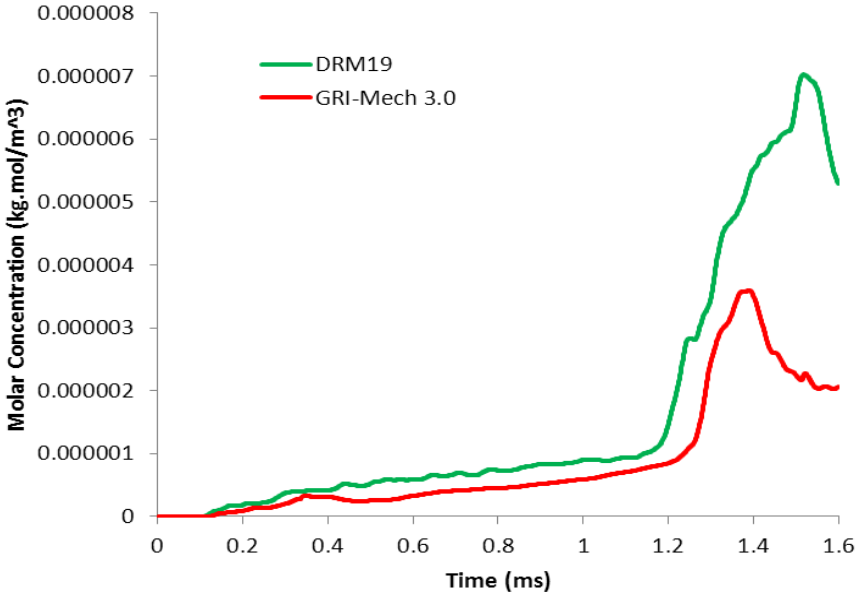

(b) Molar concentration of CH_3

Figure 5.7 CVC-Chamber-Integrated Reaction Rate for Methane-air Mixture, Predicted using GRI Mech 3.0 and DRM19

5.4.3 Kinetics for Ethylene and Propane

The skeletal reaction mechanism used for ethylene involves 32 species in 206 reversible elementary reactions [72] and is derived from the USC Mech-II detailed mechanism [73]. For propane the detailed reaction mechanism from the University of California, San Diego is used, which involves 40 species [68]. The reaction rates for different fuels are compared and discussed further in later sections.

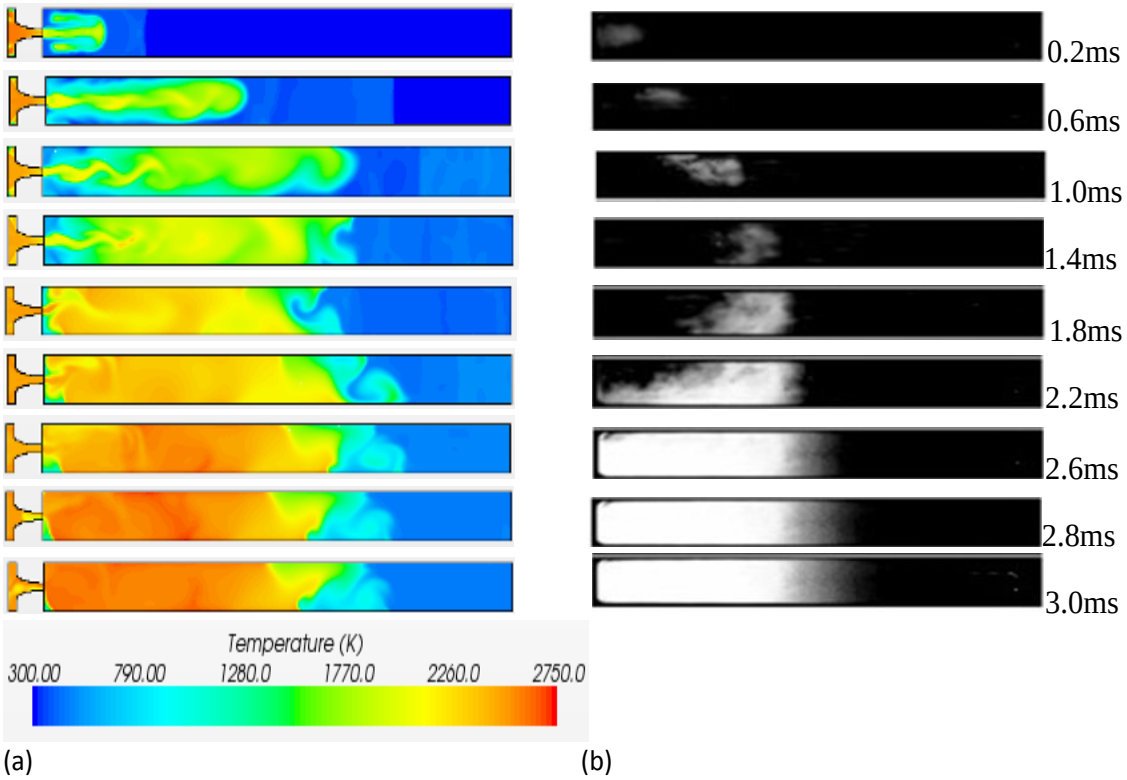

Figure 5.8 Comparison of the Combustion Progress for Stoichiometric Methane Mixture in the CVC Chamber (A) Temperature Levels from Simulations (B) Flame Luminosity in High-Speed Video Images from a Corresponding Test [8]

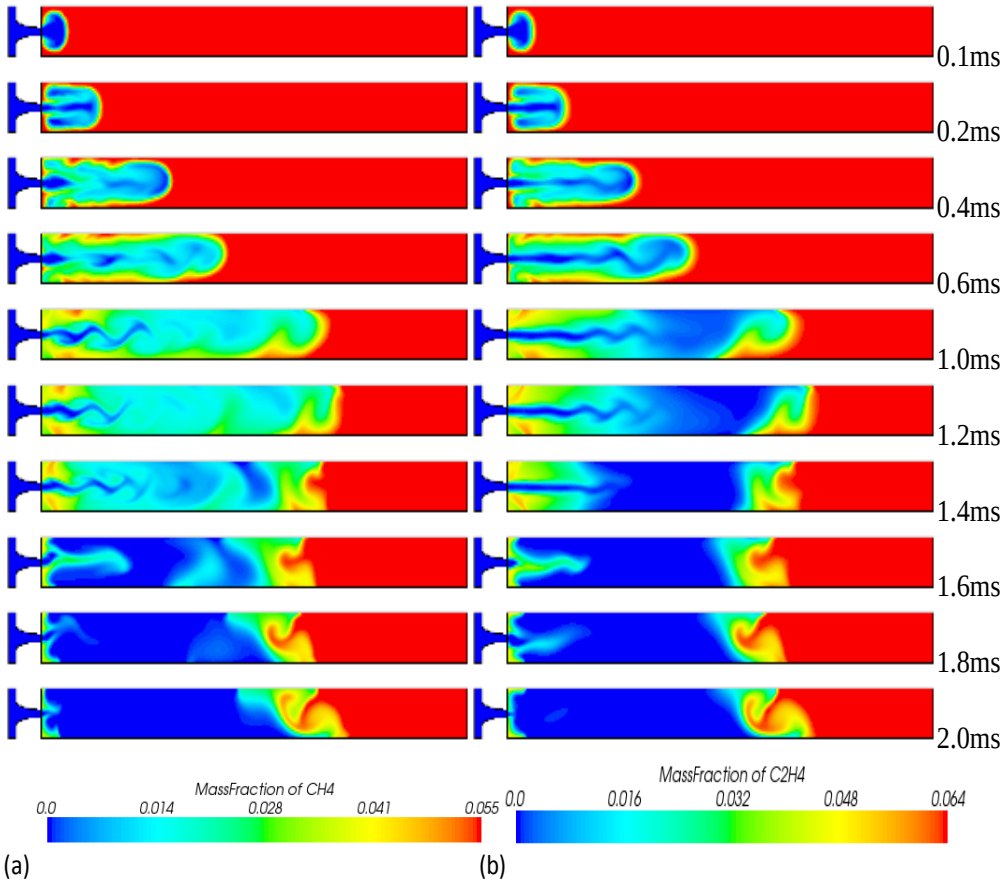

Figure 5.9 Fuel Mass Fraction (a) Methane-Air Combustion Predicted using DRM19 (21 species) Reaction Mechanism (b) Ethylene-Air Combustion Predicted using Detailed Reaction Mechanism (32 species)

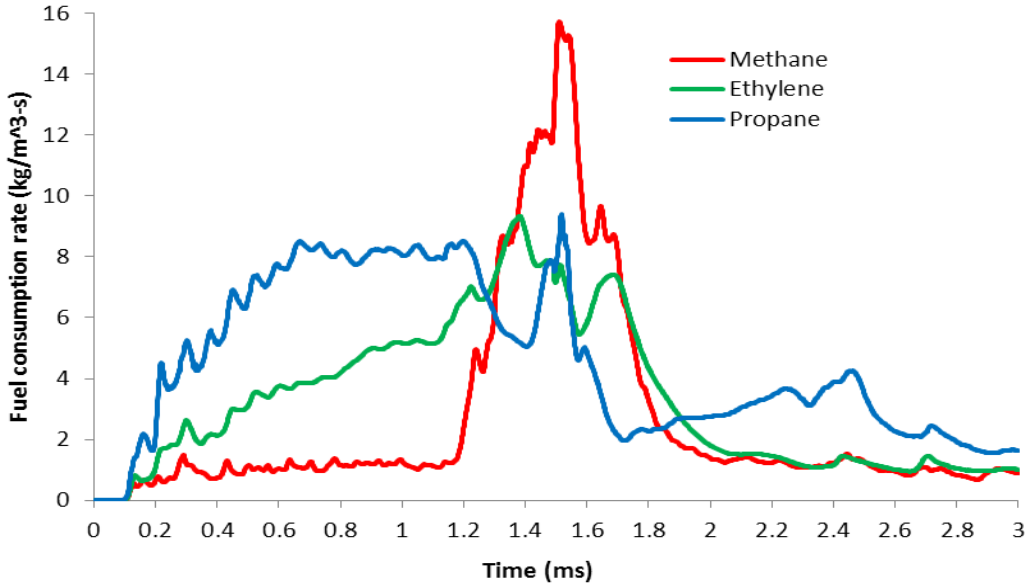

(a) CVC-chamber-integrated Fuel consumption rate

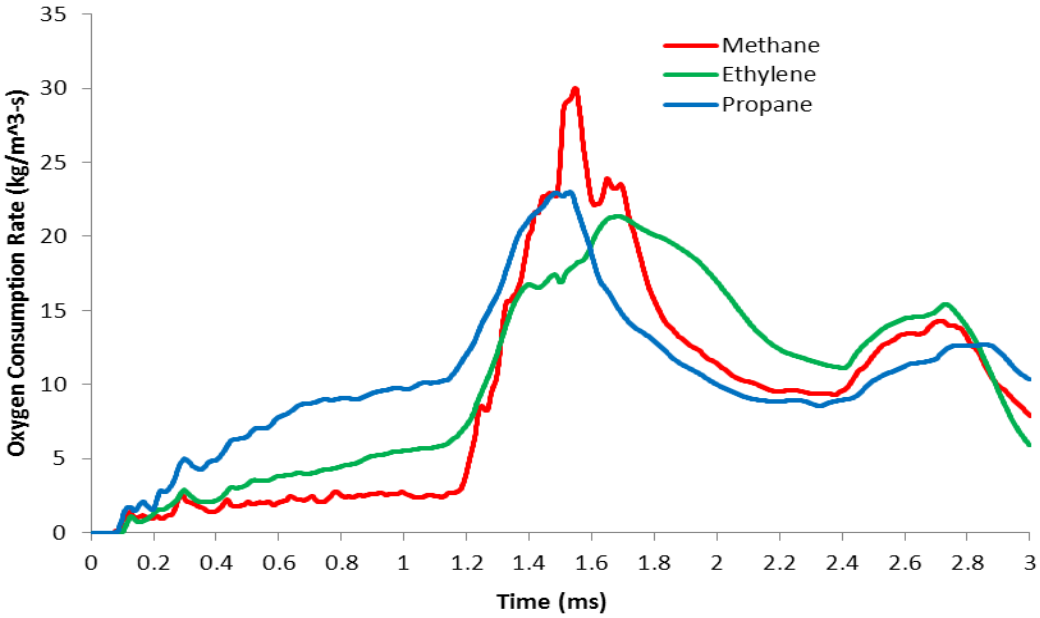

(b) CVC-chamber-integrated Oxygen consumption rate

Figure 5.10 Comparison of Fuel and Oxygen Reaction Rates in the CVC Chamber for Different Fuel Mixtures, Integrated Over the Chamber Volume

5.4.4 Ignition Delay

While there are many definitions of ignition delay time for different modes of ignition, the estimation of ignition delay time generally requires interpretation of the evidence for accelerating reaction. For shock-initiated ignition of premixed gas, Davidson and Hanson [74] reported that pressure is a good indicator of ignition at high fuel concentrations. They also found that the CH* and OH (and intermediate species C_3H_6) mole fraction histories show clear evidence of a change owing to ignition. In hot jet ignition, where the chemically active hot gas mixes with the cold combustible mixture, the definition of ignition delay must ideally consider all steps from the mixing process to the release of substantial fuel energy. With this caveat, the ignition event could reasonably be defined as occurring either at the time of maximum rate of change or at the time when the peak value of some species or variable such as [OH], [CH], or pressure is reached. Alternatively, it could be based on an extrapolation of the maximum slope to the zero signal level.

The computed fuel consumption rates for methane, ethylene, and propane are presented in Figure 5.10. In Figure 5.10(a) the consumption rate of fuel mass over time confirms the slower kinetics of methane relative to other fuels. For the same initial temperatures, significant consumption of fuel starts as early as 0.8 ms for ethylene, before the effect of reflected shock compression. For methane, consumption accelerates rapidly after shock arrival at the reacting region at 1.2 ms. The increase in fuel consumption rate at about 1.2 ms is attributed to the temperature increase by compression of the interior bulk of this region and possible smaller-scale mixing and homogenization due to baroclinic vorticity deposition in this region. For ethylene and propane, the fuel consumption occurs rather steadily from the time the hot jet enters the CVC chamber ($t = 0.2$ ms), and no sharp increase is seen upon shock compression. The boundary of the mixing region is observed to be distorted by shock interaction. As flame propagation may be occurring at this interface it may be aided by shock interaction. Oxygen consumption rate in the CVC chamber (Figure 5.10 (b)) undergoes rapid increase at shock compression for all three fuels. This reflects oxidation of intermediate hydrocarbon species that had already been created from ethylene and propane, while for methane if is primarily the initial oxidation of the

fuel. Thus the shock does have an impact in the reaction rates for all three fuels, even for ethylene and propane, but it is decisive in initiating reaction for methane at low initial temperature. Difference in ignition delay observed in the experiments of the hot-jet ignition [5] are consistent with these predictions. It is reported based on the interpretation of high-speed video images that the lowest recorded ethylene ignition delay time is 1.6 ms and for methane it is observed to be 2.9 ms [8], both for stoichiometric mixtures in the CVC chamber.

The chamber-integrated histories of several intermediate species are shown for methane, propane and ethylene fuels as shown in Figures 5.11, 5.12 and 5.13, respectively. Comparing the history of intermediate species concentration in the CVC chamber for different fuels, it is interesting that while the C_1 and C_2 intermediate species history exhibits the slower ignition activity for methane when compared with ethylene and propane. The history of OH, H, and HO_2 show similar trends for all three fuels. In the next section, we use detailed maps of the distribution of various species to attempt to understand the reason for the above trends from the reaction pathways for conversion of a fuel mixture into final products CO_2 and H_2O.

Examining methane combustion is more detail, the history of molar concentration of important intermediate species in the CVC chamber is presented in Figures 5.11(a) and 5.11(b). CH_3 concentration appears to be a useful indicator for ignition delay time quantification; it is seen in Figure 5.11(a) that a rapid increase of CH_3 occurs between t = 1.2 ms and t = 1.5 ms. Observing the molar concentration histories of OH, H, and HO_2 (Figure. 11 (b)), it appears that the production of these species peak near 2.5-3 ms, which is about a millisecond later than when the hydrocarbon intermediate with one or two carbon atoms (C_1 and C_2) species show peaks. To understand these trends better, the distribution of representative species is examined. In Figure 5.14 it is observed that the small hydrocarbon species (C_1 and C_2) are concentrated in the 'flame' at the boundary between the jet mixing region and the unburned region, while CO persists in the jet mixing region for a brief time and is always present in the flame. In contrast, OH and H are formed and

persist for a relatively longer period throughout the jet mixing region; thus the quantities of H and OH are overall is greater than the minor C species.

These observations point to the need for studying the chemical activity in the mixed region and in the boundary region separately, as both can be important for ignition and combustion activity in the chamber. In particular, it is clear that the arrival of the shock wave kicks off the formation of H, OH, and HO_2 in the bulk of the mixing region for all considered fuels. Thus, even in the case of ethylene and propane, where there is quicker initial reaction of the fuel molecule within the mixing region, shock compression increases the fuel consumption.

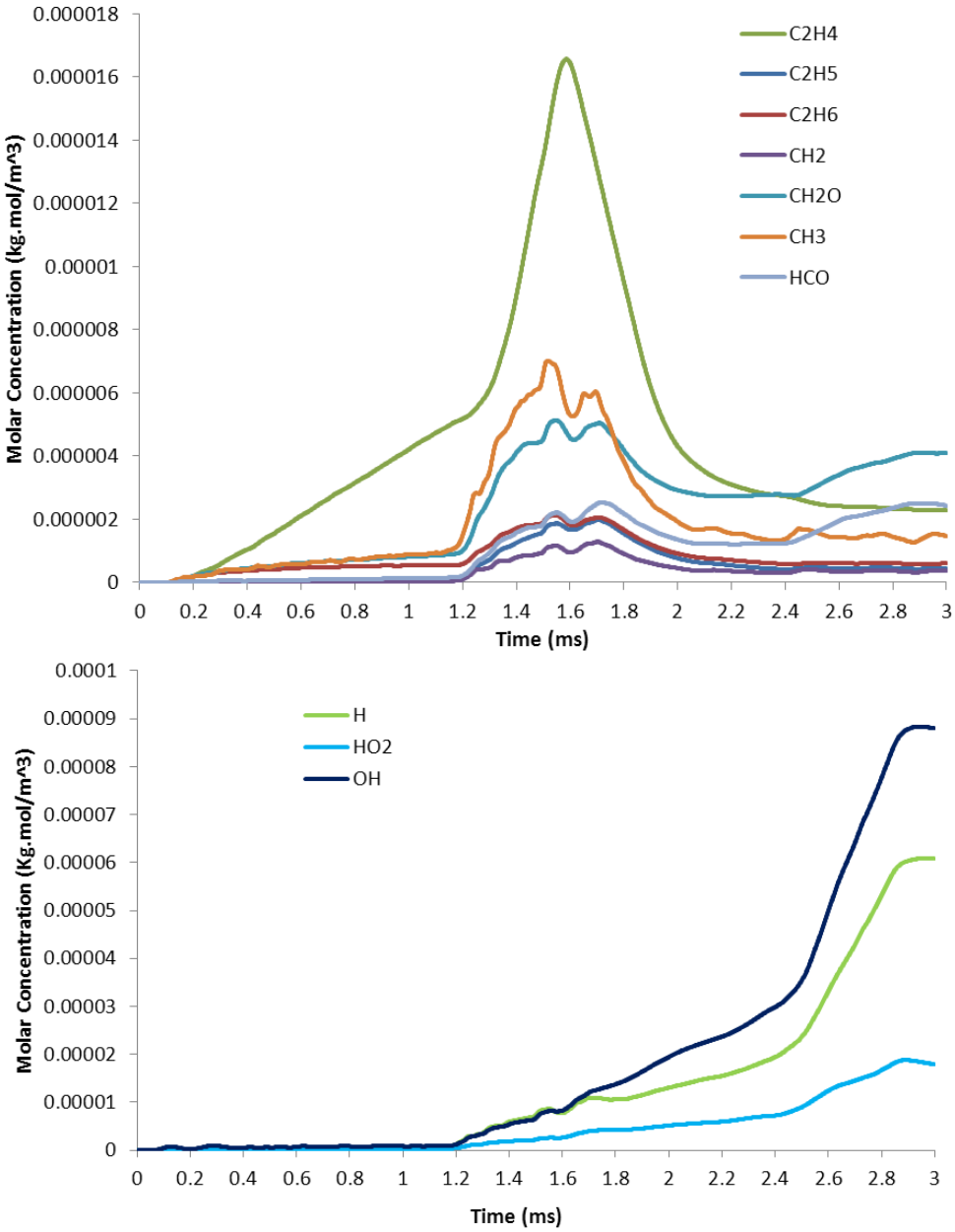

Figure 5.11 CVC Chamber-Averaged Molar Concentrations of Intermediate Species for Methane-Air Combustion

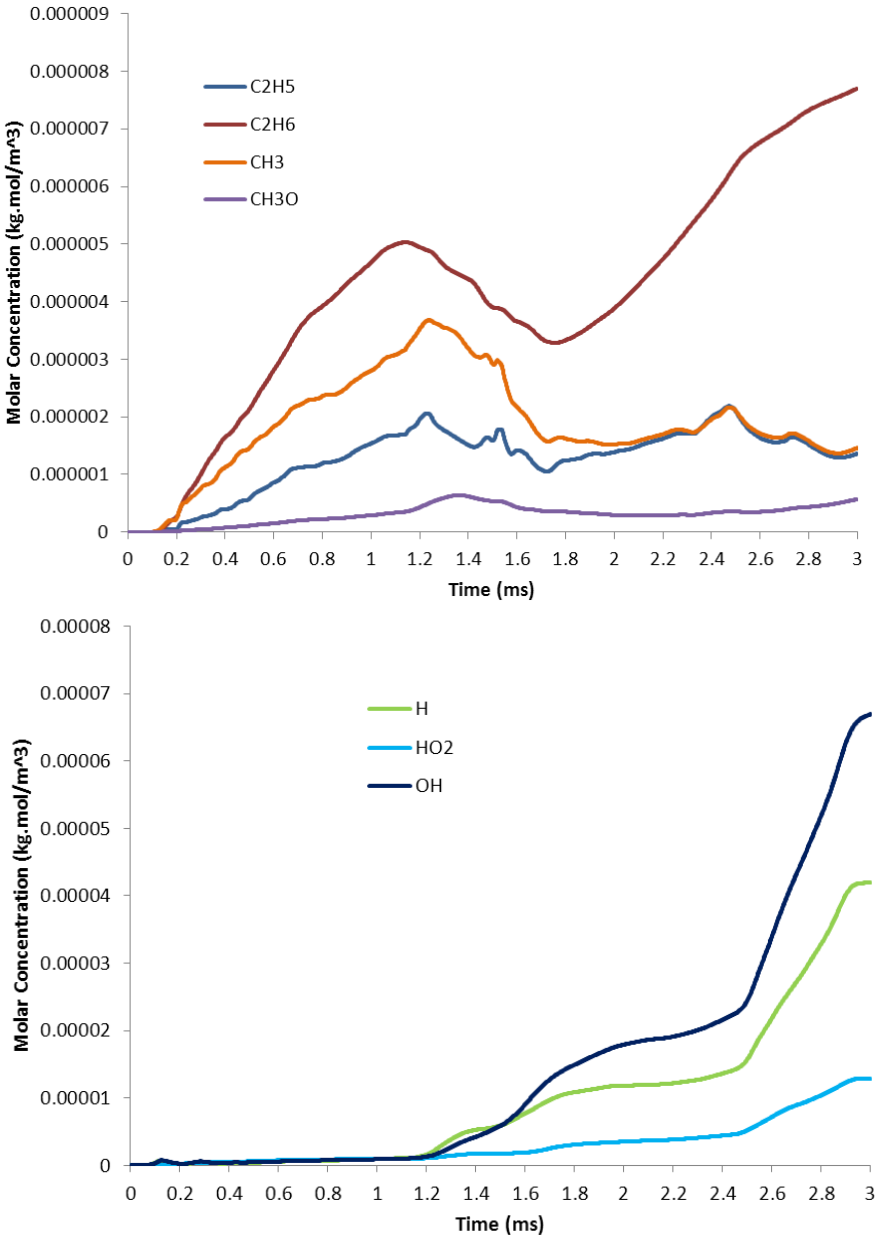

Figure 5.12 CVC Chamber-Averaged Molar Concentrations of Intermediate Species for Propane-Air Combustion

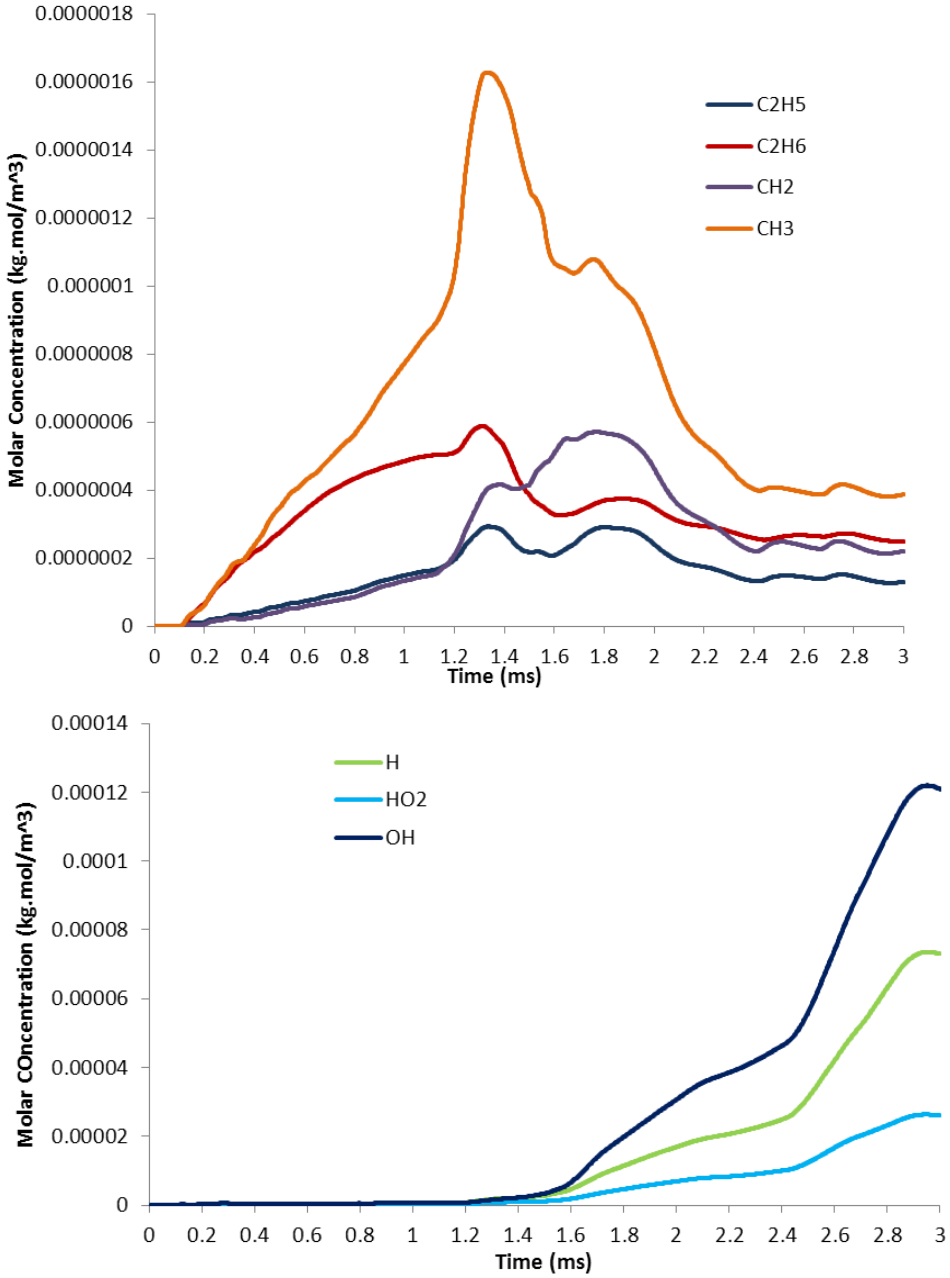

Figure 5.13 CVC Chamber-Averaged Molar Concentrations of Intermediate Species for Ethylene-Air Combustion

5.5 Reaction Pathways

In this section, reaction pathways have been discussed in detail for methane, ethylene and propane combustion. Ignition in the CVC chamber occurs when the mixture of injected gas and chamber gas is sufficiently hot and the concentrations of fuel and oxygen are sufficiently high. For methane fuel, the temperature reached in the CVC chamber mixed region, before ignition occurs at about 1.2 ms, is found to be in the range of 1600-1800 K. The reaction pathways for the combustion of methane are dependent on the initial composition and temperature. The ignition jet entrains reactants and creates vortices that may be treated as stirred reactors, as products of combustion are stirred in with reactants. In well-stirred reactors at high temperature (>2000 K), the main pathway for CH_4 combustion is [75, 76]:

$$CH_4 \rightarrow CH_3 \rightarrow CH_2O \rightarrow HCO \rightarrow CO \rightarrow CO_2 \tag{5.7}$$

At low temperature (<1500 K), one important addition found in the reaction pathway of methane combustion in well-stirred reactor is the following [75]:

$$C_2H_6 \rightarrow C_2H_5 \rightarrow C_2H_4 \rightarrow C_2H_3 \rightarrow C_2H_2 \rightarrow CO, CH_2 \tag{5.8}$$

The reaction mechanism used in this work for methane, DRM19, does not include the species C_2H_3 and C_2H_2. It does include the species C_2H_6, C_2H_5 and C_2H_4, and these may be used to infer the importance of the low-temperature pathway. From Figures 5.11(a) and 5.11(b), it is observed that the start of rapid fuel consumption at about 1.2 ms to the oxidation into CO_2 at 3.0 ms, much of the methane is consumed over a period of about 1.8 ms. The CH_2, CH_3, CH_2O and other higher hydrocarbons attains their maximum molar concentration between 1.5 ms to 1.7 ms; then decreasing through the oxidation of these species into CO. It is noted that there is again a slight increase in CH_2O and HCO around 2.6-3.0 ms. While this is consistent with the above mechanisms, the distribution of some of these species needs more attention, as given below. The molar concentration of H, OH, and HO_2 is observed to increase from about 1.2 ms until about 2.9 ms.

The appearance of hydrocarbon molecules larger than the initial reactant hydrocarbon is a feature of low-temperature oxidation processes [75]. The relative levels of C_2H_4 and other C¬2 species (Figure 5.11) indicates that the low-temperature reactions pathways may be active in the CVC jet ignition. It can be thus inferred that the two reaction pathways described above are probably both important. More detailed insight on reaction pathways through intermediate C_2/C_1 species would require more detailed and comprehensive mechanisms such as GRI Mech 3.0.

The level plots of various species in Figures 5.14-5.19 allow a more detailed examination of the processes in the mixed region near the jet and the boundary between the mixed region and. The distribution of CH_3 in Figure 5.14 shows concentrations in the mixing region initially, with rapid formation in several localized areas when the first shock compresses the mixed region at 1.2-1.3 ms. After about 2 ms CH_3 is concentrated at the boundary flame between the mixed and unburned regions. The CH_3 concentration within the flame is observed to increase again when the next shock reflection arrives from the unburned region at about 2.6 ms. This is expected as the freshly burning fuel produces CH_3 and it is quickly consumed; the enhanced mixing and compression heating by the shock increases the rate of fuel consumption locally, producing CH_3.

The subsequent intermediates of methane oxidation, CH_2O and HCO, are also highly concentrated (Figures 5.15 - 5.16) near the boundary region. The history and distribution of these intermediates parallels that of CH_3 with initial formation in the mixing region, and later concentration in the boundary region with even more pronounced peaks upon the arrival of a shock wave, especially at the 2.6 ms mark.

In contrast with the minor hydrocarbon intermediates, the distribution of OH and CO is more uniform and persistent throughout the jet mixing region. The OH concentration (Figure 5.17 and Figure 5.11) grows slowly within the mixing region, intensifying with the multiple shock passages, throughout the simulation period until 3.0 ms. The CO concentration (Figure 5.18) also grows throughout the mixing region, reaching highest

levels around 1.6-1.8 ms, and then falling. Correspondingly, the CO_2 concentration (Figure 5.19) grows rapidly after 1.8 ms as CO oxidizes.

These observations point to the need for carefully modeling the ignition process by considering the mixing and chemical kinetic processes in the jet mixing region. For methane mixture that is initially at room temperature, the heat-releasing chemical processes that involve CO and OH appear to be relatively slow compared to the mixing processes. The relatively mixed region undergoes chemical changes that are sensitive to shock heating in the experienced temperature range. These shock events are important in the success of ignition in this region.

The chemistry at the boundary between the mixed region and the unburned region must be considered separately to understand the formation of a propagating flame. The flame behavior is also influenced by shock interaction and by pre-existing and generated turbulence. This shock-driven flame acceleration is a separate phenomenon [77, 78]

For propane combustion (Figure 5.12), the chamber-integrated trends for C_1/C_2 species are seen to be rather different from that for methane, but the trends for OH/H/HO2 are quite similar. A consequence of the propane reaction pathways is the high production of ethane, C_2H_6 with peaks corresponding to the two major shock-flame interactions, while other C_1/C_2 species are seen to be consumed. C_2H_6 is generated and remains as a stable species for some time in the combustion of propane. For brevity, the details of the distribution of species is not shown for propane or ethylene.

For ethylene combustion, Westbrook et al. [79] reported that H-atom abstraction from ethylene by OH attack dominated fuel consumption based on well-stirred reactor experiments operating at atmospheric pressure and temperature in the range 1003 to 1253 K. The initial reaction during the combustion of higher alkane and alkene compounds are dominated by the β-scission process [80], which leads to the production of ethylene. While a substantial amount of ethylene is oxidized to C_1 species and formaldehyde, acetylene

may form as a result of pyrolytic reactions of ethylene. For stoichiometric to fuel rich flames, acetylene is the dominate intermediate. It can be observed from Figure 5.13 that the C_1/C_2 intermediate species C_2H_4 continuously increase from the time the hot jet entering the CVC chamber. This behavior is very different from methane combustion.

The comparison with ethylene and propane combustion is intended to highlight the relatively different kinetics of methane at low initial temperature. The importance of specific fuels such as natural gas and jet fuel for applications of wave-rotor pressure-gain combustion would indicate the importance of applying detailed kinetic models to hot-jet ignition over a range of initial temperatures corresponding to engine operating range. These are topics of ongoing and future investigations.

5.6 Shock-Flame Interaction

The ignition delay in the combustion of mixture in the CVC chamber is dependent on the delay time due to chemical kinetics as well as the delay time due to mixing and jet penetration. The internal gas dynamics of a long closed chamber typically gives rise to a shock wave that reflects and returns to the region of ignition. The chemical ignition delay time may be shortened by shock compression and further flame propagation may be enhanced by shock-flame interaction (SFI). This is observed in the case of methane mixtures initially at room temperature.

In addition, baroclinic vorticity production in the flame appears to be the main driver of the interface deformation produced at different scales [81]. Richtmyer-Meshkov instability (RMI) is caused by the positive and negative vorticity deposition along the interface that results in a mushroom-like interface deformation. Analytical studies, experiments and numerical simulations of RMI have been reviewed by Rupert [82], Zabusky [83] and Brouillette [84] respectively. Recently, a detailed study [77, 78, 81, 85] on shock-flame interactions, expansion wave-flame interaction and the contribution of area increase and kinetic amplification of fuel reaction rate for wave rotor like applications have been reported. The deformation of flame caused by the reflecting shock can be seen in

Figure 5.9 for methane and ethylene mixtures respectively. For both the fuels, the flame deformation is observed at time t = 1.6ms, indicating that the fluid dynamics of SFI following shock arrival are not coupled with chemical reactions.

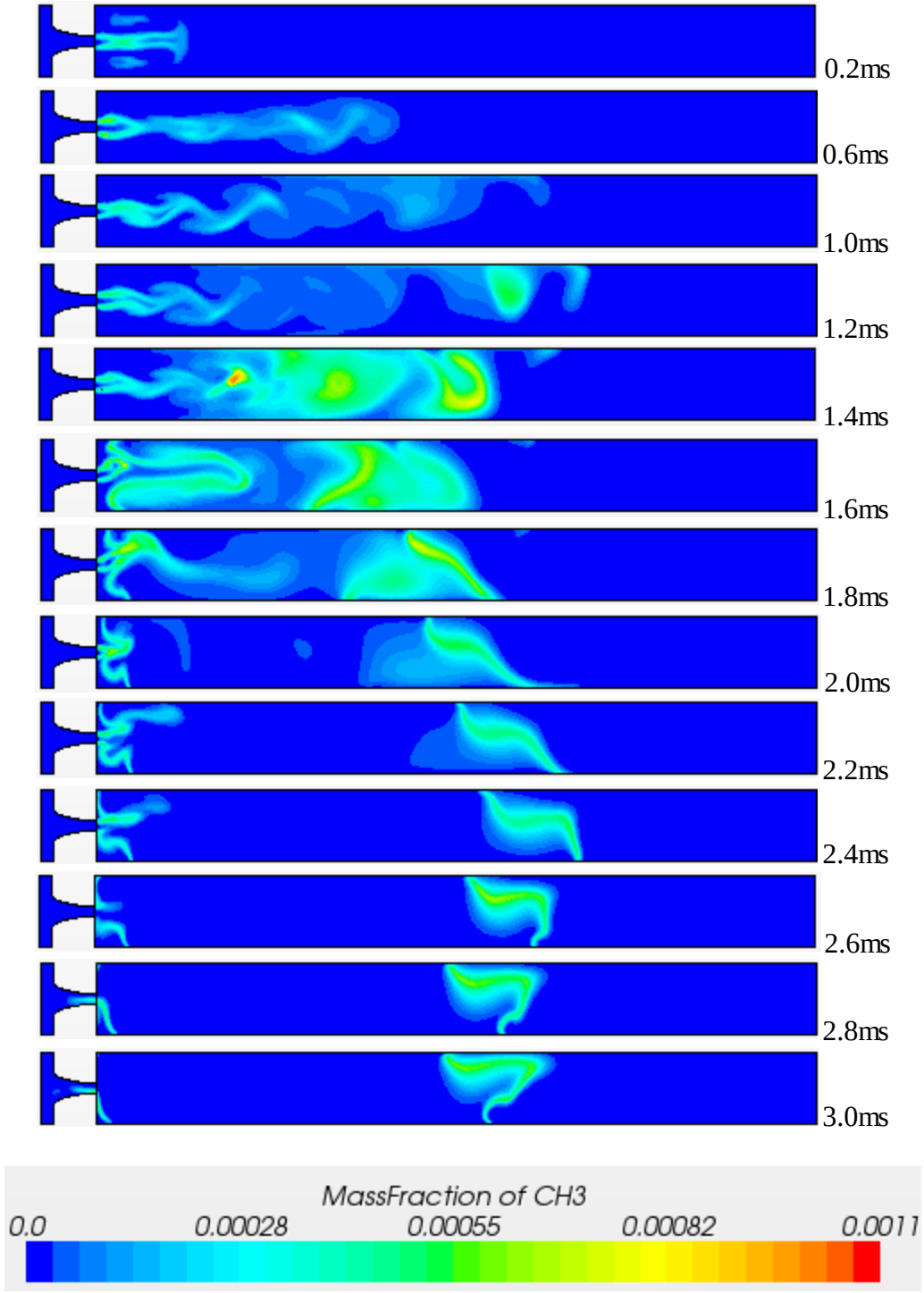

Figure 5.14 CH_3 Mass Fraction during Methane-Air Combustion Predicted using DRM19 Reaction Mechanism

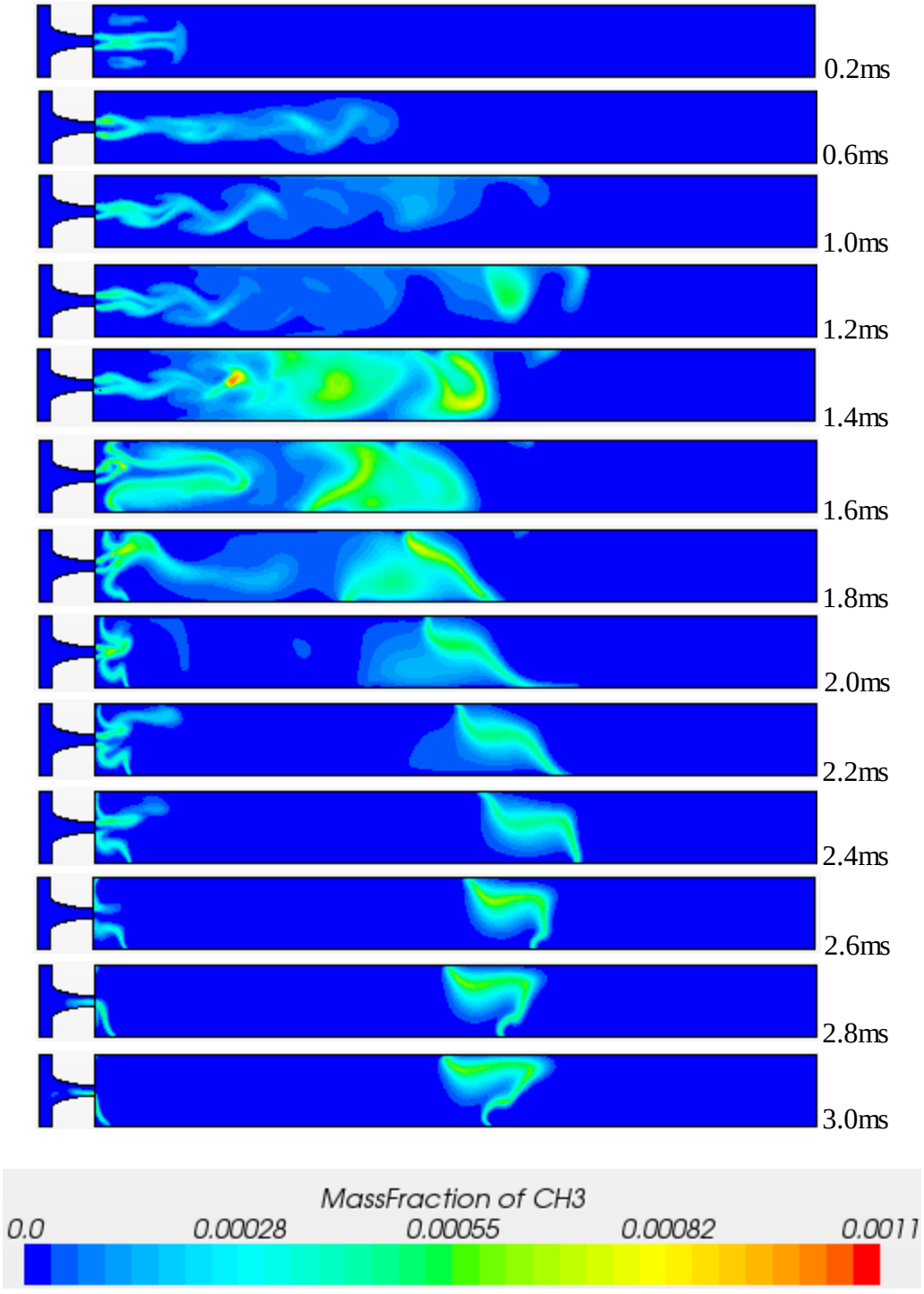

Figure 5.15 CH_2O Mass Fraction during Methane-Air Combustion Predicted using DRM19 Reaction Mechanism

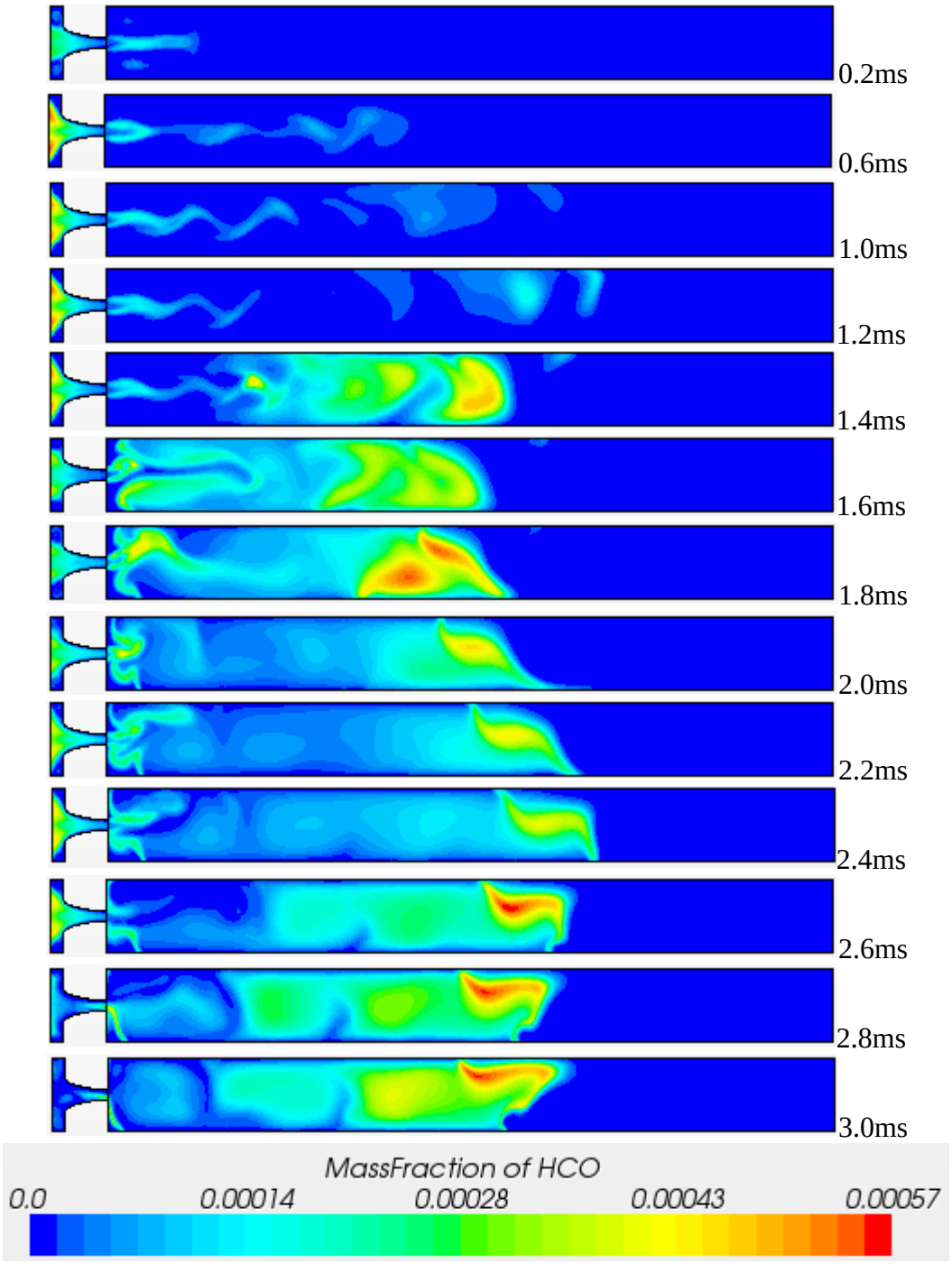

Figure 5.16 HCO Mass Fraction during Methane-Air Combustion Predicted using DRM19 Reaction Mechanism

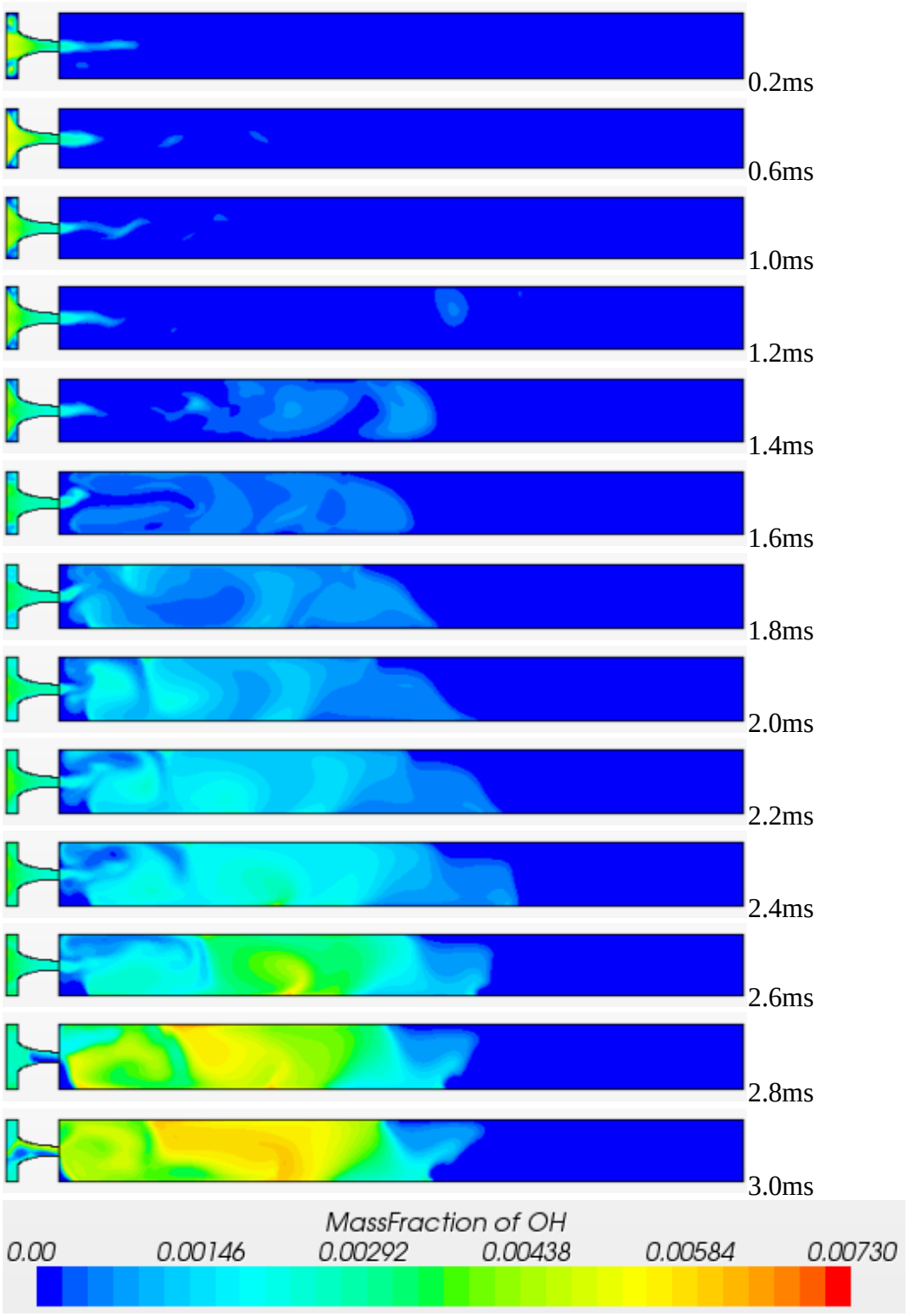

Figure 5.17 OH Mass Fraction during Methane-Air Combustion Predicted using DRM19 Reaction Mechanism

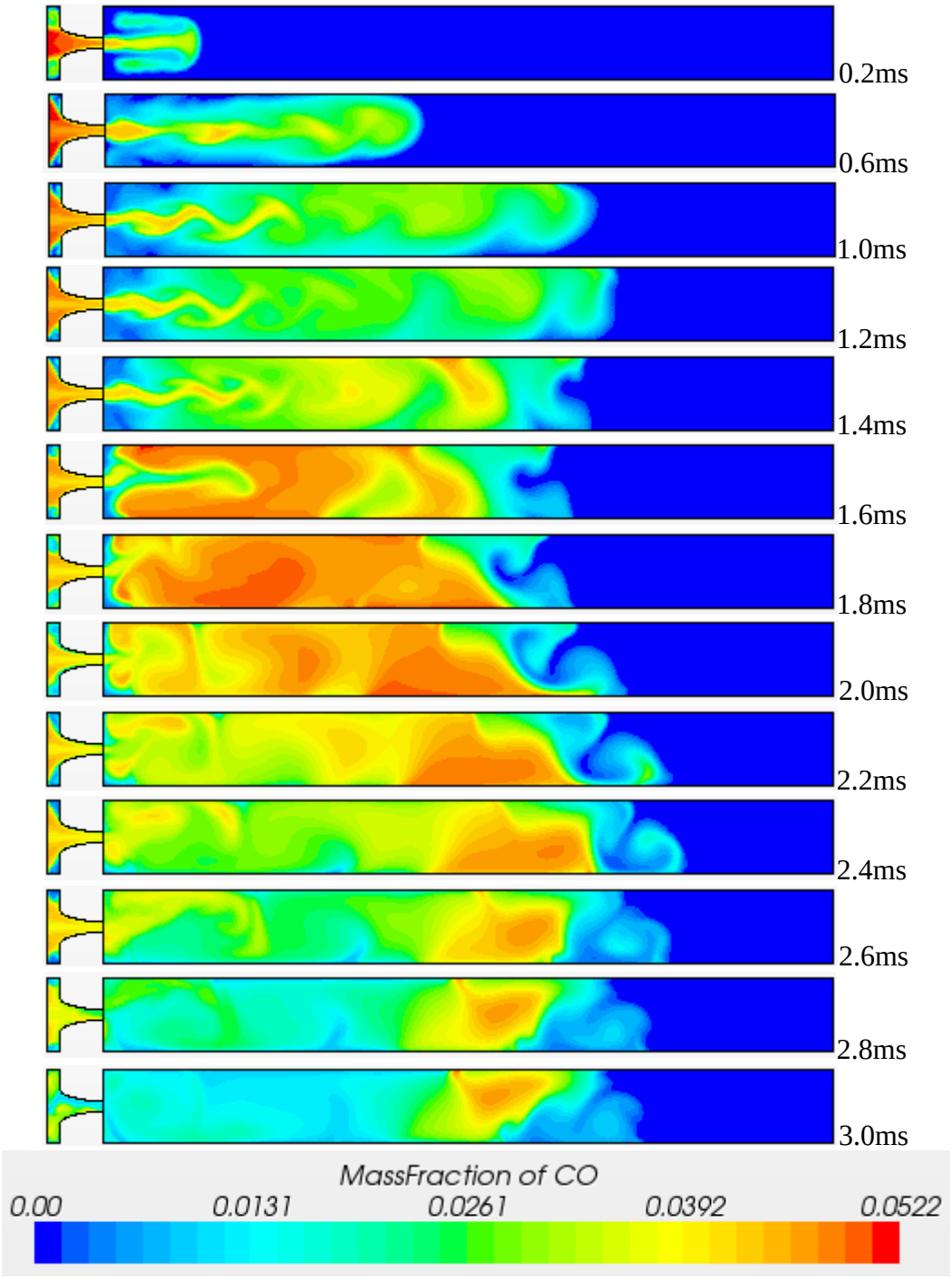

Figure 5.18 CO Mass Fraction during Methane-Air Combustion Predicted using DRM19 Reaction mechanism

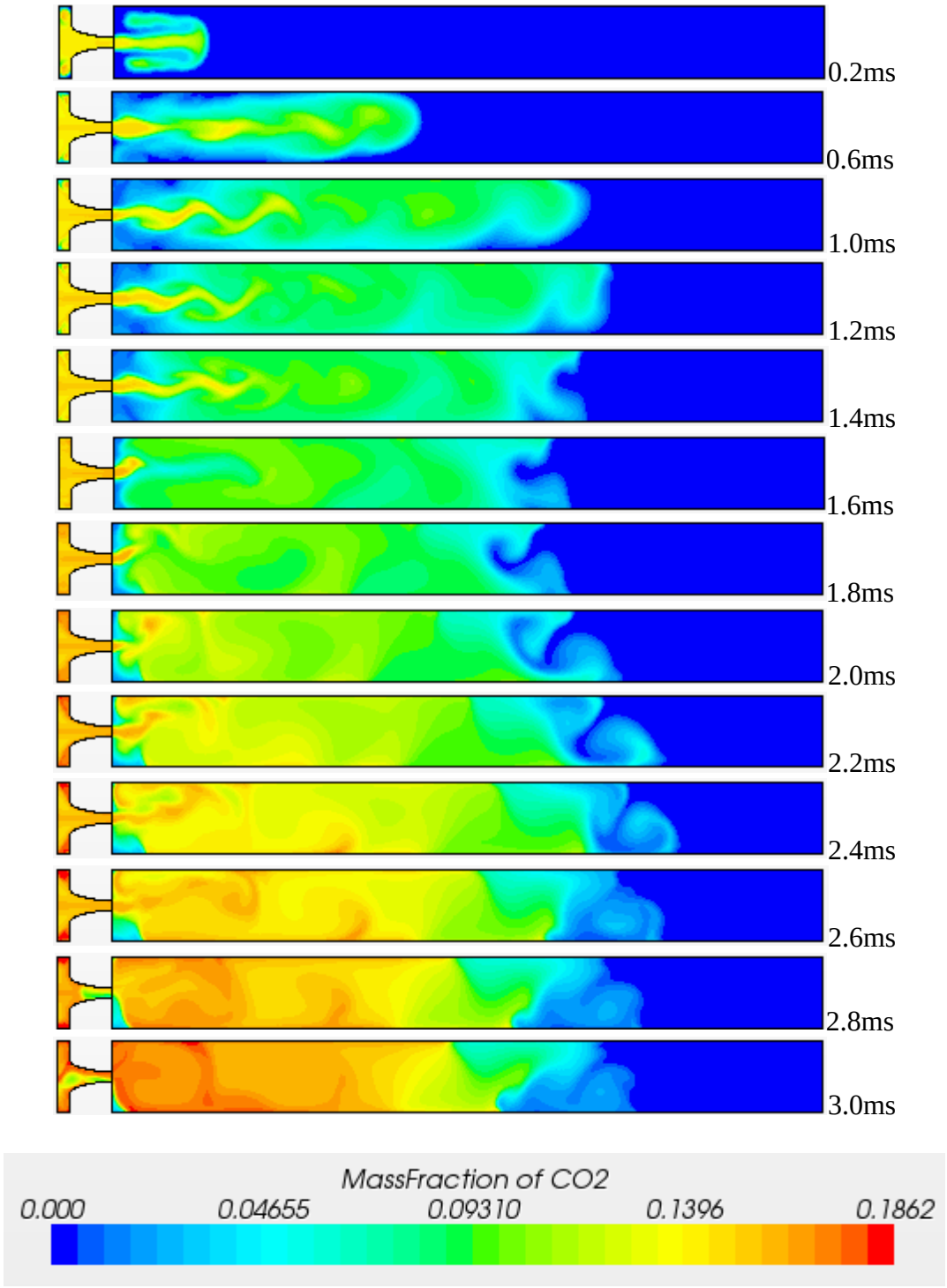

Figure 5.19 CO_2 Mass Fraction during Methane-Air Combustion Predicted using DRM19 Reaction Mechanism

In order to verify that the timing of shock arrival controlled the timing of significant chemical reaction, the length of the CVC chamber was increased to 20 inches from original 16 inches, which would delay the reflecting shock return. This case is simulated for the combustion of methane using DRM19, and results are compared with the original geometry. The gas density history for the original geometry and extended length CVC chamber are shown in Figures 5.20 and 5.21, respectively. Shock wave reflection for the extended length CVC chamber is seen at time t = 1.0 ms, later than for the original geometry (t = 0.8 ms). Similarly, the deformation of the flame front is seen at about t = 1.8 ms for extended length CVC chamber, later than t = 1.4 ms for original geometry. The fuel consumption rate and oxygen consumption rates for two cases are presented in Figure 5.22. The longer CVC chamber causes a delay of approximately 0.2 ms in the sudden rise of fuel and oxygen consumption rates. This is a significant finding for wave rotor constant volume combustors (WRCVC) of different lengths compared to the rig considered in the present work. Although the timing of methane ignition is clearly linked to the shock arrival, the actual mechanism for the role of SFI and shock compression can be further investigated. SFI causes a significant increase in the flame surface and thus in micro-scale mixing. The shock wave also increases temperature by compression and thus accelerates many kinetic rates. In the future work, it would also be important to study the effect of the shock wave on ignition for other fuel mixtures.

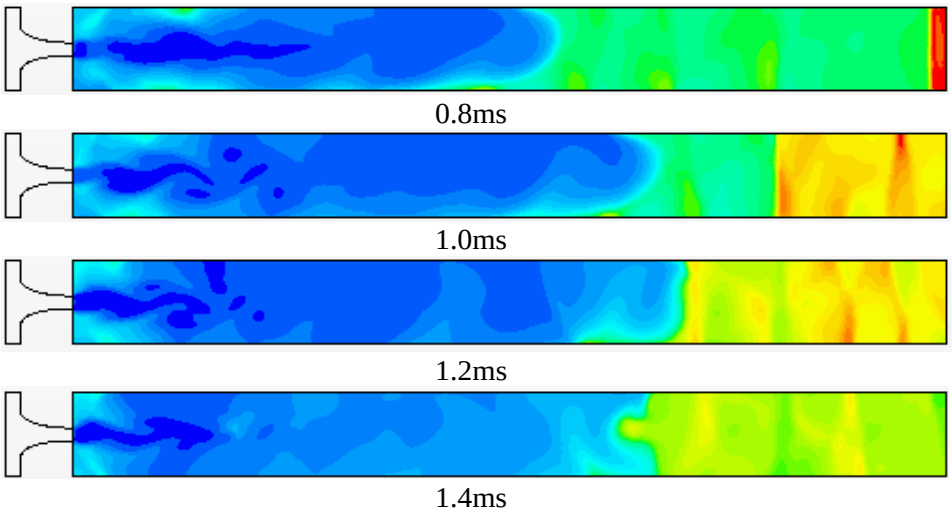

Figure 5.20 Shock-Flame Interaction during Methane-Air Combustion in Original Length (16 inches) CVC chamber, Shown by Gas Density History

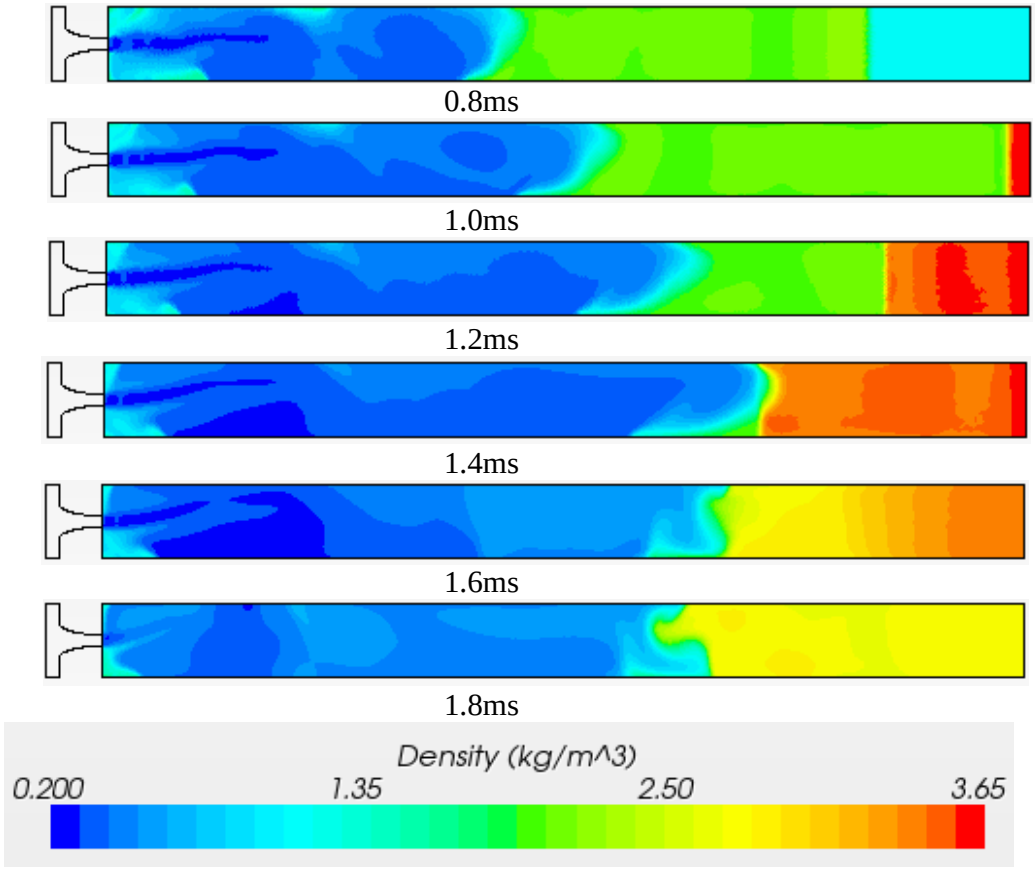

Figure 5.21 Shock-Flame Interaction during Methane-Air Combustion in Extended Length (20 inches) CVC Chamber, Shown by Gas Density History

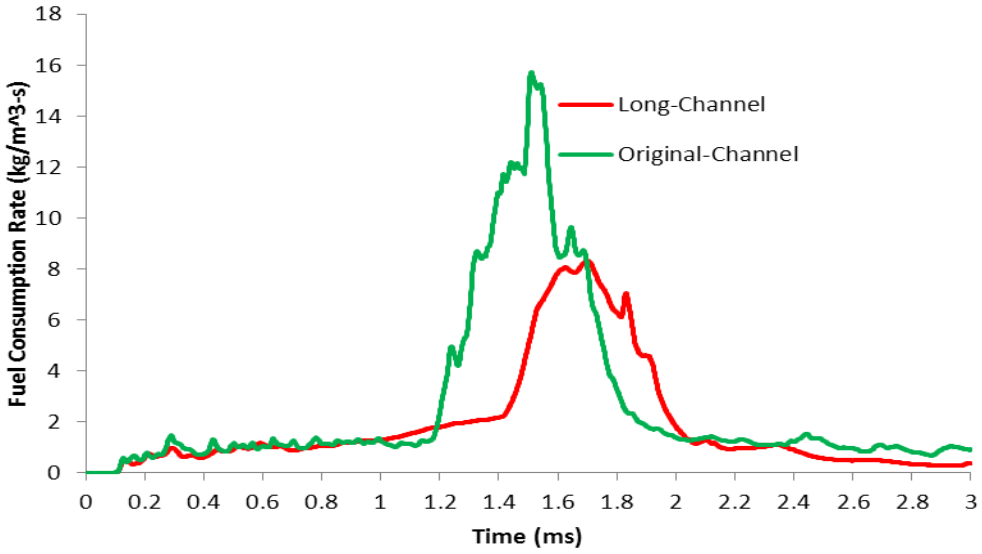

(a) Fuel (methane) consumption rate

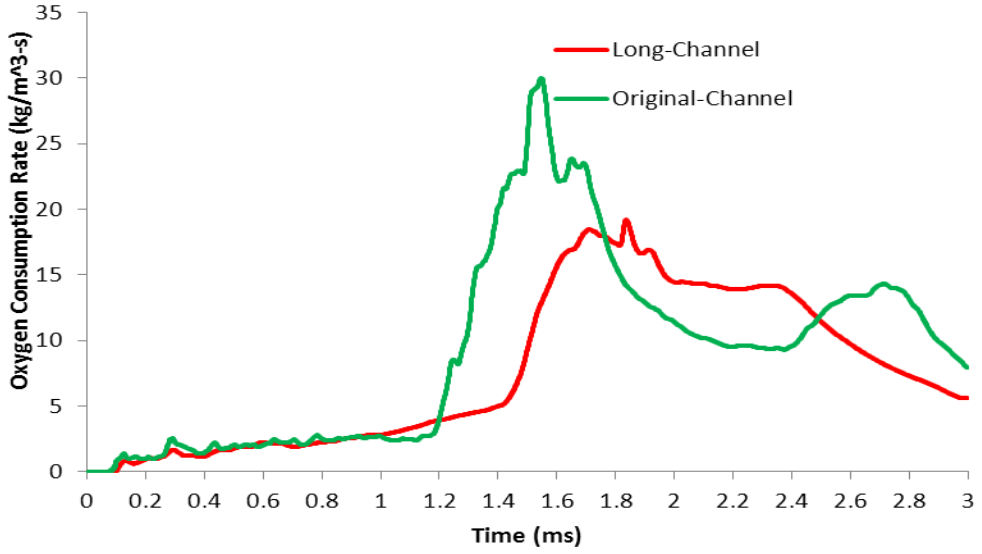

(b) Oxygen consumption rate

Figure 5.22 Effect of Shock-Flame Interaction Timing in Different Length CVC Chambers, Evidenced by Methane Fuel and Oxygen Consumption Rate History

5.7 Traversing Jets

The reaction mechanism used for ethylene involves 32 species in 206 reversible elementary reactions [72]. For methane, a detailed reaction mechanism DRM19 is used, which involves 21 species in 84 reversible reactions.

The initial pressure in the pre-chamber is specified as the pressure at diaphragm rupture measured from experiments [5]. The initial temperature and composition of the pre-chamber is obtained by chemical equilibrium calculation of major product species for combustion of ethylene-air with the equivalence ratio of 1.1. The calculation used the program developed by Depcik, which correlates well with the NASA equilibrium code. The initial conditions for the pre-chamber and CVC chamber are listed in Table 1.

Table 5.1. Initial Conditions for the Simulations

Thermodynamic Properties and Mass Fractions	Pre-chamber	CVC Chamber	
		Methane	Ethylene
Pressure (kPa)	649.0	101.325	101.325
Temperature (K)	2770	298	298
O_2	0.0069176	0.219231	0.217271
N_2	0.719410	0.725824	0.719240
CO_2	0.142050	0	0
CO	0.050400	0	0
H_2	0.000739	0	0
H_2O	0.080490	0	0
CH_4	0	0.054945	0
C_2H_4	0	0	0.063488

5.7.1 Ignition Delay and Jet Speed

There are many definitions of ignition delay time used in the literature, most of which refer to auto ignition by rapid or shock compression of a fuel-oxidant mixture with no trace of other highly reactive species initially present. Hot jet ignition and auto ignition have common and different challenges in defining the ignition delay time. Ignition could reasonably be defined as occurring either at the time of maximum rate of change or at the

time when the peak value of some species or variable such as [OH], [CH], or pressure is reached, or could be based on an extrapolation of the maximum slope to the zero signal level. Davidson and Hanson [74] reported that, in general, pressure rise is a good indicator of ignition at high fuel concentrations. They also found that the CH^* (formed by the reaction, $C_2H + O \rightarrow CH^* + CO$, where CH^* represents the excited state) and OH (and intermediate species C_3H_6) mole fraction histories show clear evidence of a change owing to ignition for the cases investigated. Hot jet ignition also involves a physical delay for mixing with the cold combustible gas. The active radical species introduced may influence reaction initiation of the fresh fuel, but may also be quenched during entrainment of cold mixture, depending on the entrainment ratio and mixing rate. Examination of fuel consumption rate or production rates of some of the intermediate species may not adequately define ignition delay.

High-speed video images taken through a transparent window of the experimental CVC with traversing hot-jet ignition are presented in Figure 5.23, for methane mixture in the CVC chamber, with optically obscured volume indicated in green. The camera spectral response is 400-1000 nm, capturing visible and near-infrared luminosity of hydrocarbon combustion, which comes from soot radiation. In Figure 5.23(a), ignition of a stoichiometric methane-air mixture by a centered stationary jet is observed. In Figure. 5.23(b), ignition of a lean methane-air mixture is observed, with pre-chamber spin rate of 150 rpm, which corresponds to a jet traverse speed of 0.983 m/s and a traverse time of 40.5 ms. At this speed jet barely moves away from the side wall before ignition is completed. Thus the jet structure, penetration, and entrainment for the near-wall position, rather than the traversing motion, is likely to be its distinguishing characteristic. Therefore, this slowly traversing case will be referred to as the ‘near-wall’ jet. It can be seen that the jet initially travels along the wall and later impinges on the bottom wall. Rapid onset of combustion can be seen to start at around 1.4 ms after the impingement of the jet and progresses towards both ends of the CVC chamber.

Experimental data has not been published for faster traversing jets; this work is intended to anticipate that data with numerical simulations. More advanced optical diagnostic tools often seek to measure excited species such as OH, but it is not obvious what measurements would provide a reliable indication of ignition and ignition delay time. The pre-chamber spin rates and the corresponding jet traverse speeds and the traverse times for the numerical simulations reported are listed in Table 5.2. It is expected that numerical simulations will capture the jet behavior and ignition trends similar to the experiments, and provide a deeper understanding of the interplay between physical and chemical processes. However, it is not expected that the jet impingement time and ignition delay time from simulations would match quantitatively with experimental data due to lack of realism of the two-dimensional approximation in the simulations. The forthcoming discussion is based entirely on computer simulations, motivated and anchored by the currently limited experimental data, and to provide guidance for future experiments. In Figure. 5.24, the mass fraction levels of the combustion of stoichiometric ethylene/air and methane/air mixtures in the CVC chamber are presented for the near-wall jet. The traversing jet is seen to impinge on the CVC chamber bottom wall at 0.4 ms forming counter-rotating vortices that entrain the CVC mixture. It is also observed that the 'flame surface' boundary between unburned ethylene air mixture and the entrained and consumed region retreats towards the injection end of the channel at about 1.2 ms, and immediately afterwards the flame surface becomes more highly convoluted. This is due to a shock wave that is generated by the jet initiation and initial heat release, and travels away from the flame. Upon reflection at the opposite end, the shock wave returns to reverse the general direction of gas motion (giving the appearance of flame retreating) and more importantly, deposits significant baroclinic vorticity on the non-planar flame surface, significantly increasing in flame area. The shock wave also increases gas temperatures in the combusting region, thus accelerating kinetic rates. Thus in all cases, a significant increase in fuel consumption is observed at this time. Although the overall vortex dynamics and entrainment flows are very similar, it can be seen within the mixed regions that ethylene reacts significantly faster than methane. As methane is less reactive than ethylene, its greater sensitivity to jet mixing patterns and rates may be understood with deeper examination of the chemical kinetics of reaction. In the

temperature level plots presented in Figure. 5.255 for the near-wall jet, higher temperature rise in the CVC chamber can be observed for ethylene/air mixture compared to methane/air mixture. The constant-volume combustion adiabatic flame temperature for methane and ethylene are found to be 2821 K and 3116 K respectively for atmospheric initial conditions assuming single step reaction.

Table 5.2. Jet Traverse Speed and Traverse Time

Spin Rate (rpm)	Traverse Speed (m/s)	Traverse Time (ms)
150	0.983	40.5
750	4.917	8.1
2000	13.112	3.1

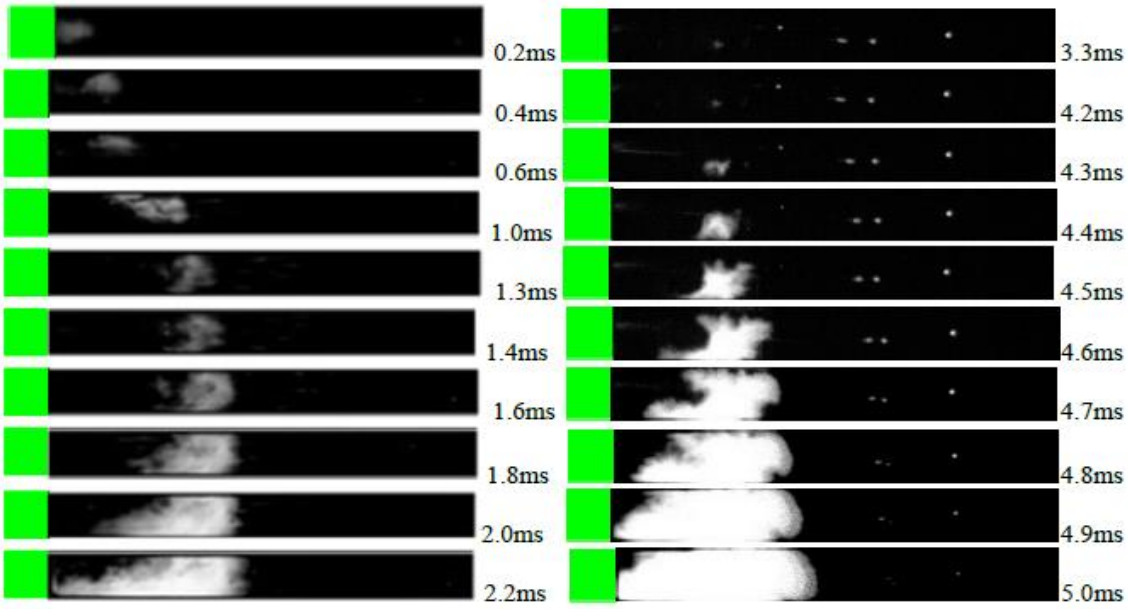

(a) (b)

Figure 5.23 High-Speed Video Images of Ignition of (A) Φ = 1 Methane Mixture in the Main CVC Chamber, for Centered Stationary Jet [7] (b) Φ = 0.8 Methane Mixture in the Main CVC Chamber for Near-Wall Jet

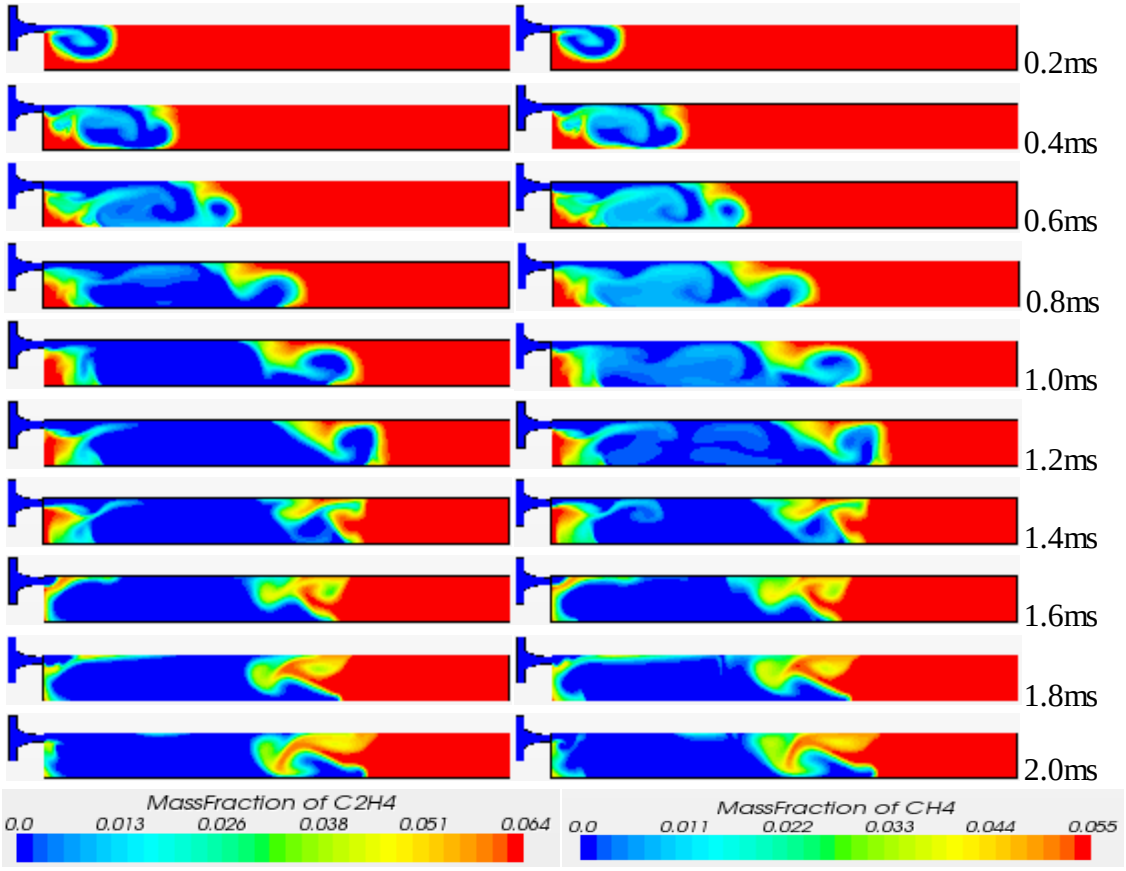

Figure 5.24 History of Fuel Mass Fraction for Ethylene (Left) and Methane (Right) in Stoichiometric Mixtures for Near-Wall Jet

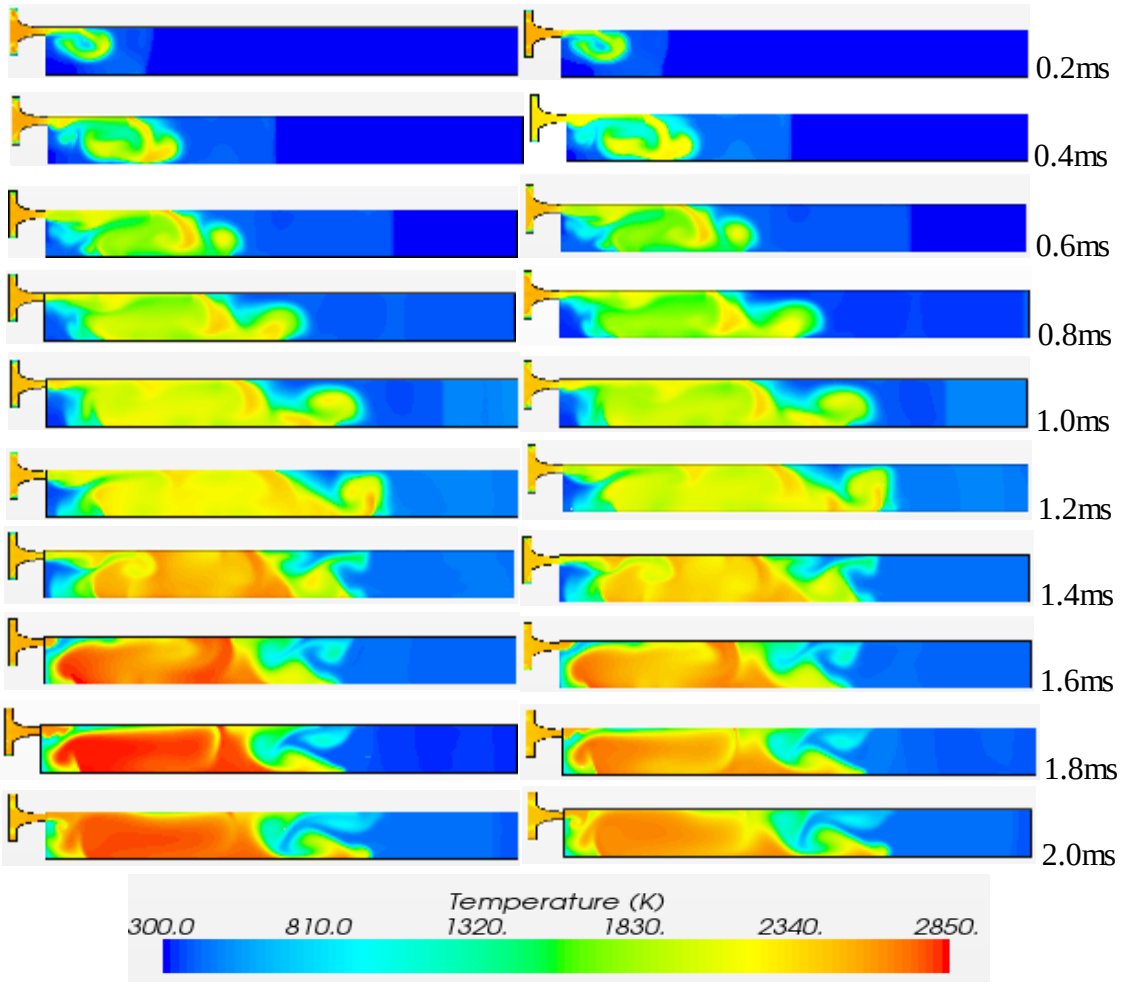

Figure 5.25 History of Temperature Levels for Ethylene (Left) and Methane (Right) in Stoichiometric Mixtures for Near-Wall Jet

To analyze the effect of traversing jet speed, the averaged fuel consumption history in the CVC chamber for the ethylene mixture at different jet traversing speeds is compared with the centered stationary case in Figure 5.26. The trends in ethylene fuel consumption are similar for the traversing jet at different speeds and for the centered stationary jet, with rapid combustion rates after about 1.2 ms after start of injection, but with some differences. Because of the low autoignition temperature of ethylene, higher combustion temperature, and fast reaction rates, the Damkohler Number (Da, ratio of reaction rate to mixing rate of vortices) is large, and ignition occurs early and relatively independent of variations in jet and entrainment behavior. For all traverse cases, the arrival of the reflected shock at about 1.2 ms does accelerate the reaction rate moderately.

The fuel consumption histories in the CVC chamber for methane mixture predicted from simulations are presented in Figure 5.27 for the centered stationary jet and different traversing jet speeds. In case of methane mixture in the CVC chamber, reaction is initially relatively slow, more so for the centered stationary jet. It is seen that the fuel consumption rate sharply increased between 1.2 ms to 1.5 ms, consistent with the returning shock compression and flame distortion during this period, but with significantly more effect for the centered stationary jet than the near-wall slowly traversing jet. For the near-wall jet, the peak fuel consumption rate is relatively lowest. The relatively slow kinetics and high autoignition temperature of methane results in a greater role for jet and entrainment behavior in determining local Damkohler number and the ignition delay time. This faster-traversing hot jets move through positions from near-wall towards and past the centerline position, thus having more complex vortex generation and entrainment dynamics.

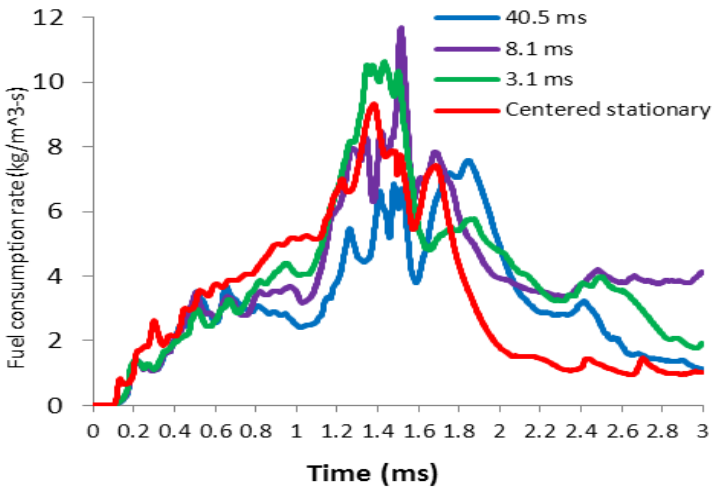

Figure 5.26 CVC Chamber-Averaged Fuel Consumption Rate for Traversing Jets and Centered Stationary Jet, for Stoichiometric Ethylene-Air Mixture

For a better understanding of methane combustion progress and heat release with varying jet behavior, the CVC temperature levels are plotted in Figure 5.28. One noticeable difference is that the temperature rise is lower in case of centered stationary jet when compared to all the traversing jet cases. For example, at 2.0 ms, temperature is higher for the jets traversing at the three speeds compared to the centered stationary jet. Moreover, earlier temperature rise is seen in case of near-wall jet speed case compared to other cases. It appears that the initial jet position and traverse speeds can significantly affect the time of the combustion and its progress. Closer observation of the gas distribution and temperature field at about 1.0 ms, before the shock-flame interaction, shows that the centered jet has significantly more penetration and thus entrains more fuel-air mixture, but has lower overall temperature, probably due to the lower concentrations of injected hot gas as a result. Consumption of fuel is also lower at 1.0 ms for this jet (Figure 5.27). Thus for the centered jet, more fuel is mixed with hot gas creating a leaner mixture with more unreacted fuel, which is then rapidly consumed when the shock interacts. It is further seen that the heat release and temperature rise occur later for the centered jet, and the overall consumption rate plummets when the mixed region expands by about 2.0 ms.

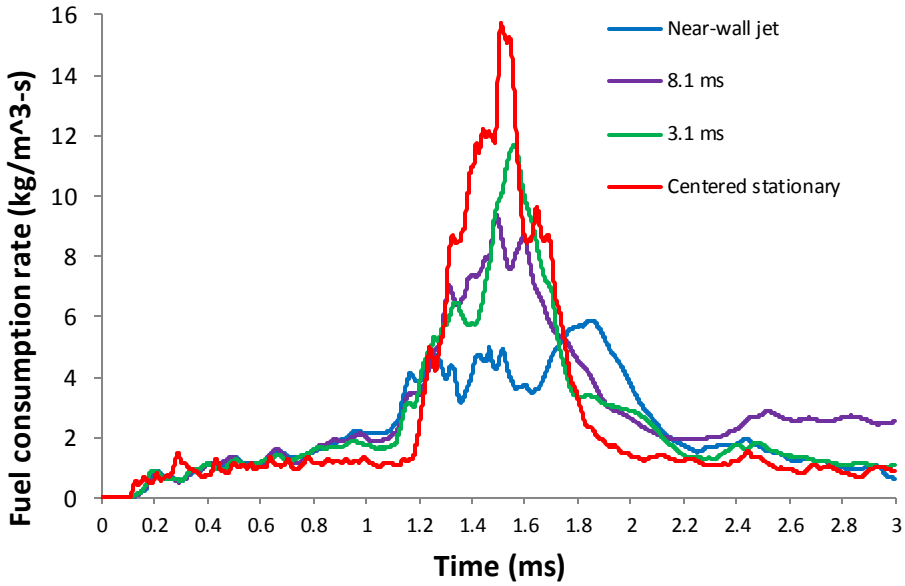

Figure 5.27 CVC Chamber-Averaged Fuel Consumption Rate for Traversing Jets and Centered Stationary Jet, for Stoichiometric Methane-Air Mixture

To analyze the combustion progress and reaction pathways, the production and consumption behavior of several significant intermediate species is presented below.

5.7.2 Reaction Pathways and Combustion Progress

The significantly different consumption rate of fuel in the CVC chamber for methane mixture for the near-wall and centered stationary jets could be explained by looking at the prominent intermediate species. An important C_2 intermediate species in the combustion of methane is ethylene, C_2H_4, which was earlier studied as a fuel itself. Figure 5.29 is a comparison of the mass fraction of ethylene for the centered stationary case and different traversing jet cases of methane combustion. It can be seen that there is very high production of ethylene from 1.4 ms to 1.8 ms for the centered stationary case with highest mass fraction at 1.6 ms. Interestingly, such high ethylene production is not seen for the near-wall jet case. This sudden production of ethylene is also less prominent for the faster traversing jet cases when compared to the centered jet case. This may be explained by the enhanced mixing with lower entrainment for the near-wall jet, due to jet impingement producing counter-rotating vortices. To gain further insight, the mass fraction of

intermediate species OH is compared in Figure 5.30. It shows that the high production of OH starts as early as 1.6 ms for near-wall jet case while for the centered jet case the same level of OH production is seen much later at around 2.4 ms. It can also be observed that the production of OH is seen to occur in the enhanced mixing zone where the counter-rotating vortices evolve after the jet impinges on the wall. It can be concluded that for the near-wall jet case the enhanced mixing in a smaller volume causes the faster completion of reaction.

Further insight may be obtained by examining the globally averaged histories of two important C1 and C2 hydrocarbon intermediate species, CH_3 and C_2H_4, shown in Figure 5.31. These species are relatively unstable and exist more in newly reacting regions such as the propagating flame front and slower mixing regions. It can be seen for the centered stationary jet that CH_3 and C_2H_4 are present in significant amounts and then consumed. On the other hand, for the near-wall and traversing jets, the presence of CH_3 and C_2H_4 is lower, indicating that production is more closely followed by consumption. In contrast to C1 and C2 species, OH and H are key radical species that are generated during continuing chain-propagation reactions of the combustion process. The presence of OH and H is seen (Figure 5.32) to increase dramatically between 1.6 ms to 2.6 ms for all the cases, but with higher levels for the near-wall jet compared to the centered stationary and faster traverse cases. This supports the hypothesis that a jet with reduced entrainment and enhanced mixing can lead to faster progress of combustion. Based on OH and H, the ignition delay would appear to about 2 ms, but based on fuel consumption, and earlier time is indicated. This highlights the importance of not relying on a single or indirect measure of ignition activity.

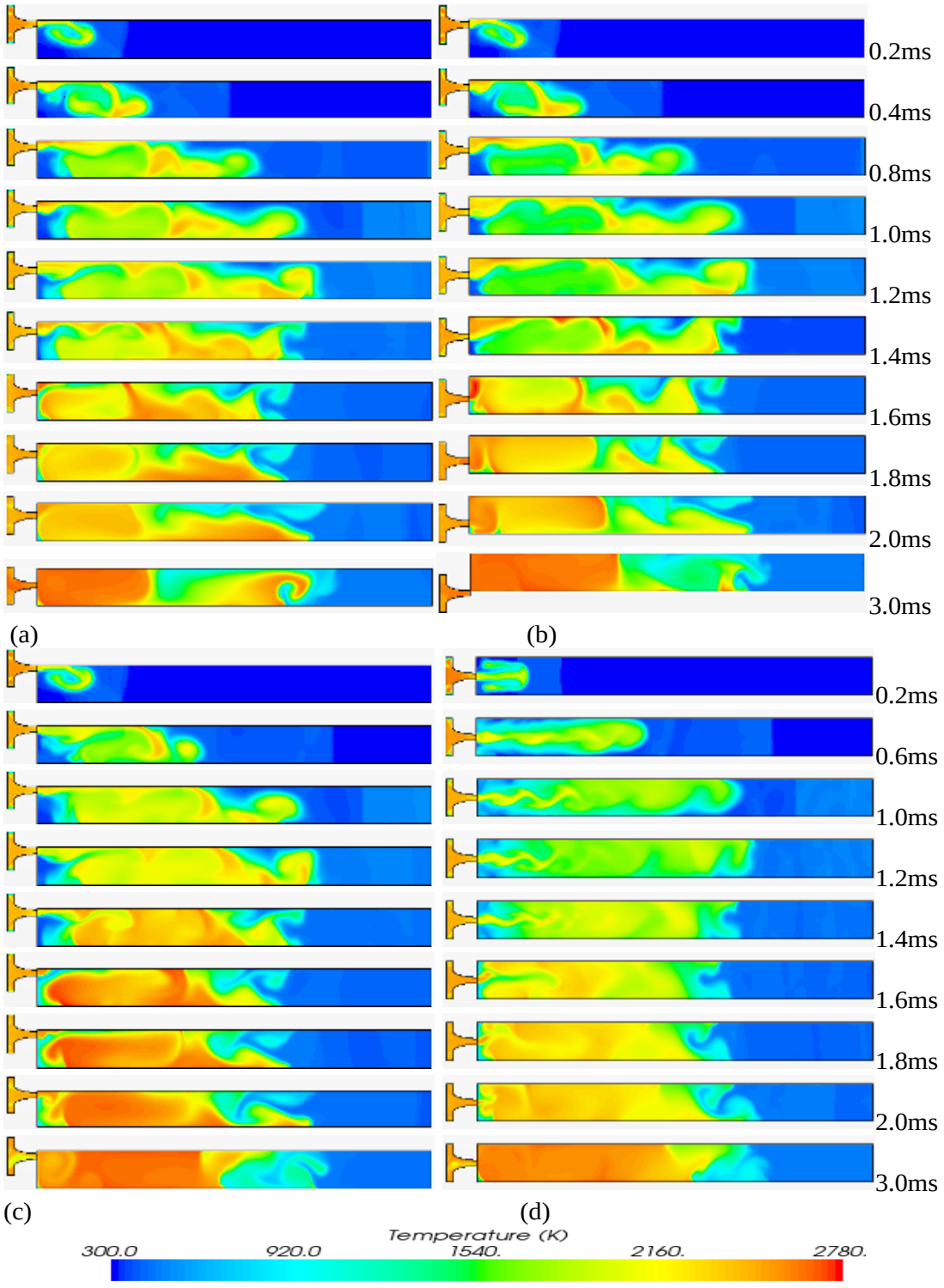

Figure 5.28 Temperature Levels for Methane Mixture for (a) 8.1 ms Traverse (b) 3.1 ms Traverse (c) Near-Wall (d) Centered Stationary

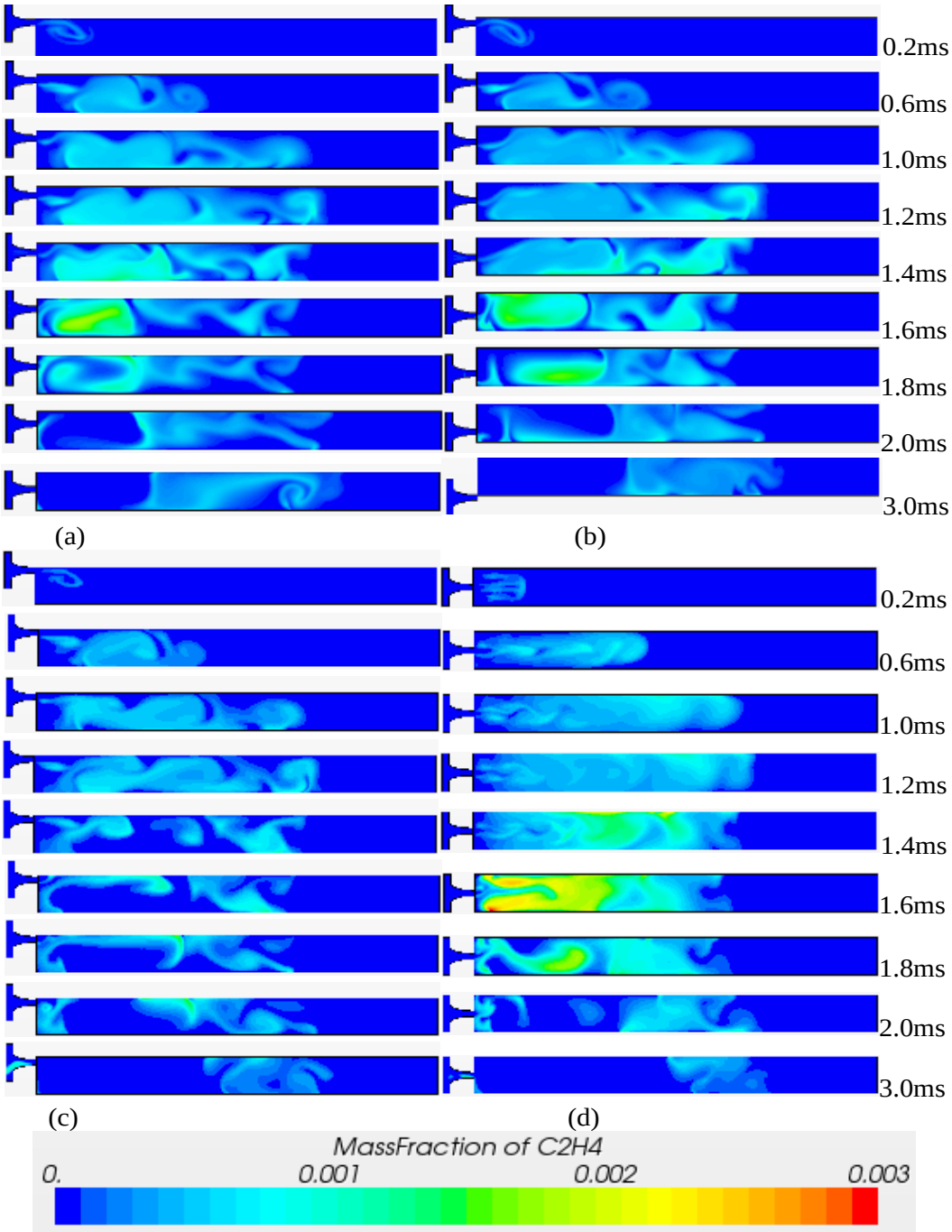

Figure 5.29 C_2H_4 Mass Fraction Contours for Methane Mixture at (a) 8.1 ms Traverse Jet (b) 3.1 ms Traverse Jet (c) Near-Wall Jet and (d) Centered Stationary Jet

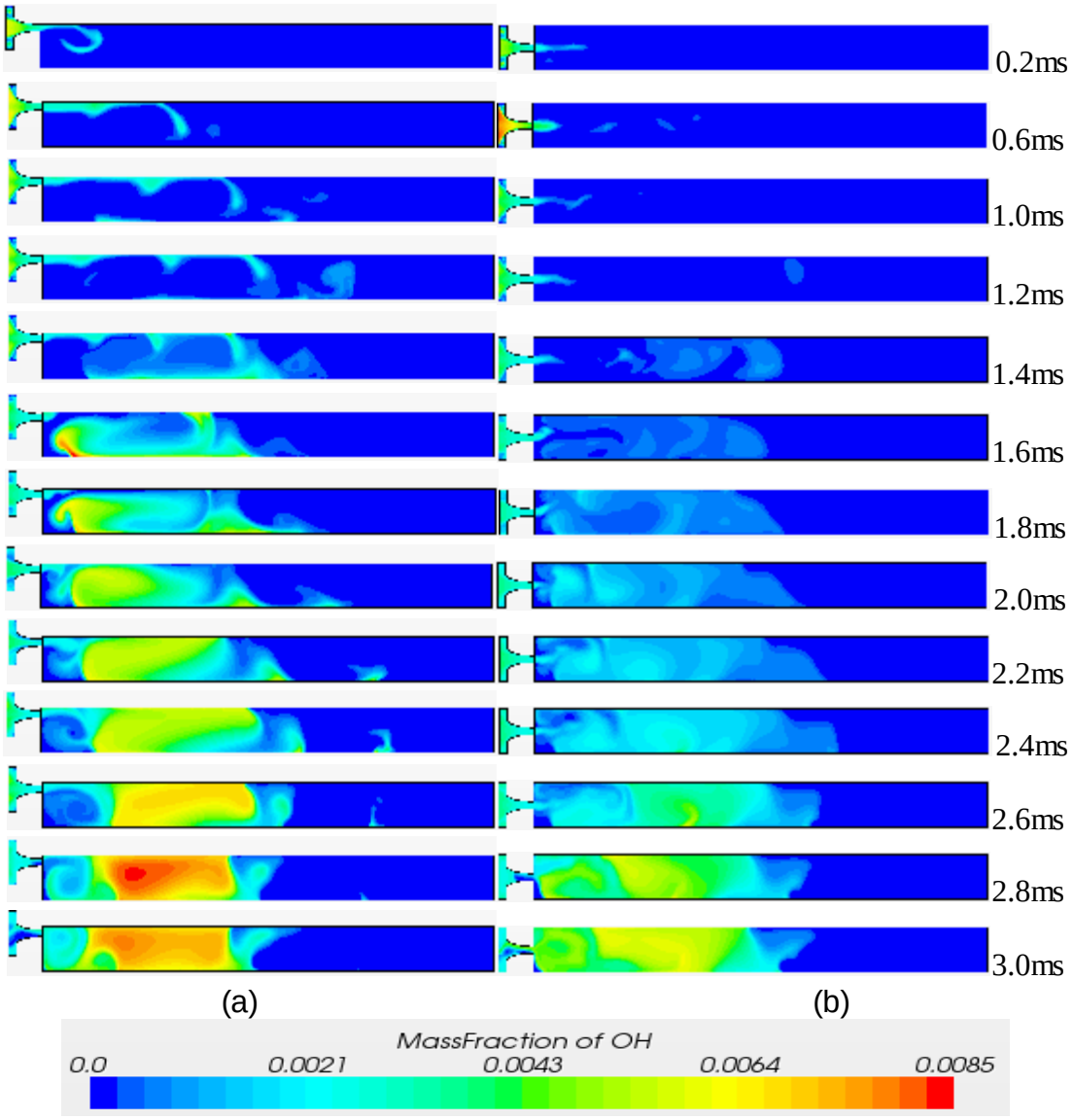

Figure 5.30 OH Mass Fraction Contours for Methane Mixture in (a) Near-Wall Jet and (b) Centered Stationary Jet

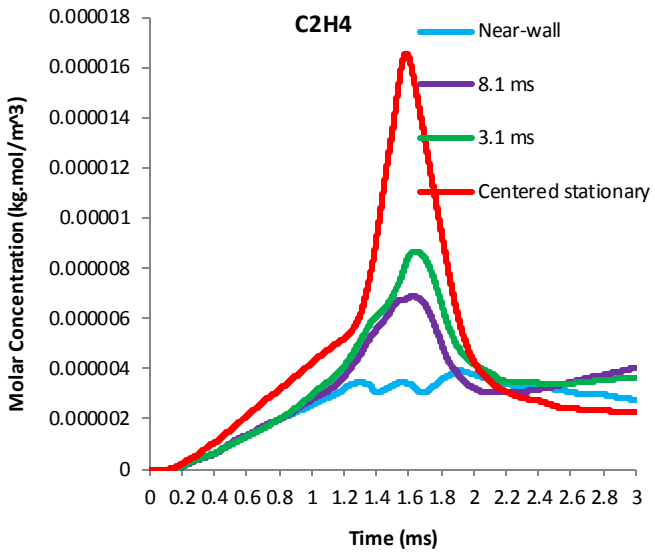

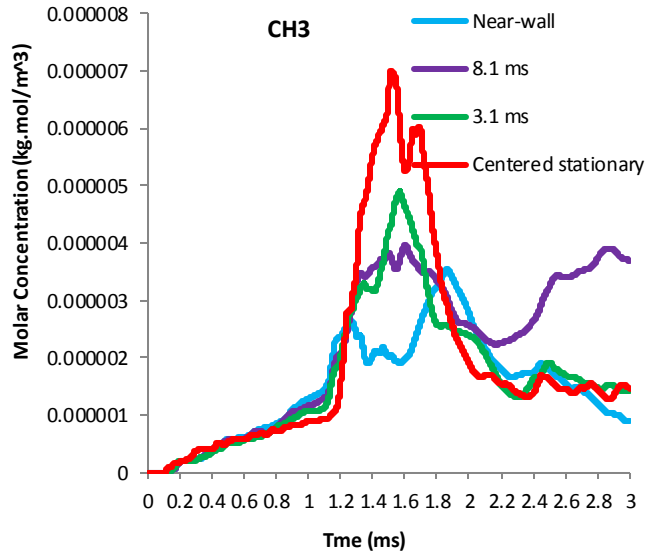

(b)

Figure 5.31 CVC Chamber-Averaged Molar Concentration Histories of (a) CH_3 and (b) C_2H_4 Intermediate Species in the CVC Chamber for Stoichiometric Methane Mixture

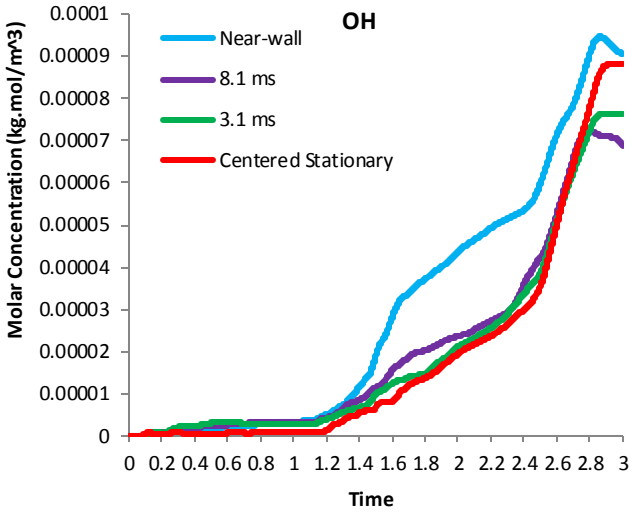

(a)

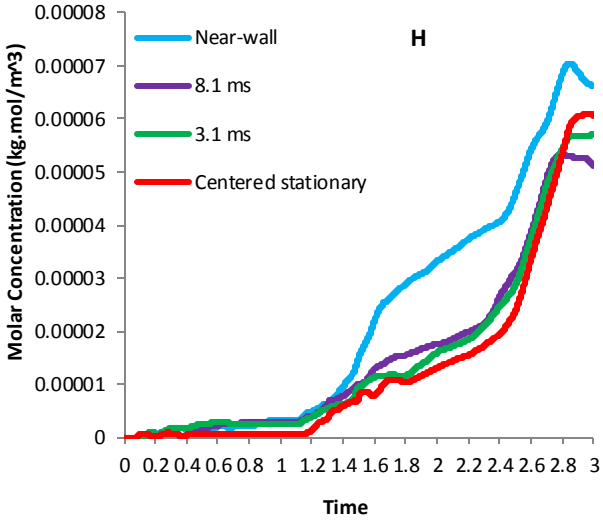

(b)

Figure 5.32 CVC Chamber-Averaged Molar Concentration Histories of OH And H Intermediate Species in the CVC Chamber for Stoichiometric Methane Mixture

6. EFFECT OF JET CHEMICAL ACTIVITY AND COMBUSTION MODELS

6.1 Introduction

A jet of hot gas can serve as an ignition source in combustion devices, such as automotive engines, pulsed detonation engines and wave rotor combustors. Hot-jet ignition involves complex flow phenomena such as vortex evolution, fluid mixing, and turbulence generation. Further, the penetrating and distributed nature of ignition can be affected by mixture non-uniformity and can be advantageous for ignition success, thermal management, and emissions control. The jet itself may be inert or chemically reactive. In a hot jet produced by partial or recent combustion of an adjacent mixture, active radicals present may significantly affect the ignition process of the premixed mixture to be ignited, usually in a constant volume combustor (CVC). In a wave rotor constant volume combustor, rapid ignition and combustion also involves complex interactions of pressure waves with flames in the transient jet. In the present chapter, detailed numerical simulations are carried out to understand the effect of jet composition present in a turbulent hot jet on the ignition in an experimental constant-volume combustor. A transient but physically immobile hot jet is modeled in three ways: as an inert jet (nitrogen and argon), relatively inert and as a chemically active hot jet. Combustion is modeled in the main constant-volume chamber for methane, hydrogen and blended methane-hydrogen mixtures. The composition of the chemically active jet is determined from chemical equilibrium for rich ethylene mixture in a pre-chamber supplying the jet. Combustion is modeled in the main constant-volume chamber for stoichiometric methane mixture.

6.2 Inert Jet and Stable-Species Jet

Three different compositions are considered: a) products of combustion of rich combustion of ethylene and air, at equivalence ratio of 1.1, considering the major stable species as listed in Table 5.1, b) pure nitrogen, which is the major component of a typical jet, but is inert with respect to the major species considered; and c) pure argon.

The simulations with argon are intended to provide a sense of the variability of ignition processes when no active radicals are present in the jet. The argon and nitrogen jets differ due to thermal rather than chemical properties of the jet, and the jet behavior is affected by different gas density and different energy content due to variation in specific heats. The difference between argon and nitrogen jets at the same temperature then provides a point of reference to compare the difference between inert nitrogen and combustion-product jet composition due to chemical rather than thermal differences. The combustion products jet contains H_2 and O_2 which react to form small amounts of intermediate species H and OH. The presence of OH in the jet can significantly affect the combustion process as many of the reactions are started by OH attack [75]. For more detailed investigation of the effect of the small intermediate species present in the hot jet on the CVC chamber ignition, the small intermediate species need to be considered in the future works.

In Figure 6.1 the mass fraction levels for different hot jet composition for stoichiometric methane mixture in the CVC is presented for the three different jet compositions. Significant fuel consumption is seen only after 2.8 ms in case of inert argon jet while inert nitrogen jet shows this as early as 1.6 ms. It should also be noted that while shock-flame interaction causing the sudden compression plays decisive role in the ignition of the methane mixture as observed in earlier works [86], this shock compression is not sufficient to cause ignition in the case of argon jet. Careful examination of the frames in Figure 1 at 1.2 ms and 1.6 ms reveals backward movement and large distortion of the flame front, indicating a shock wave interaction with the flame. More detailed insight is possible from the fuel consumption rate averaged in the CVC chamber as presented in Figure. 6.2

for three different jets. For the sake of standardized presentation, the fuel consumption rate is averaged over the entire CVC chamber, although it is recognized that the fuel consumption activity is spatially localized. The fuel consumption trends for nitrogen jet and combustion products jet are similar with a relative delay of about 0.2 ms for the nitrogen jet. The low heat capacity of argon compared to nitrogen is attributed to lower ignition delay time in shock tube studies with argon as diluent. The chemistry heat release rate averaged in the main chamber presented in Figure. 6.3 indicates that the combustion is much faster in case of nitrogen inert jet.

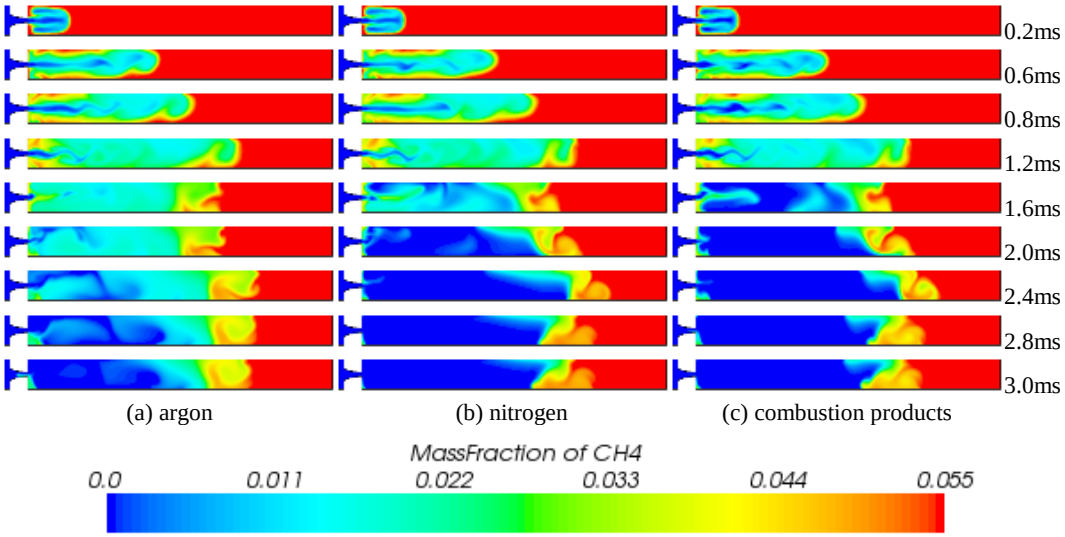

Figure 6.1 Fuel Mass Fraction Levels for Stoichiometric Mixture of Methane for Different Hot Jet Composition

For the analysis of combustion characteristics after ignition, the temperature levels for three different jet composition cases are presented in Figure 6.4. There appear to be large differences in the flame temperatures of combusting gases, between the case of the nitrogen jet and combusted gas jet, even though the ignition-delay difference (defined by rapid increase in fuel consumption) was relatively small. At some locations the difference between the two cases is as much as 700 K. The intermediate species production/consumption as well as reaction pathways for the combustion are thus important to analyze for this understanding this difference. As expected for the lower energy content of the argon jet, the temperatures are relatively lower.

The molar concentration histories in the CVC chamber are presented for important single-carbon (C_1) and two-carbon (C_2) species (respectively, CH_3 and C_2H_4), in Figures 6.5 and 6.6 respectively for different hot jets considered. Similar to previous line plots, the concentrations are averaged over the entire CVC chamber for standardization, but should be interpreted carefully, considering spatial localization. It is observed that that there is higher but relatively slower production of C_1 and C_2 species after ignition in case of nitrogen jet compared to combustion products jet. The molar concentration histories for the more stable species like OH, CO and H are also analyzed in order to understand the combustion completion leading to final products. The molar concentration history of CO averaged in the CVC chamber is presented in Figure. 6.7. It is observed from the figure that a large amount of CO is supplied from the pre-chamber in case of the combustion products jet and therefore the total amount of CO in the CVC chamber is significantly higher for this case. However, the production trend of CO in the CVC chamber for nitrogen hot jet and combustion products hot jet is similar. The molar concentration histories of H and OH in the CVC chamber are presented in Figures 6.8 and 6.9 respectively. Significantly larger amount of these two species are seen to be produced in case of combustion products hot jet as compared to the nitrogen inert hot jet case. This implies that while the fuel consumption is not significantly delayed in case of nitrogen hot jet compared to combustion products hot jet, but the combustion progress is still significantly delayed. The faster production of C_1 and C_2 species in when the hot jet contains even stable combustion products is apparently due to the ready disassociation of the jet species compared to the need for hot nitrogen to transfer enough thermal energy to break bonds in fuel and oxidant species before chemical reactions can begin. Thus temperature rise and the higher production of other reactive species, H and OH, are seen with the combustion products jet.

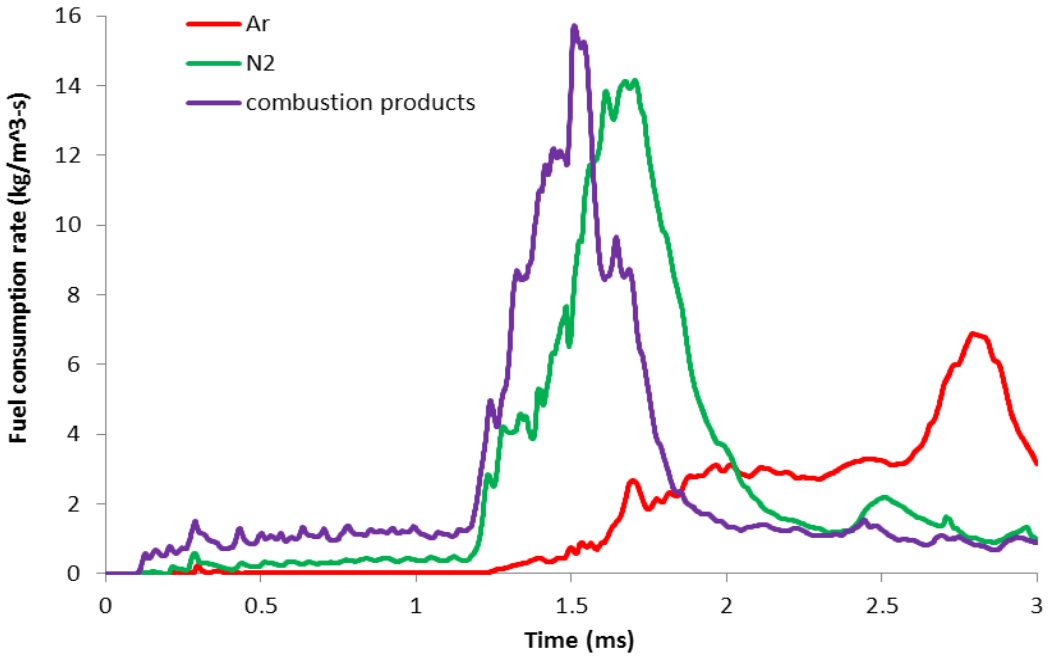

Figure 6.2 Fuel Consumption Rate Averaged in CVC Chamber for Hot Jets of Different Composition

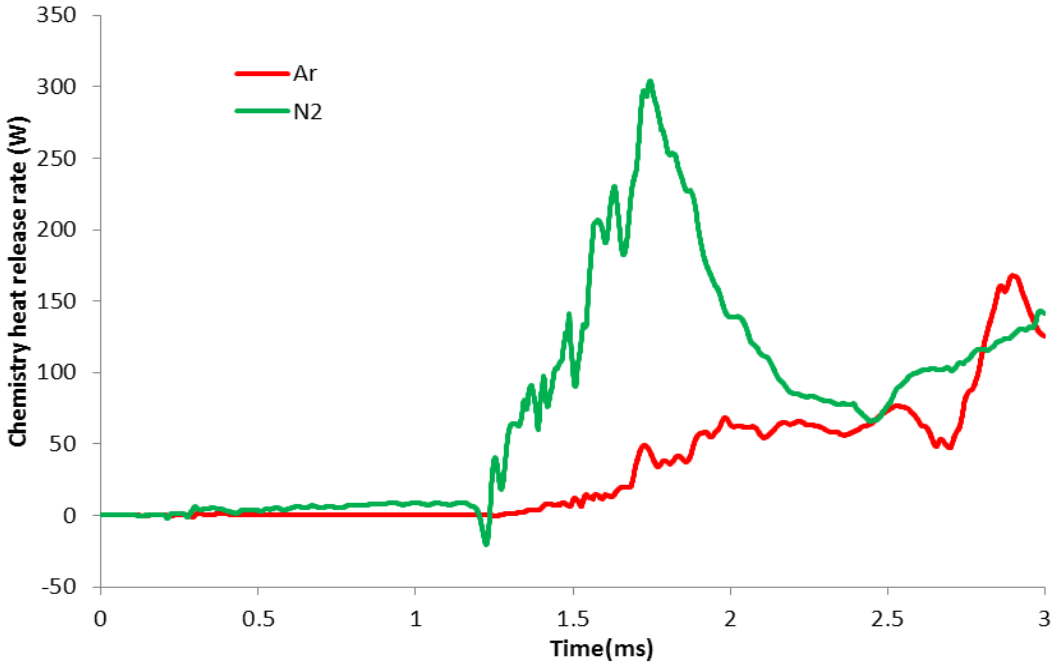

Figure 6.3 Chemistry Heat Release Rate Averaged in CVC Chamber for Argon and Nitrogen jets

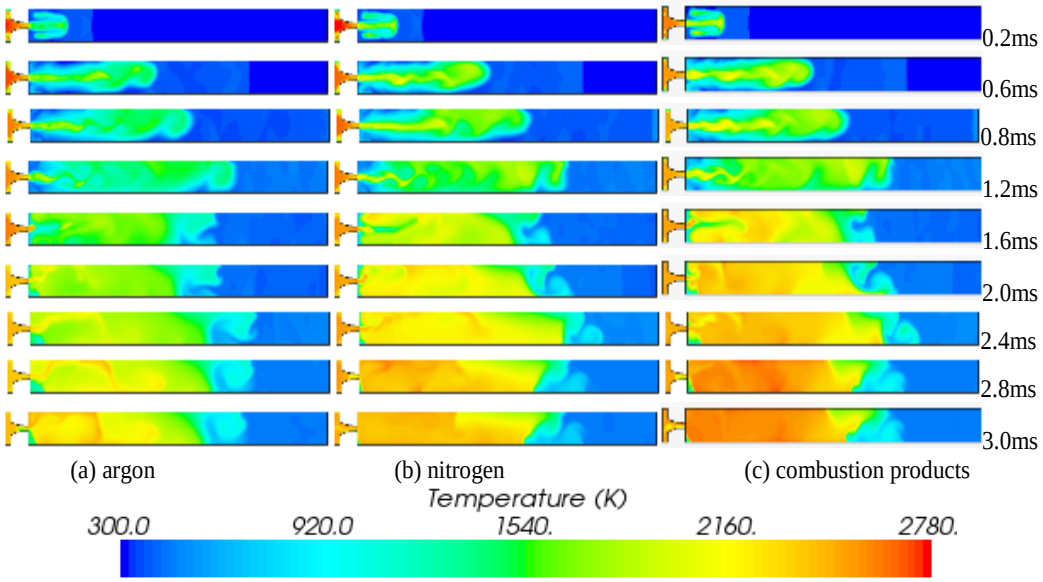

Figure 6.4 Temperature Levels for Stoichiometric Mixture of Methane for Different Hot Jet Composition

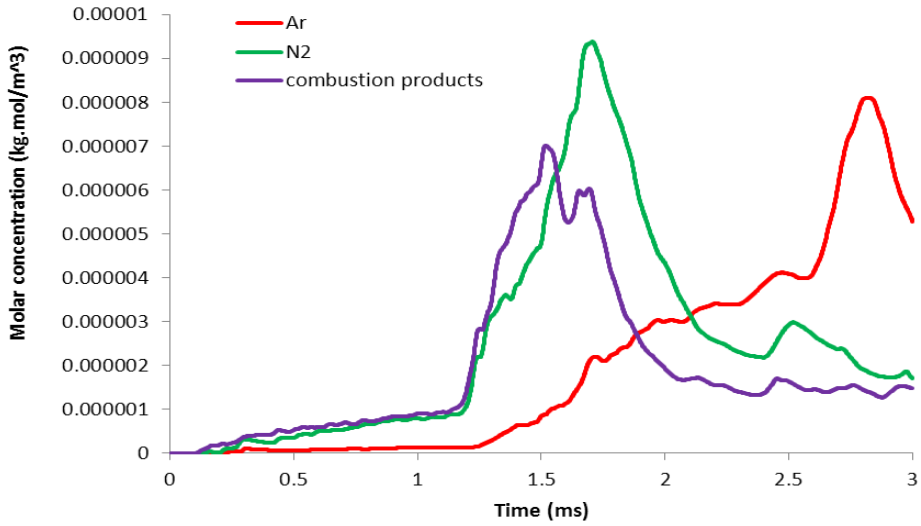

Figure 6.5 Molar Concentration of CH_3 Averaged in CVC Chamber for Hot Jets of Different Composition

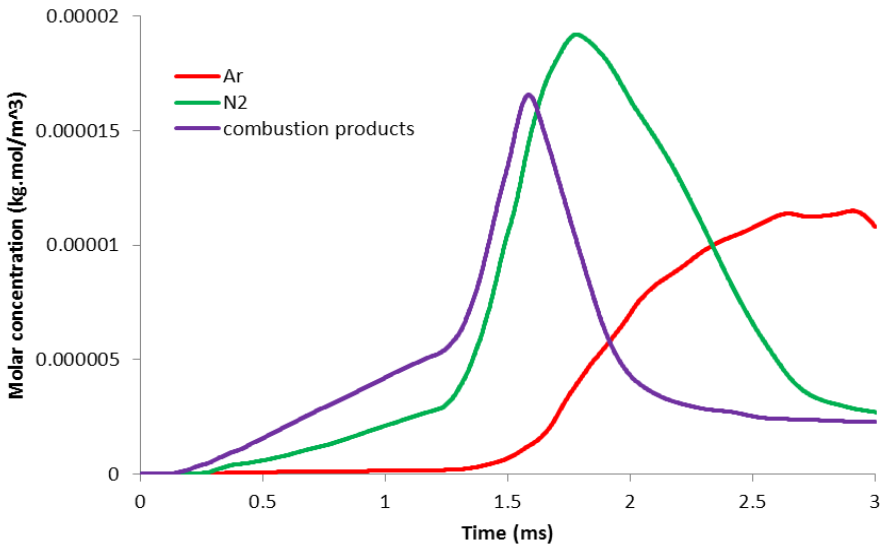

Figure 6.6 Molar Concentration of C_2H_4 Averaged in CVC Chamber for Hot Jets of Different Composition

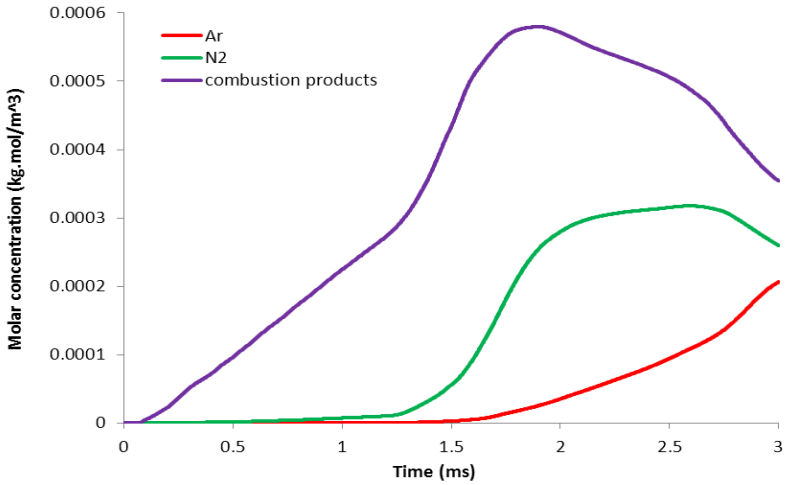

Figure 6.7 Molar Concentration of CO Averaged in CVC Chamber for Hot Jets of Different Composition

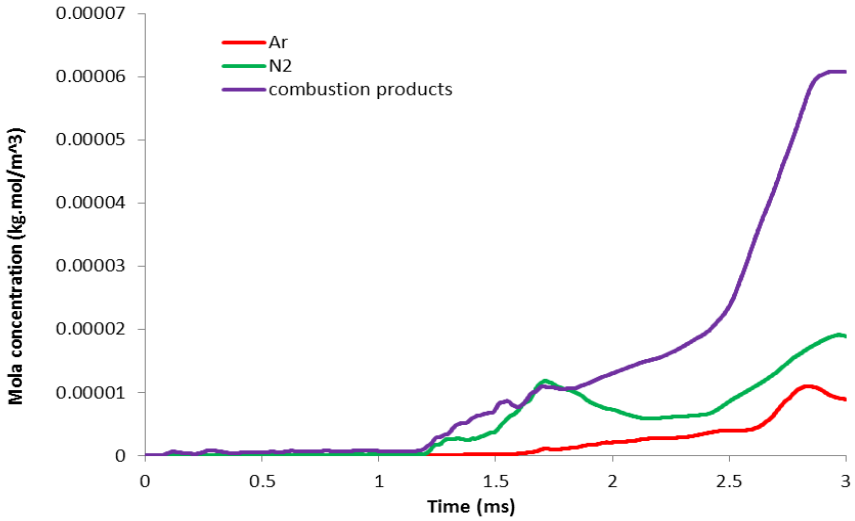

Figure 6.8 Molar Concentration of H averaged in CVC chamber for hot jets of different composition

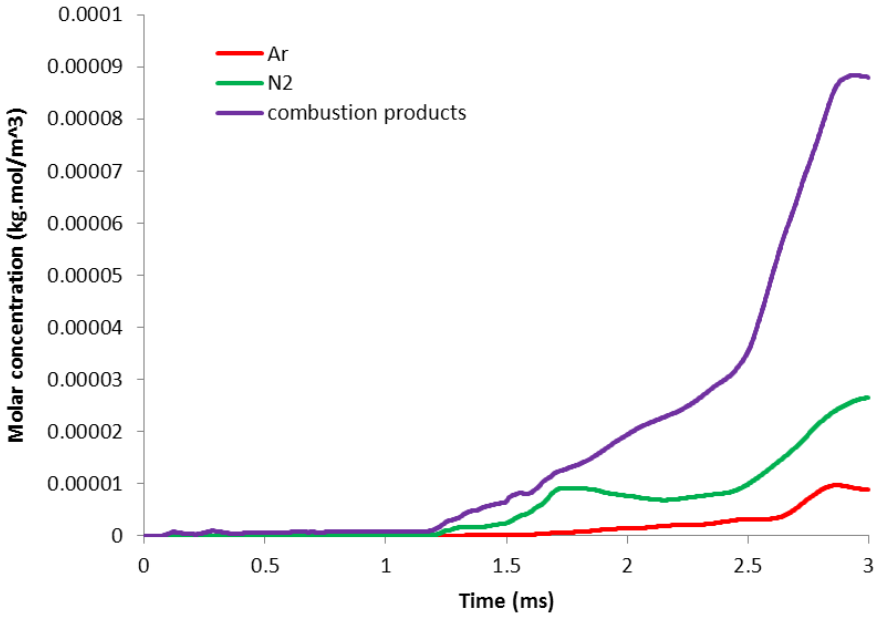

Figure 6.9 Molar Concentration of OH averaged in CVC chamber for hot jets of different composition

6.3 Effect of Minor Species

The effect of radical species in the jet is examined here, with the expectation that the radicals will have an impact in regions where the reaction rate is kinetically controlled. Fuel mass fraction contours for stoichiometric methane mixture in the main chamber at

different time levels for stable-species hot jet and radical-inclusive hot jet cases are presented in Figure 6.10. The total fuel consumption rate for the two cases is presented in Figure 6.11. When minor radical species of the detailed mechanism are included in the hot jet composition, the fuel is consumed more rapidly compared to the hot jet with only stable species. For methane, the inclusion of radical species present in very small amount appears to affect both the initial reaction rate in the CVC chamber, and the pace of cumulative reaction progress. The peak fuel consumption rate is seen about 0.2 ms earlier for the radical-inclusive hot jet. For methane fuel, the peak rate is controlled by the arrival of a reflected shock at essentially the same time (about 1.2 ms) for both cases; however, the radicals appear to sensitize the mixture such that the response to the shock compression is much quicker.

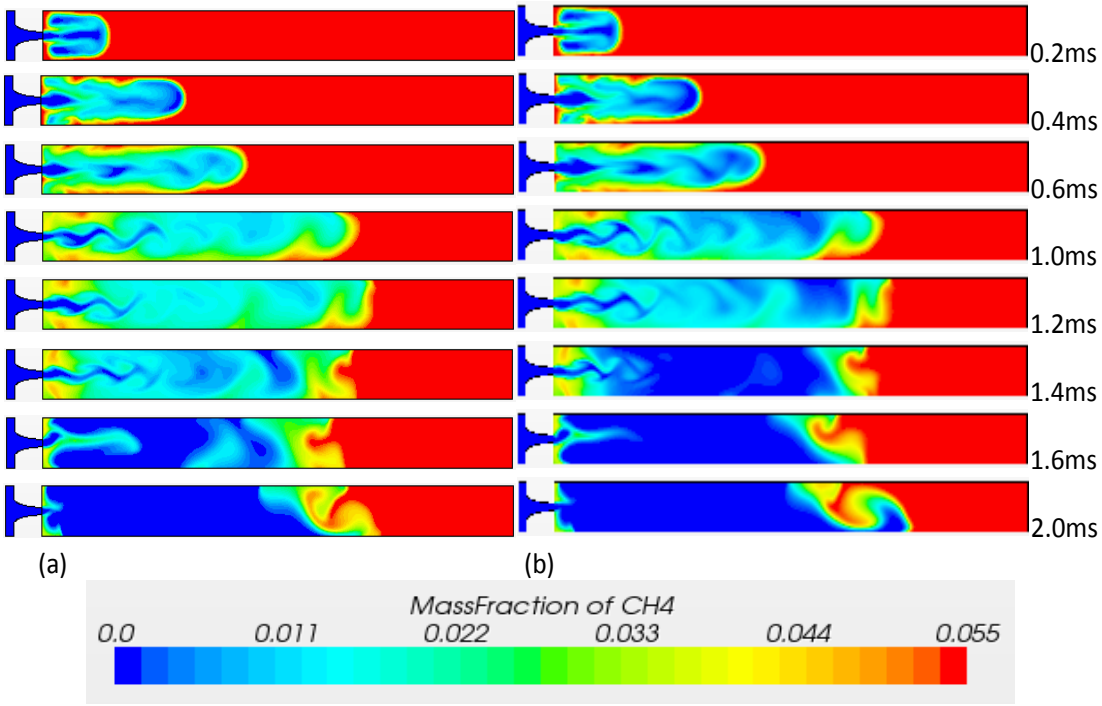

Figure 6.10 Fuel Mass Fraction for Stoichiometric Methane Mixture (a) Stable-species Hot Jet (b) Radical-Inclusive Hot Jet

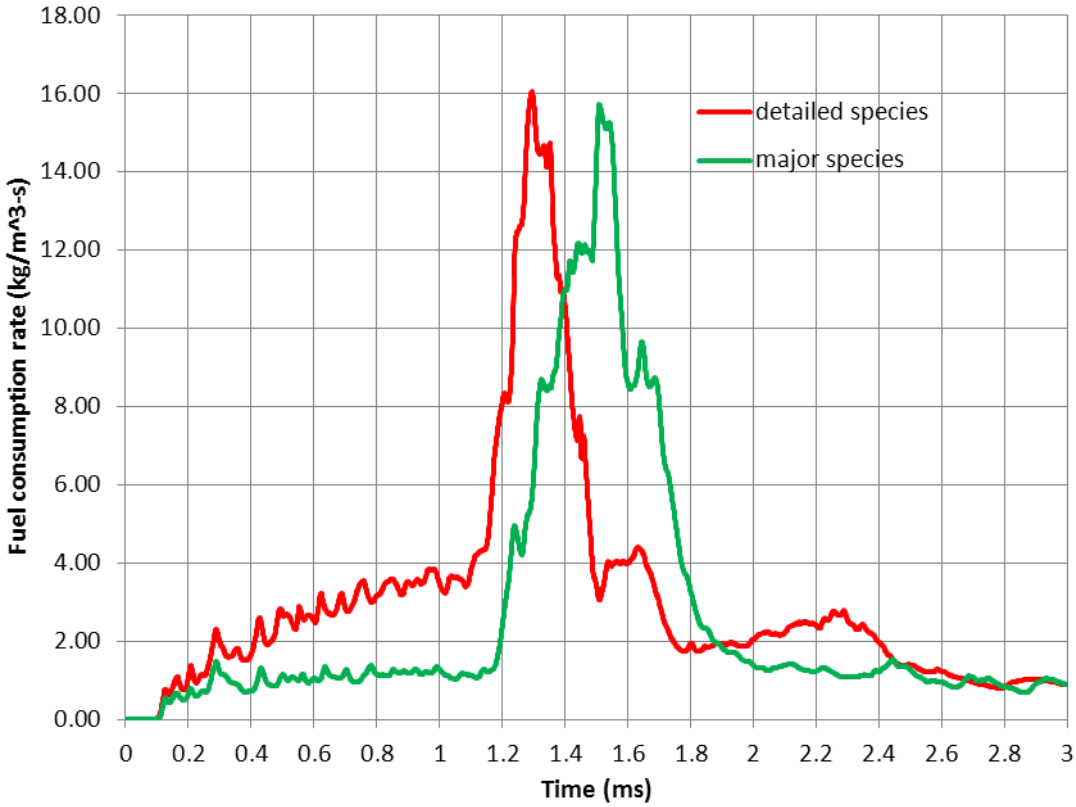

Figure 6.11 CVC Chamber Averaged Fuel Consumption Rate for Stoichiometric Methane Mixture for the Hot-Jet with Only Major Stable-species and including Radical Species of the Detailed Mechanism

6.4 Experimental Observations

For a qualitative comparison of the ignition characteristics and the combustion progress, high-speed video images of flame luminosity in ignition experiments are presented in Figure. 6.12. The main chamber mixture is stoichiometric methane. Two sets of images for two experiments with identical geometry and intended initial conditions are presented. There are noticeable differences in the observed pattern of luminosity of the jet ignition process. Quantitative comparison of ignition of the planar two-dimensional simulation with experiments is not intended. Nevertheless, the jet penetration, vortex structure, and distributed reaction zones in the simulation and experiment have similar features. The hot jet penetrates and mixes with the main chamber mixture for some time before a sudden increase in luminosity is seen around 2 ms in the experiment. Prediction of soot formation and radiation is not included in the current simulations.

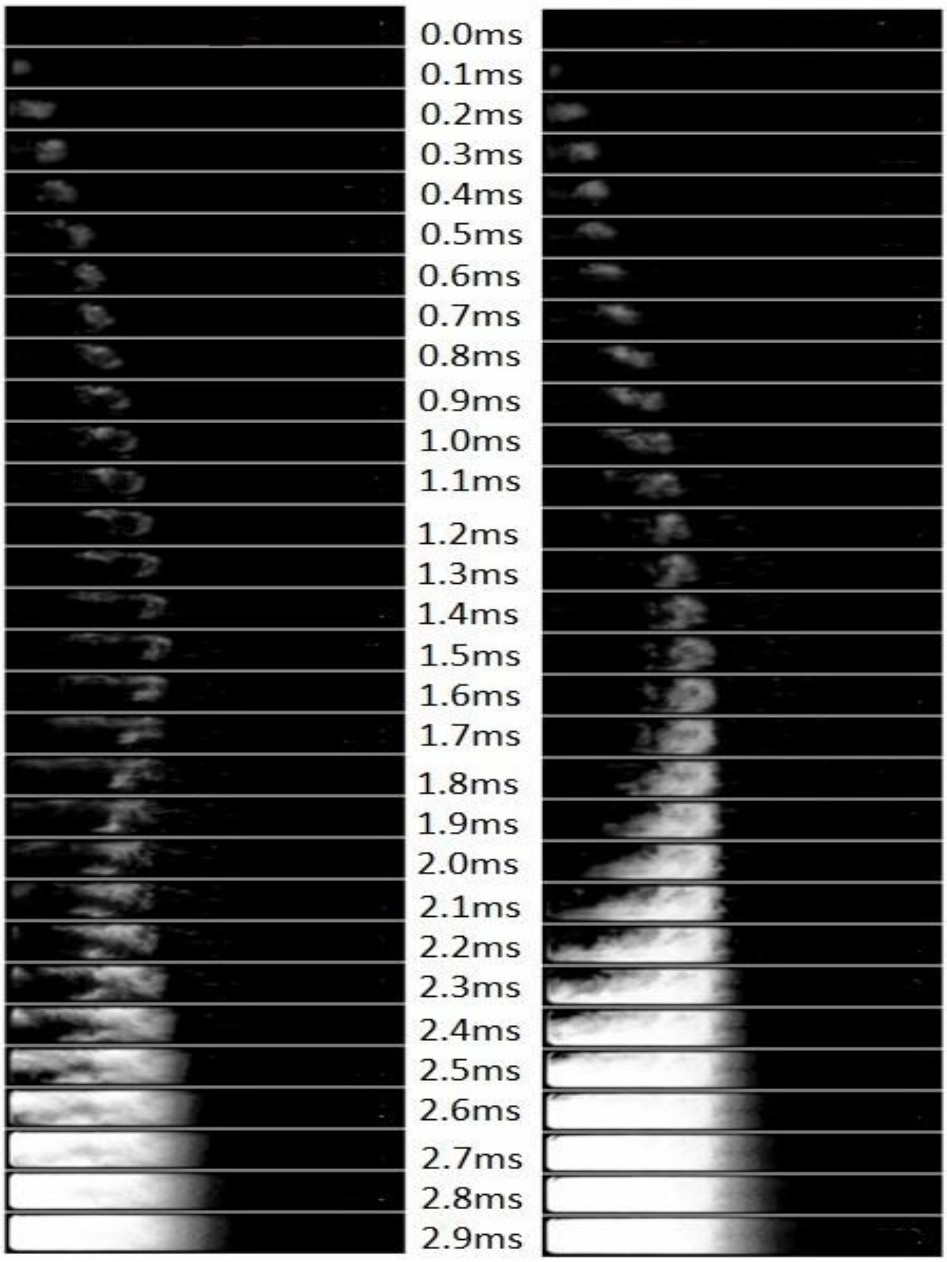

Figure 6.12 High-speed Video Images of Ignition of a Stoichiometric Methane-Air Mixture in the Main CVC Chamber, for two tests with the same Conditions [5]

6.5 Fuel Composition and Blending

Three different fuel compositions are examined by numerical simulation: pure methane, pure hydrogen and a methane-hydrogen blend. The blend used as fuel for the

present simulation is 60% CH_4 and 40% H_2 by volume. It is noted that the one mole of CH_4 requires two moles of O_2 for combustion, whereas one mole of H_2 requires 0.5 moles of O_2. This implies that the total oxygen consumption for this blended fuel is shared by methane and hydrogen in the ratio of 12:2, or 86% by methane.

Simulations have been conducted using the hot jet of stable combustion products for stoichiometric mixture with air for three fuels, with otherwise identical conditions and the same numerical grid and methods. The overall reaction progress can be best tracked by monitoring oxygen consumption Methane combustion generates hydrogen, making the tracing of fuel consumption problematic for the blend fuel. A comparison of oxygen consumption for pure hydrogen, pure methane and blend mixture is presented in Figure 6.13. It is evident that the reaction rate for hydrogen is significantly higher than for methane, both initially and throughout the ignition process. It can also be noticed that the reflecting shock is implicated in the high reaction rates in all the three cases. The pure hydrogen case shows much greater chemical sensitivity through faster response to the shock arrival. However, the blending of a small amount of hydrogen (as measured by oxygen demand) does not significantly help the ignition of methane, within the limits of the chemical kinetics considered. It should also be noted that the reaction mechanism used for blend mixture combustion is same as used for pure methane (DRM19). This reduced mechanism does not have all the detailed elementary reactions of hydrogen combustion and therefore a more detailed reaction mechanism would be necessitated for better understanding of combustion in blend mixture case. Thus it is premature to make stronger conclusions.

The concentration of H and H_2 present in the reacted zone depends upon various factors such as, H_2 mass fraction in the mixture, H_2 injected from pre-chamber, production of H_2 from decomposition of CH_4 and consumption of H_2 as the reaction progresses. As the combustion progress the hydrogen production is seen to shift towards the nozzle end of the channel and the flame. At high temperature, the increase in concentration of H radicals due to presence of H_2 is expected to induce a fast procession of $H + CH_4 \rightarrow CH_3 + H_2$.

Comparison of H concentration in the plot in Figure. 6.14 indicates production of excess H radicals in the blended mixture compared to pure methane as CH_4 consumption rate starts to increase around 1.1ms until it reaches the maximum value. Then there is significant scavenging of H radicals as consumption rate of CH_4 starts to die down from 1.3ms. This trend is not noticeable for pure methane mixture where H radicals continue to increase steadily signaling change in reaction chemistry during the ignition event. A similar trend is observed for OH radical concentration. This indicates the active progression $O+H_2<=>H+OH$ mechanism during the main ignition event.

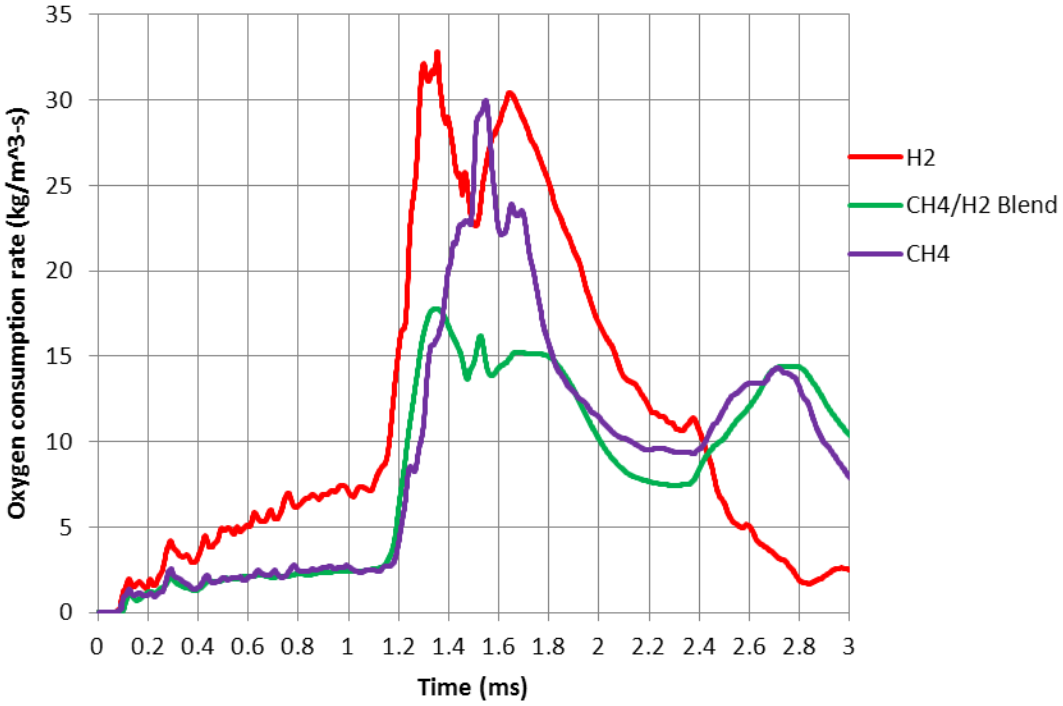

Figure 6.13 CVC Chamber Averaged Consumption Rate of Oxygen for Different Stoichiometric Mixtures

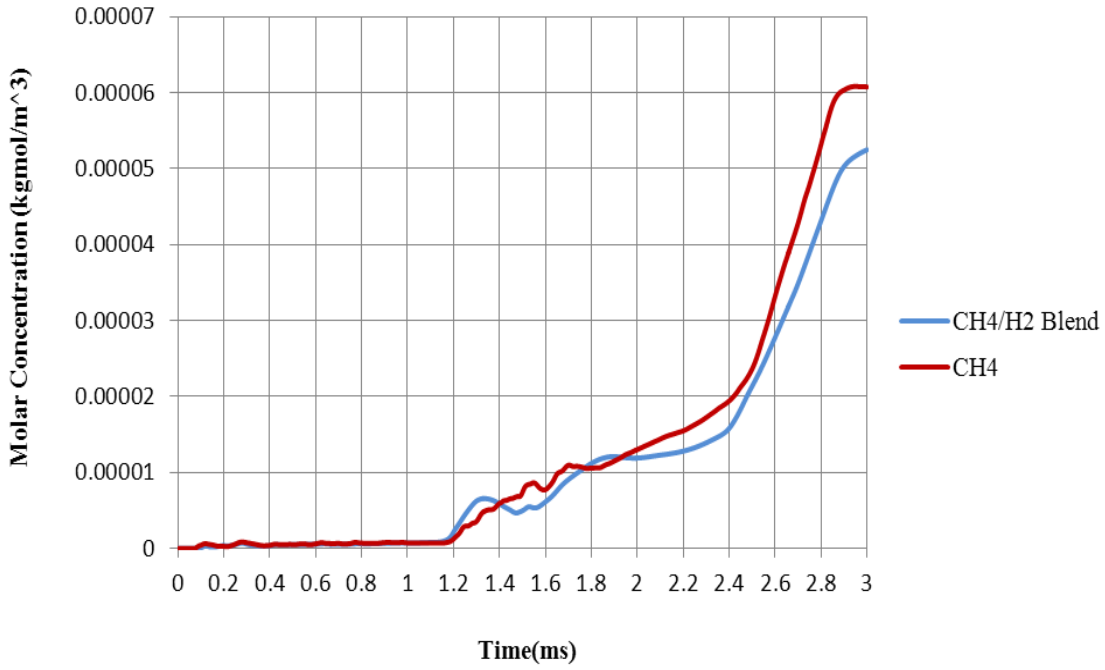

Figure 6.14 CVC Chamber Molar Concentration of H for Methane-Hydrogen Blend and Pure Methane in Main Chamber

6.6 Effect of Combustion Models

The eddy-break up model relates the rate of reaction to the dissipation rate of turbulent eddies containing products and reactants. The dissipation rate of turbulent eddies is assumed to be proportional to the ratio of the turbulent kinetic dissipation and turbulent kinetic energy, ε/k [41]. When being mixing controlled the finite-rate chemistry version of the EBU model would be expected to behave identically to the standard model [40].

A peculiar situation that may occur when combining the EBU model with a multistep reaction mechanism is that several reactions will proceed at the same rate. The reason for this is that the mixing rate of a species that is only present at low concentration is likely to be the limiting factor. If this species is taking part in several reactions, the rates of these reactions are all the same and are given by the mixing rate of this particular species; although it is probably more reasonable that the fastest reaction consumes the most [40].

Kong and Reitz [87] employed combined approach of turbulent mixing and chemical kinetics for HCCI engine and concluded that the effects of turbulent mixing on the reaction rates needed to be considered to correctly simulate the combustion and heat release rates.

In the present work, simulations are carried out using hybrid eddy break mode (which includes both mixing time scale and kinetics time scale) and kinetics only model to understand the effect of these two approaches on combustion modeling.

The fuel mass fraction levels are shown for hybrid EBU model and kinetics only model in Figure 6.15. It can be observed that the fuel consumption in case of kinetics only model is continuous and uniform from the time hot jet enters the main chamber. On the other hand for the hybrid EBU model there seems to be a lag in significant consumption of fuel. These observations can be seen in Figure 6.16 which shows the averaged fuel consumption rate in the main chamber. The fuel consumption for hybrid EBU is seen to significantly increase after 1.2 ms when there is sudden consumption of fuel in the main chamber. To understand process of the decomposition of fuel and eventual conversion into final products, the intermediate species formation are analyzed. In Figure 6.17, the mass levels of an important intermediate species CH_3 is presented at different points of time for the two combustion models. It is seen that in case of hybrid EBU the production of CH_3 is significantly larger and more distributed while in case of kinetics only mode it is produced only on interface between burnt and unburnt region, that is, flame. Looking at OH mass fraction in Figure 6.18 it is observed that there is significantly higher and early production of OH in case of kinetics only model. It can be inferred from this that the combustion completion is faster and more in case of kinetics only model. This can be further observed from the temperature levels at different point of time during combustion in the main chamber presented in Figure 6.19.

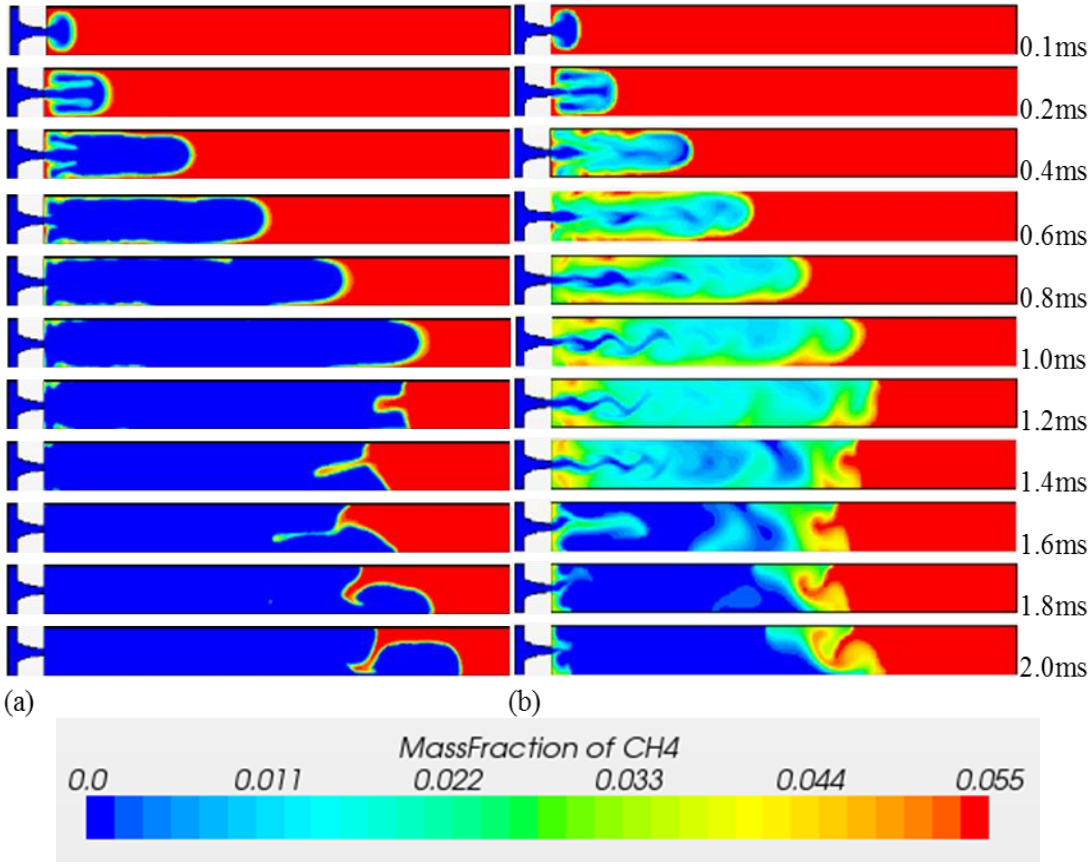

Figure 6.15 Fuel Mass fraction contours for methane using DRM19 (21 species) reaction mechanism (a) Kinetics Only Model (b) Hybrid Eddy Break Model

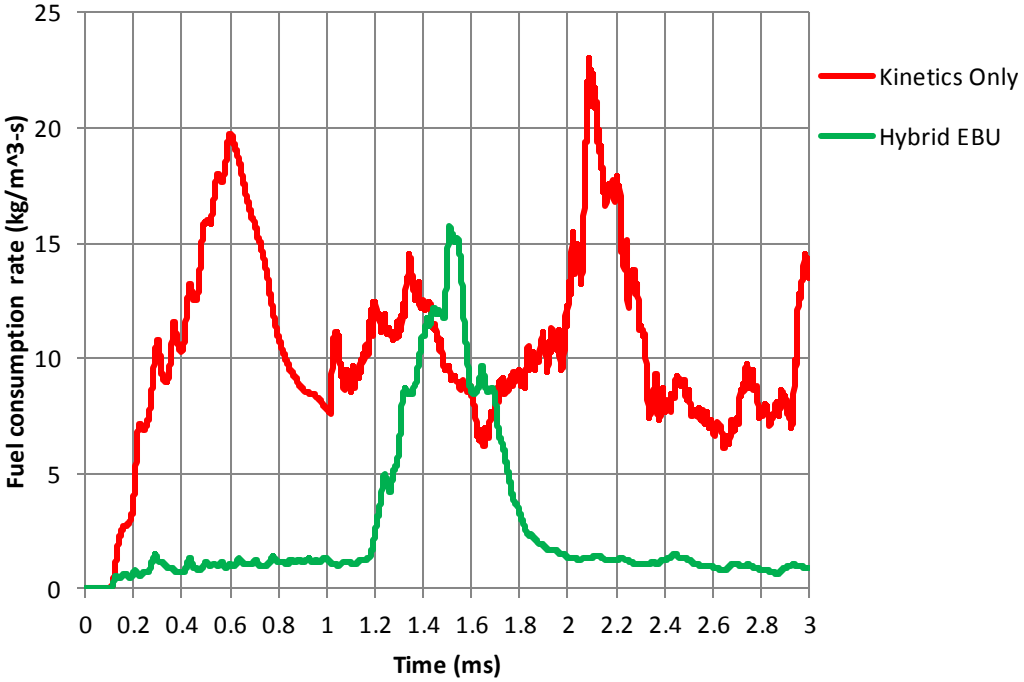

Figure 6.16 Averaged Fuel Reaction Rate in Main Chamber for Stoichiometric Methane Mixture for Kinetics Only and Hybrid EBU Combustion Models

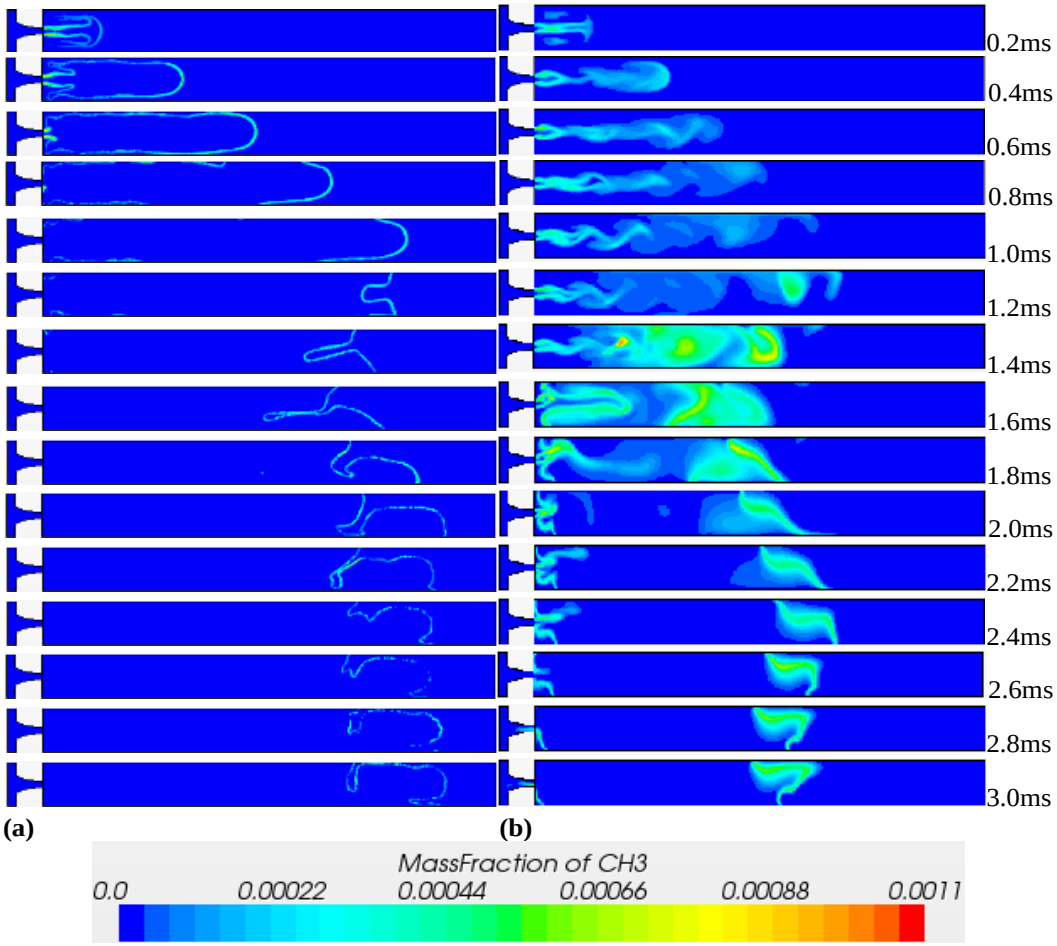

Figure 6.17 CH_3 Mass Fraction at Different Time Levels for Methane using DRM19 (21 species) Reaction Mechanism (a) Kinetics Only Model (b) Hybrid Eddy Break Up Model

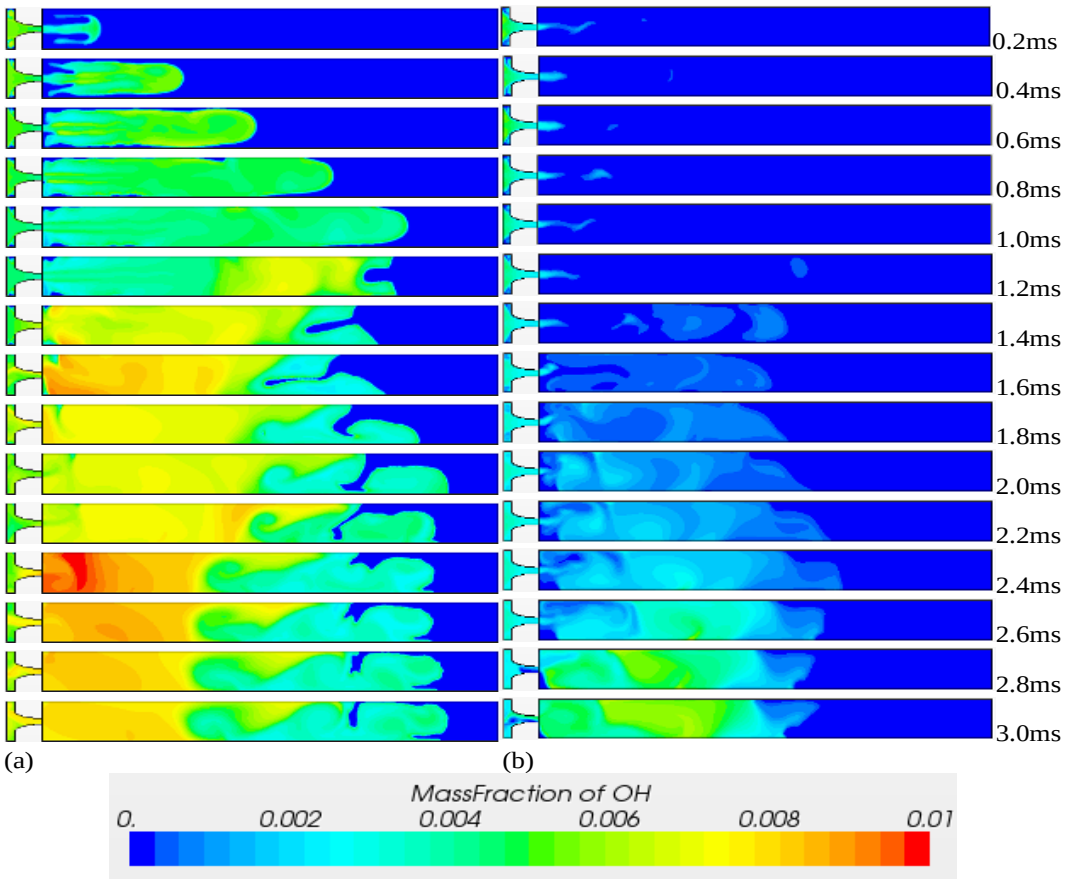

Figure 6.18 OH Mass Fraction at Different Time Levels for Methane Using DRM19 (21 Species) Reaction Mechanism (a) Kinetics Only Model (b) Hybrid Eddy Break Up Model

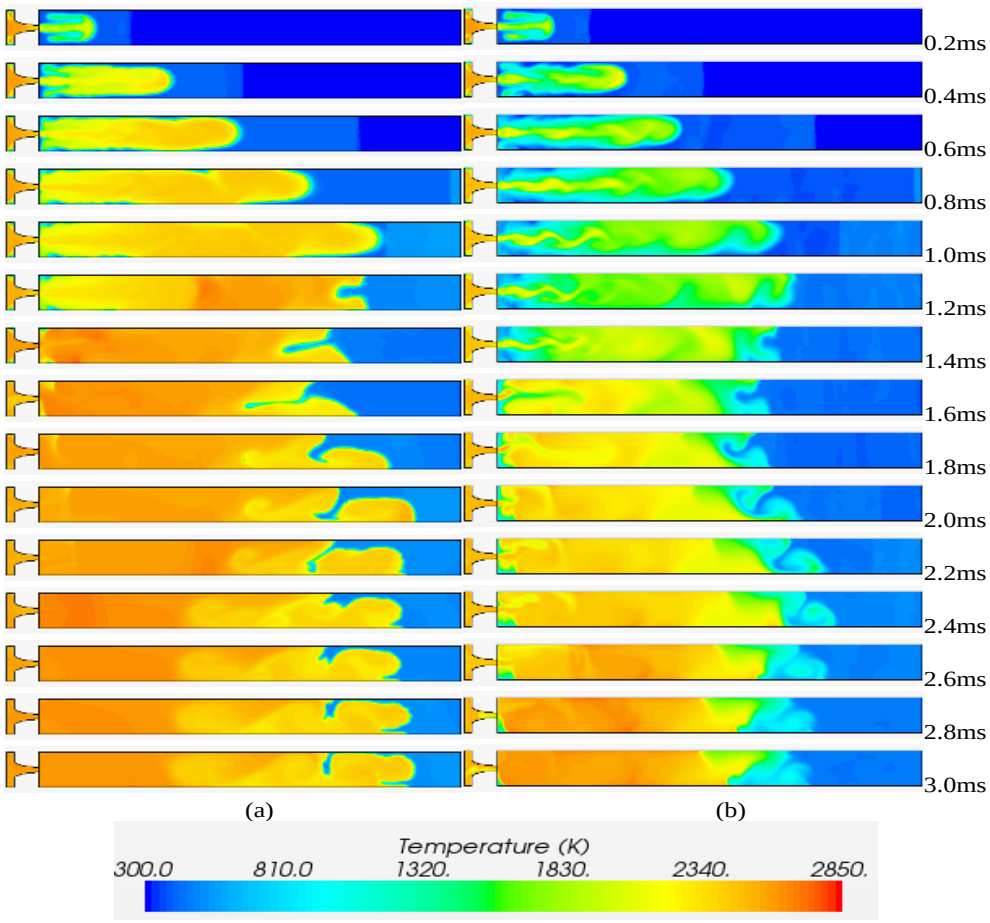

Figure 6.19 Temperature at Different Time Levels for Methane Using DRM19 (21 Species) Reaction Mechanism (A) Kinetics Only Model (B) Hybrid Eddy Break Model

7. CONCLUSION AND RECOMMENDATIONS

7.1 Conclusions

The hot jet ignition process for hydrocarbon-air mixtures was analyzed using numerical simulations of non-reacting and reacting processes in a constant-volume combustor. Detailed study was carried out for jet mixing and behavior, ignition delay, reaction pathways, and shock-flame interaction. Simulations were conducted using hybrid turbulence-kinetic schemes and kinetics-only schemes using detailed, skeletal and global reaction mechanisms.

The mixing of hot jet with cold mixture in the main chamber is compared with high speed video images from experiments, with the qualification that predictions from two-dimensional simulations cannot be quantitatively matched with the measurements in the actual three-dimensional experimental geometry. The ignition delay time and jet behavior are also compared with experimental data. The amount of mixing and temperature level are analyzed using High Temperature Mixedness (HTM). Traversing jet at different speeds shows different jet behavior in the main chamber compared to stationary centered jet. Near-wall jet shows enhanced mixing due to counter-rotating vortices as the jet impinges on wall.

The reacting simulations show the inadequacy of global reaction mechanisms for studying ignition delay and combustion progress. Detailed and skeletal reaction mechanisms are able to give more insight on ignition process both quantitatively and qualitatively. The ignition delay is found to be higher for methane mixture compared to ethylene and propane mixtures for both stationary and traversing jet cases. The traversing hot jet in the near-wall jet case has lower ignition delay than the stationary jet for methane mixture.

Shock-flame interaction is found to play significant role in the ignition and combustion processes, particularly for the case of the relatively less reactive methane at the given initial temperature. The ignition for methane mixtures happens after shock returns and causes compression of the non-combusted mixture leading to sudden fuel consumption. Delaying the shock return from main chamber end wall also delays the ignition for methane mixture.

Reaction pathways for combustion of methane mixture in the main chamber is mainly via disintegration into C1/C2 species and then their subsequent consumption for hybrid turbulence-kinetics scheme. The reaction pathways for kinetics-only scheme shows the continuous consumption of fuel from beginning and production of C1/C2 species mainly in the flame region. Traversing jets combustion shows different reaction pathways compared to stationary jet. For methane mixture the near wall jet shows less production of C1/C2 species and more production of relatively stable species like OH.

The choice of combustion modeling schemes; hybrid and kinetics-only has significant impact on ignition delay predictions, reaction pathways, and combustion progress. The kinetics-only scheme does not take into account turbulent mixing and hence less suited for the hot jet ignition process in the present investigation.

7.2 Recommendations for Future Work

The present work carried out detailed numerical investigation of combustion in hot jet ignition process using a constant-volume combustor. The following recommendations are made for future work based on the current work:

1. Detailed numerical simulations should be carried out using three-dimensional geometry configuration for better quantitative comparison of numerical results with experimental data.
2. The effect of shock-compression and shock-flame interaction on ignition and flame propagation in constant-volume combustor should be analyzed in detail. The effect of shock-flame interaction should be separated from the jet traverse for understanding its effect on ignition.
3. Design of experiments study can be carried out from the information obtained from CFD to reduce the number of tests needed in future.
4. In the present work, the hybrid and kinetics-only schemes were compared for only methane mixture in the main chamber. The effect of turbulence-chemistry interaction can be studied in more detail for different fuel mixtures and equivalence ratio.
5. Heat transfer was not modeled in the present work. More realistic heat transfer modeling should be included in the future work.
6. The leakage between the prechamber and main chamber was not modeled in the present work. It would be good to consider leakage in future works.
7. The modeling of hot-jet ignition should be extended to a range of initial mixture temperature that is high enough to be representative of typical combustor operation. Many of the conclusions of this work may be qualified by the significantly higher chemical reaction rates at higher temperatures, relative to jet mixing rates and fluid dynamic processes of shock-flame interaction.

LIST OF REFERENCES

LIST OF REFERENCES

[1] E. Toulson, H. J. Schock, and W. P. Attard, "A Review of Pre-Chamber Initiated Jet Ignition Combustion Systems," *SAE Paper*, p. 2263, 2010.

[2] W.P. Attard, E. Toulson, A. Huisjen, X. Chen, G. Zhu, and H. Schock, "Spark Ignition and Pre-chamber Turbulent Jet Ignition Combustion Visualization," *SAE Paper*, p. 823, 2012.

[3] D. H. Lieberman, K. L. Parkin, and J. E. Shepherd, "Detonation Initiation by a Hot Turbulent Jet for Use in Pulse Detonation Engines," in *38th Joint Propulsion Conference*, Indianapolis, IN, 2002.

[4] Y. Matsutomi, S. E. Meyer, S. D. Wijeyakulasuriya, Z. Izzy, M. R. Nalim, M. Shimo, M. Kowalkowski, and P. H. Snyder, "Experimental Investigation on the Wave Rotor Combustor," in *46th Joint Propulsion Conference*, Nashville, TN, 2010.

[5] U.I. Perera, S.D. Wijeyakulasuriya, and M.R. Nalim, "Hot Combustion Torch Jet Ignition Delay Time for Ethylene-Air Mixtures," in *49th AIAA Aerospace Sciences Meeting*, Orlando, FL, 2011.

[6] P. Akbari and M. R. Nalim, "Review of Recent Developments in Wave Rotor Combustion Technology," *AIAA Journal of Propulsion & Power*, vol. 25, pp. 833-844, 2009.

[7] J.J. Keller, "Pressure wave machine with constant-volume combustion as a superstage for gas turbines," *Asea Brown Boveri*, Technical Rept. CRBT 90-20. 1990.

[8] I. U. Perera, "Experimental Investigation into Combustion Torch Jet Ignition of Methane-Air, Ethylene-Air, and Propane-Air Mixtures," MS Thesis, Purdue University, Indianapolis, 2010.

[9] E. Toulson, H. J. Schock, and W. P. Attard, "A Review of Pre-Chamber Initiated Jet Ignition Combustion Systems," *SAE Paper*, p. 2263, 2010.

[10] W. P. Attard, and H. Blaxill, "A Lean Burn Gasoline Fuelled Pre-Chamber Jet Ignition Combustion System Achieving High Efficiency and Low NOx at Part Load," *SAE Paper*, p.1146, 2012.

[11] H.G. Wolfhard, "The ignition of combustible mixtures by hot gases," *Jet Propulsion*, vol. 28, Iss. 12, pp. 798-804, 1958.

[12] Z. J. Fink, and M. Vanpée, "Overall kinetics of hot gas ignition," *Combustion Science and Technology*, vol. 11, 5-6, pp. 229-238, 1975.

[13] R. J. Cato, and J. M. Kuchta, "Hot Gas Ignition Temperatures of Hydrocarbon Fuel Vapor-Air Mixtures," *Bureau of Mines*, Tech. Rep. AD0643518, 1966.

[14] V. I. Tarzhanov, I. V. Telichko, V. G. Vil'danov, V. I. Sdobnov, A. E. Makarov, S L Mukhin, I. G. Koretskii, V. A. Ogarkov, V. V. Vlasov, A. D. Zinchenko, A. V. Vorob'ev, A. N. Grachev, V. A. Matkin, and V. A. Potashnikov, "Detonation of Propane-Air Mixtures under Injection of Hot Detonation Products," *Combustion Explosion and Shock Waves*, vol. 42, pp. 336-345, 2006.

[15] F. Mayinger, M. Jordan, A. Eder, I. S. Zaslonko, V. P. karpov, and S. M. Frolov, "Flame-Jet Ignition of fuel-Air Mixtures. Experimental Findings and Modeling," in *17th International Colloquium on the Dynamics of Explosions and Reactive Systems (ICDERS)*, Heidelberg, Germany, 1999.

[16] M. Bilgin, "Stationary and Rotating Hot Jet Ignition and Flame Propagation in a Premixed Cell," Ph.D. Dissertation, Aeronautics and Astronautics Dept, University of Washington, Seattle, WA, 1998.

[17] M. Bilgin, J.J. Keller, and R.E. Breidenthal, "Ignition and flame propagation with rotating hot jets in a simulated wave engine test cell," in *34th AIAA/ASME/SAE/ASEE Joint Propulsion Conference*, 1998.

[18] D. Baronia, M.R. Nalim, and P. Akbari, "Numerical study of wave rotor ignition and flame propagation in a single-channel rig," *43rd AIAA/ASME/SAE/ASEE Joint Propulsion Conference*, Cincinnati, OH, 2007.

[19] M. C. Turkish, "3 valve stratified charge engines: Evolvement, Analysis and Progression," *SAE Technical Paper*, 1974.

[20] T. Date, and S. Yagi, "Research and Development of Honda CVCC Engine," *SAE Technical Paper*, 1974.

[21] Kyaw, Z.H. and H.C. Watson, "Hydrogen Assisted Jet Ignition for Near Elimination of NOx and Cyclic Variability in the S.I. Engine." *Twenty-Fourth Symposium on Combustion*, vol. 24(1), p. 1449-1455, 1992.

[22] F. Hamori, "Exploring the Limits of Hydrogen Assisted Jet Ignition." PhD thesis, *University of Melbourne*, 2005.

[23] P. Mehrani, "Flame Propagation and Knock in a HAJI Engine." PhD Thesis, *University of Melbourne*, 2008.

[24] P. Mehrani, and H.C. Watson, "A search for maximum efficiency and NOx reduction through spark-ignition engine design optimisation at lambda=1", *Institution of Mechanical Engineers, Part D: Journal of Automobile Engineering*, vol. 222, Num. 5, pp. 875-88, 2008.

[25] M.R. Nalim, H. Li, and P. Akbari, "Air-Standard Aerothermodynamic Analysis of Gas Turbine Engines With Wave Rotor Combustion", *Journal of Engineering for Gas Turbines and Power-Transactions of the ASME*, vol. 131, No. 5, 2009.

[26] J.Y. Kim, A.J. Ghajar, T. Tang, and G.L. Foutch, "Comparison of Near-Wall Treatment Methods for High Reynolds Number Backward-Facing Step Flow," *International Journal of Computational Fluid Dynamics*, vol. 19, No. 7, pp. 493-500, 2005.

[27] Y. Halupovich, B. Natan, and J. Rom, "Numerical solution of the turbulent supersonic flow over a backward facing step," *Fluid Dynamics Research*, vol. 24, pp. 251-273, 1999.

[28] R.J. Hartfield, S.D Hollo, and J.C. McDaniel, "Planar measurement technique for compressible flows using laser induced iodine fluorescence," *AIAA Journal*, vol. 31 (3), pp. 483-490, 1993.

[29] B.E. Launder, G.J. Reece, and W. Rodi, "Progress in the Development of a Reynolds-Stress Turbulent Closure," *Journal of Fluid Mechanics*, vol. 68(3), pp. 537-566, 1975.

[30] W.P. Jones, and B.E. Launder, "The prediction of laminarization with a two-equation model of turbulence," *Int. J. Heat Mass Transfer*, vol. 15 (2), pp. 301-317, 1972.

[31] B.E. Launder, and B.I. Sharma, "Application of the Energy Dissipation Model of Turbulence to the Calculation of Flow Near a Spinning Dis," *Letter in Heat and Mass Transfer*, vol. 1, no. 2, pp. 131-138, 1974.

[32] T.H. Shih, W.W. Liou, A. Shabbir, Z. Yang, and J. Zhu, "A New *k*- Eddy Viscosity Model for High Reynolds Number Turbulent Flows -Model Development and Validation", *NASA TM* 106721, 1994.

[33] P.R. Spalart, and S.R. Allmaras, "A One-Equation Turbulence Model for Aerodynamic Flows," *AIAA Paper* 92-0439, 1992.

[34] F.R. Menter, "Two-equation eddy-viscosity turbulence modeling for engineering applications," *AIAA Journal,* vol. **32**(8), pp. 1598-1605, 1994.

[35] V. Ponyavin, C. Yitung. D.W. Pepper, and H.T. Hsieh, "Numerical Modeling of the turbulent supersonic flow over a backward Facing step," *Proceedings of IMECE04*, pp. 527-534, 2004.

[36] A. Roshko, and G.J. Thomke, "Observations of turbulent reattachment behind an axisymmetric downstream-facing step in supersonic flow," *AIAA Journal*, vol. 4 (6), pp. 975-979, 1966

[37] A. Karimi, S.D. Wijeyakulasurya, and M.R. Nalim, "Numerical Study of Supersonic Flow over Backward-Facing Step for Scramjet Application," in *48th AIAA/ASME/SAE/ASEE Joint Propulsion Conference*, Atlanta, Georgia, 2012.

[38] D. Garre´ton, and O. Simonin, "First Aerodynamics of Steady State Combustion Chambers and Furnace Workshop," *EDF-DER*, Chaton, 1994.

[39] AC. V. Silva, F. H. R. França, and H. A. Vielmo, "Analysis of the Turbulent, Non-Premixed Combustion of Natural Gas in a Cylindrical Chamber With And Without Thermal Radiation," *Combustion Science And Technology*, vol. 179:8, pp. 1605-1630, 2007.

[40] A. Brink, C. Mueller, P. Kilpinen, and M. Hupa, "Possibilities and Limitations of the Eddy Break-Up Model, Brief Communication," *Combustion And Flame*, vo. 123, pp.275–279, 2000.

[41] D.B. Spalding, "Mixing and Chemical Reaction in Steady Confined Turbulent Flames," *Thirteenth Symposium (International) on Combustion*, The Combustion Institute, Pittsburgh, PA, pp. 649–657, 1971.

[42] B.F. Magnussen, and B.H. Hjertager, "Development of the eddy-break-up model of turbulent combustion," *Sixteenth Symposium (International) on Combustion*, The Combustion Institute, Pittsburgh, PA, pp. 719–729, 1976.

[43] C.K. Westbrook, and F.L. Dryer, "Simplified Reaction Mechanism for the Oxidation of Hydrocarbon Fuels in Flames," *Combustion Science and Technology*, vol. 27, pp. 31 43, 1981.

[44] W.P. Jones, and R.P. Lindstedt, "Global Reaction Schemes for Hydrocarbon Combustion," *Combust. Flame*, vol. 73, pp. 233–249, 1981.

[45] H.C. Magel, U. Schnell, and K.R.G. Hein, "Simulation of Detailed Chemistry in a Turbulent Combustor Flow," *Twenty-sixth International Symposium on Combustion*, Combustion Institute, Naples, Italy, pp.67-74, 1996.

[46] L. Song, and J. Abraham, "Entrainment Characteristics of Transient Turbulent Round, Radial and Wall-Impinging Jets: Theoretical Deductions," *Journal of Fluid Engineering*, vol. 125, pp. 605-612, 2003.

[47] J. Kechiche, H. Mhiri, G. Palec, and P. Bournot, "Numerical study of the inlet conditions on a turbulent plane two-dimensional wall jets," *Energy Conversion and Management*. vol. 45, pp. 2931-2949, 2004.

[48] J.C.S. Lai, and D. Lu, "Effect of wall inclination on the mean flow and turbulence characteristics in a two-dimensional wall jet," *International Journal of Heat and Fluid Flow*, vol. 17, Iss. 4, pp. 377-385, 1996.

[49] C. Horne, "A preliminary experimental investigation of the flowfield of a planar wall jet," in *AIAA 14th Annual Meeting and Technical Display*, Washington D.C, 1978.

[50] H. Fujimoto, G. Hyun, M. Nogami, and K. Hirakawa, "Characteristics of Free and Impinging Gas Jets by Means of Image Processing," *SAE Technical Paper*, 1997.

[51] G. Bruneaux, "Combustion structure of free and wall-impinging diesel jets by simultaneous laser-induced fluorescence of formaldehyde, poly-aromatic hydrocarbons, and hydroxides," *International Journal of Engine Research*, vol. 9 no. 3, pp. 249-265, 2008.

[52] G. Bruneaux, "Mixing Process in High Pressure Diesel Jets by Normalized Laser Induced Exciplex Fluorescence Part II: Wall Impinging Versus Free Jet," *SAE Technical Paper*, 2005.

[53] J. Yu, V. Vuorinen, H. Hillamo, T. Sarjovaara, O. Kaario, and M. Larmi, "An experimental investigation on the flow structure and mixture formation of low pressure ratio wall-impinging jets by a natural gas injector," *Journal of Natural Gas Science and Engineering*, vol. 9, pp.1-10, 2012.

[54] T.J. Craft, and B.E. Launder, "On the Spreading Mechanism of the Three-Dimensional Turbulent Wall Jet," *Journal of Fluid Mechanics*, vol. 435, pp. 305-326, 2001.

[55] B.G. Newman, R.P. Patel, S.B. Savage, and H.K. Tjio, "Three-Dimensional Wall Jet Originating from a Circular Orifice," *Aeronautical Quarterly*, vol. 23, pp. 188-200, 1972.

[56] M.R. Davis, and H. Winarto, "Jet Diffusion from a Circular Nozzle above a Solid Plane," *Journal of Fluid Mechanics*, vol. 101, No. 1, pp. 201-221, 1980.

[57] N. Fujisawa, and H. Shirai, "Mean Flow and Turbulence characteristics of Three-Dimensional Wall Jet along Plane Surface," *Transactions of Japan Society for Aeronautical and Space Sciences*, vol. 32, pp. 35-46, 1989.

[58] H. Abrahamsson, and B. Johansson, L. L¨ofdahl, "An Investigation of the Turbulence Field in the Fully Developed Three-dimensional Wall-Jet, *Internal Rep 97/1*, Chalmers University of Technology, Sweden, 1997.

[59] B.E. Launder, and W. Rodi, "The Turbulent Wall Jet Measurements and Modeling," *Annual Review of Fluid Mechanics*, vol. 15, pp. 429-459, 1983.

[60] L. Song, and J. Abraham, "Entrainment Characteristics of Transient Turbulent Round, Radial and Wall-Impinging Jets: Theoretical Deductions," *Journal of Fluid Engineering*, vol. 125, pp. 605-612, 2003.

[61] P. Chinnathambi, "Experimental Investigation on traversing hot jet ignition of lean hydrocarbon-air mixtures in a constant volume combustor," M.S.M.E Thesis, IUPUI, 2013.

[62] STAR-CCM+, User Guide, Version 5.06.010, CD-adapco, 2010.

[63] S.D. Wijeyakulasuriya, U.I. Perera, and M.R. Nalim, "Mixing and Ignition Potential of a Transient Confined Turbulent Jet in a Wave Rotor Constant Volume Combustor," in *46th AIAA/ASME/SAE/ASEE Joint Propulsion Conference and Exhibit*, Nashville, TN, 2010.

[64] K. Murphy, M.S.M.E. Thesis, Department of Mechanical Engineering, Indiana University-Purdue University, Indianapolis, unpublished.

[65] C. Depcik, "Open-ended thermodynamic cycle simulation," MS Thesis, University of Michigan, Ann Arbor, 2000.

[66] S. Gordon, and B.J. McBride, "Computer program for calculation of complex chemical equilibrium compositions and applications," *NASA Reference Publication*, 1311, 1996.

[67] D.J. Hautman, F.L. Dryer, K.P. Schug, and I. Glassman, "A Multiple-step Overall Kinetic Mechanism for the Oxidation of Hydrocarbons," *Combustion Science and Technology*, v.25, pp.219-235, 1981.

[68] UCSD, Chemical-Kinetic Mechanisms for Combustion Applications, San Diego Mechanism web page, Mechanical and Aerospace Engineering (Combustion Research), University of California at San Diego), 2005. Last accessed May 2012 http://web.eng.ucsd.edu/mae/groups/combustion/sdmech/sandiego20050615/sandiego20050615.mec

[69] G.P. Smith, D.M. Golden, M. Frenklach, N.W. Moriarty, B. Eiteneer, M. Goldenberg, C.T. Bowman, R.K. Hanson, S. Song, W.C. Gardiner, and V.V. Lissianski, Q. Zhiwei http://www.me.berkeley.edu/gri_mech/,

[70] A. Kazakov, and M. Frenklach, Last accessed May 2012, http://www.me.berkeley.edu/drm/

[71] M. Amir, T. Sadegh, and G. Mohsen, "Numerical study of influence of molecular diffusion in the MILD combustion regime," *Combustion Theory and Modeling*, vol. 14, pp.747–774, 2010.

[72] Z. Luo, C.S. Yoo, E.S. Richardson, J.H. Chen, C.K. Law, and T.F. Lu, "Chemical explosive mode analysis for a turbulent lifted ethylene jet flame in highly-heated coflow," *Combustion and Flame*, vo. **159,** pp. 265-274., 2012.

[73] H. Wang, X. You, V. A. Joshi, S.G. Davis, A. Laskin, F. Egolfopoulos, and C.K. Law, USC Mech Version II. High-Temperature Combustion Reaction Model of H2/CO/C1-C4 Compounds. http://ignis.usc.edu/USC_Mech_II.htm, May 2007.

[74] D.F. Davidson, and R.K. Hanson, Interpreting shock tube ignition data, international journal of chemical kinetics, **36**, 9, *Wiley Online Library*, pp. 510-523.

[75] S.R.Turns, "An Introduction to Combustion," Second Edition, 2005.

[76] P. Glarborg, J.A. Miller, and R.J. Kee, "Kinetic modeling and sensitivity analysis of nitrogen oxide formation in well-stirred reactors," *Combustion and Flame*, vo. 65, Iss. 2, pp. 177-202, 1986.

[77] V. Kilchyk, M. R. Nalim, and C. Merkle, "Laminar premixed flame fuel consumption rate modulation by shocks and expansion waves," *Combustion and Flame*, vol. **158**, pp. 1140-1148, 2011.

[78] V. Kilchyk, M.R. Nalim, and C. Merkle, "Shock and expansion wave – laminar flame interaction," *6th International Colloquium on Pulsed and Continuous Detonations*, Moscow, Russia, 2008.

[79] C. Westbrook, M. Thornton, W. Pitz and P. Maltes, "A Kinetic Study of Ethylene Oxidation in a Well Stirred Reactor." *22th Symposium (International) On Combustion*, pp. 863-871, 1988.

[80] H. Wang and A. Laskin, "A Comprehensive Kinetic Model of Ethylene and Acetylene Oxidation at High Temperatures." Progress Report, *Princeton University*, 1998.

[81] V. Kilchyk, "Pressure-wave amplification of flame area in wave rotor channels," PhD Thesis, *Purdue University, West Lafayette*. 2009.

[82] V. Rupert, "Shock-interface interaction: Current research on the Richtmyer-Meshkov problem," *Proceedings of the 18th International Symposium on Shock Waves*, Sendai, Japan, 1991.

[83] N. Zabusky, "Vortex paradigm for accelerated inhomogeneous flows: Visiometrics for the Rayleigh-Taylor and Richtmyer-Meshkov environments," *Annual Review, Fluid Mechanics*, vol. 31, pp.495–536, 1999.

[84] M. Brouillette, "The Richtmyer-Meshkov instability," *Annual Review of Fluid Mechanics*, vol.34, pp.445–468, 2002.

[85] V. Kilchyk, M.R. Nalim, and C. Merkle, "Baroclinic vortex sheet production by shocks and expansion waves," *Shock Waves*, vol. 20, pp. 367–380, 2010.

[86] A. Karimi, P. Chinnathambi, M. Rajagopal, and M. R. Nalim, "Hot-Jet Ignition of Hydrocarbons and Hydrogen in Air: Effect of Jet Chemical Activity," in 49th AIAA/ASME/SAE/ASEE Joint Propulsion Conference, San Jose, CA, 2013.

[87] S.C. Kong, and R.D. Reitz, "Application of detailed chemistry and CFD for predicting direct injection HCCI engine combustion and emissions," *Proceedings of the Combustion Institute*, vol. 29, Iss.1, pp. 663-669, 2002.